Stony Brook University

OFFICIAL COPY

The official electronic file of this thesis or dissertation is maintained by the University Libraries on behalf of The Graduate School at Stony Brook University.

© All Rights Reserved by Author.

Inhibitors of Amyloid Formation by Islet Amyloid Polypeptide

A Dissertation Presented

By

Fanling Meng

To

The Graduate School

in Partial Fulfillment of the

Requirements

for the Degree of

Doctor of Philosophy

in

Chemistry

Stony Brook University

August 2010

Stony Brook University

The Graduate School

Fanling Meng

We, the dissertation committee for the above candidate for the Doctor of Philosophy degree, hereby recommend acceptance of this dissertation.

Daniel P. Raleigh, Ph. D., Dissertation Advisor

Professor, Department of Chemistry

Peter Tonge, Ph. D., Chairperson of Defense

Professor, Department of Chemistry

Stanislaus Wong, Ph. D., Third Member

Professor, Department of Chemistry

David Eliezer, Ph. D., Outside Member

Professor, Department of Biochemistry, Weill Medical College of Cornell University

This dissertation is accepted by the Graduate School

Lawrence Martin
Dean of the Graduate School

Abstract of Dissertation

Inhibitors of Amyloid Formation by Islet Amyloid Polypeptide

By

Fanling Meng

Doctor of Philosophy
in
Chemistry

Stony Brook University
2010

Amyloid deposition is a characteristic component of many human diseases, including Alzheimer's disease, Parkinson's disease and type 2 diabetes. Human islet amyloid polypeptide (IAPP also known as amylin) is the major protein component of the pancreatic islet amyloid associated with type 2 diabetes. There is considerable interest in developing inhibitors of amyloid formation, both because of their obvious therapeutic potential but also because they can provide powerful tools for mechanistic studies. There is a large body of work on inhibitors of the Alzheimer beta amyloid peptide (Aβ), but less attention has been paid to the development of IAPP amyloid inhibitors. In this dissertation, peptide based inhibitors were rationally designed and a general strategy was developed whereby two moderate inhibitors of amyloid formation can be rationally selected via kinetic assays and combined to yield a highly effective inhibitor. Small molecule inhibitors were also developed. Rifampicin is reported to inhibit Aβ amyloid

formation, but it does not prevent amyloid formation by IAPP and does not disaggregate preformed IAPP amyloid fibrils, instead it interferes with standard fluorescence based assays of amyloid formation. Simple sulphonated triphenyl methane derivatives are potent inhibitors of *in vitro* amyloid formation by IAPP. The tea-derived flavanol, (–)-Epigallocatechin 3-Gallate, is an effective inhibitor of *in vitro* IAPP amyloid formation and disaggregates preformed amyloid fibrils derived from IAPP.

IAPP is produced as a prohormone, proIAPP, and processed in the secretory granules of the pancreatic beta cells. Partially processed forms of proIAPP are found in amyloid deposits. It has been suggested that incomplete processing plays a role in amyloid formation by promoting interactions with sulfated proteoglycans of the extracellular matrix. Biophysical proof of principle evidences are provided for the role of proIAPP processing intermediate and sulfated proteoglycans in amyloid formation. Simple sulfonated triphenyl methyl derivatives inhibit amyloid formation by proIAPP processing intermediate and also inhibit glycosaminoglycans mediated amyloid formation by proIAPP processing intermediate. These studies may give a better understanding of the mechanism of amyloid formation and provide valuable insight into the development of effective therapeutic strategies for a wide range of amyloidogenic diseases.

Table of Contents

List of Figures

List of Tables

List of Symbols and Abbreviations

Aβ	The proteolytical fragment of amyloid precursor protein which is responsible for amyloid formation in Alzheimers disease
$A\beta_{1-40}$	The 40 residue isoform of Aβ
AD	Alzeheimer's disease
AGEs	Advanced glycosylation end products
Apo E	Apolipoprotein E
APP	Amyloid precursor protein
CD	Circular dichroism spectroscopy
CGRP	Calcitonin gene-related peptide
DIPEA	*N*,*N*-diisopropylethylamine
DMF	*N*,*N*-dimethylformamide
DMSO	Dimethyl sulfoxide
EGCG	(–)-Epigallocatechin 3-gallate, (2*R*,3*R*)-5,7-dihydroxy-2-(3,4,5-trihydroxyphenyl)-3,4-dihydro-2*H*-1-benzopyran-3-yl 3,4,5-trihydroxybenzoate
EM	Electron microscopy
Fmoc	9-fluorenylmethoxycarbonyl
GAG	Glycosaminoglycan

HBTU	*O*-benzotriazol-1-yl-*N*,*N*,*N*',*N*'-tetramethyluronium hexafluorophosphate
HFIP	Hexafluoroisopropanol
HOBT	*N*-hydroxybenzotriazole monohydrate
HPLC	High performance liquid chromatography
HSPGs	Heparan sulfate proteoglycans
IAPP	Human islet amyloid polypeptide
MALDI-TOF MS	Matrix assisted laser desorption ionization-time of flight mass spectrometry
SAP	Serum amyloid P
STEM	Scanning transmission electron microscopy
PAL-PEG	5-(4'-Fmoc-aminomethyl-3',5-dimethoxyphenyl) valeric acid
PAM	Peptidylglycine alpha-amidating monooxygenase
PC2	Subtilisin-like prohormone convertase enzyme 2
PC(1/3)	Subtilisin-like prohormone convertase enzyme 1/3
proIAPP	Pro-islet amyloid polypeptide
$proIAPP_{1-48}$	A peptide corresponding to residues 1-48 of human pro-islet amyloid polypeptide
$proIAPP_{1-48}$/heparan sulfate	$ProIAPP_{1-48}$ with heparan sulfate

proIAPP$_{1-48}$/dermatan sulfate	ProIAPP$_{1-48}$ with dermatan sulfate
proIAPP$_{1-48}$/chondroitin sulfate	ProIAPP$_{1-48}$ with chondroitin sulfate
t_{50}	The time required to reach the midpoint of amyloid formation during a kinetic experiment
TEM	Transmission electron microscopy
TFA	Trifluoroacetic acid
Y37F$_{CN}$ IAPP	Human islet amyloid polypeptide with a p-cyanoPhe for Tyr-37 subtitution

Acknowledgements

The whole work in the dissertation is guided by my research advisor, Prof. Daniel P. Raleigh. I appreciate his invaluable guidance, enthusiastic support, and continuous encouragement during my research. I am very proud to have him as my Ph. D. advisor.

I would also like to express my gratitude to the other members in my academic committee. I sincerely appreciate my committee chair, Prof. Peter Tonge, and the third member, Prof. Stanislaus Wong, for their help and encouragement throughout my advancement in the Ph. D. program. I would also like to thank Prof. David Eliezer from Weill Medical College of Cornell University, who kindly served as my outside committee member.

Thanks to my group members, past and present, Dr. Andisheh Abedini, Dr. Benben Song, Dr. Yuan Bi, Dr. Bing Shan, Dr. Ruchi Gupta, Dr. Burcu Anıl, Dr. Jae-Hyun Cho, Dr. Ying Li, Dr. Yuefeng Tang, Dr. Hümeyra Taşkent, Peter Marek, Shifeng Xiao, Ping Cao, Wenli Meng, Vadim Patsalo, Trisha Barua, Bowu Luan, Ivan Peran, Hui Wang, Cynthia Tu and Harris. I greatly enjoyed the time I spent together with them. I specially thank Dr. Andisheh Abedini and Dr. Benben Song for training me when I started my lab work in my first year; thank Shifeng Xiao, Vadim Patsalo and Peter Marek for helping me with techniques and Ping Cao for collaborating on several projects.

Many of my research projects are collaborations with other research groups, without which my dissertation could not have been completed. I must thank Prof. C. Bruce Verchere, Ms. Annette Plesner and Ms. Kathryn J. Potter from University of British Columbia for cytotoxicity studies; Prof. Martin Zanni and Dr. Chris Middleton from University of Wisconsin- Madison for 2D IR studies; Dr. Mahiuddin Ahmed and

Mr. Darryl Aucoin for helping me with atomic force microscopy; Prof. Nicole S. Sampson for providing fluorescence spectrometers.

I would like to thank my family for their love and continuous support.

List of Publications

1. Andisheh Abedini, **Fanling Meng** and Daniel P. Raleigh. "A Single Point Mutation Converts Highly Amyloidogenic Human Islet Amyloid Polypeptide into a Potent Inhibitor of Fibrillization." (2007) *Journal of the American Chemical Society,* **129** 11300-11301

2. **Fanling Meng**, Andisheh Abedini, Benben Song and Daniel P. Raleigh. "Amyloid Formation by proIAPP Processing Intermediates: Examination of the Role of Protein-Heparan Sulfate Interactions and Implications for Islet Amyloid Formation in Type 2 Diabetes." (2007) *Biochemistry*, **46** 12091-12099.

3. **Fanling Meng**, Peter Marek, Kathryn J. Potter, C. Bruce Verchere and Daniel P. Raleigh. "Rifampicin does not Prevent Amyloid Fibril Formation by Human Islet Amyloid Polypeptide but does Inhibit Fibril Thioflavin-T Interactions: Implications for Mechanistic Studies Beta-cell Death" (2008) *Biochemistry*, **47** 6016-6024.

4. Andisheh Abedini, Ruchi Gupta, Peter Marek, **Fanling Meng**, Daniel P. Raleigh, Sylvia Tracz and Humyra Taskent. "Post Translational Modifications and Amyloid Formation" (2010) *Protein Misfolding Diseases: Current and Emerging Principles and Therapies.* Edited by Christopher M. Dobson, Jeffery W. Kelly and Marina Ramirez-Alvarado. Published by John Wiley and Sons.

5. **Fanling Meng**, Andisheh Abedini, Annette Plesner, Katherine J. Potter, C. Bruce Verchere and Daniel P. Raleigh. "Sulfated Triphenyl Methane Derivatives are Potent Inhibitors of Amyloid Formation by Human Islet Amyloid Polypeptide and Protect against the Toxic Effect of Amyloid Formation" (2010) *Journal of Molecular Biology,* **400**, 555-566.

6. Ping Cao, **Fanling Meng,** Andisheh Abedini and Daniel P. Raleigh. "The Ability of Rodent Islet Amyloid Polypeptide To Inhibit Amyloid Formation by Human Islet Amyloid Polypeptide Has Important Implications for the Mechanism of Amyloid Formation and the Design of Inhibitors." (2010) *Biochemistry,* **49** 872-881.

7. **Fanling Meng,** Daniel P. Raleigh, and Andisheh Abedini "The Rational Combination of Kinetically Selected Inhibitors *in Trans* Leads to the Highly Effective Inhibition of Amyloid Formation."(2010) *Journal of the American Chemical Society,* in revision.

8. **Fanling Meng**, Andisheh Abedini, Annette Plesner, Katherine J. Potter, C. Bruce Verchere and Daniel P. Raleigh. "The Flavanol (–)-epigallocatechin 3-gallate Inhibits Amyloid Formation by Islet Amyloid Polypeptide, Disaggregates Amyloid Fibrils and Protects Cultured Cells against IAPP Induced Toxicity" (2010) *Biochemisry,* in press.

9. **Fanling Meng** and Daniel P. Raleigh. "Inhibit Glycosaminoglycan Mediated

Amyloid Formation by Islet Amyloid Polypeptide and pro-Islet Amyloid Polypeptide Processing Intermediate" (2010) *submitted to Journal of Molecular Biology.*

1. Introduction

Amyloids are insoluble fibrous protein or peptide aggregates sharing specific structural features. Amyloid formation play an important role in many diseases, including Alzheimer's, Parkinson's and Huntington's diseases, the transmissible spongiform encephalopathies, type 2 diabetes mellitus and various forms of systemic amyloidosis (*1-2*). More than 20 different proteins or peptides are known to form amyloid deposits which are associated with human pathologies. Amyloid plaques are found in different affected tissues, including the pancreas in type 2 diabetes and the brain in neurodegenerative diseases (Table 1-1).

1.1 General features of amyloid fibrils

A large number of proteins and polypeptides can form amyloid. Despite the different amino acid sequences of the proteins or peptides known to form amyloid, protein amyloids share many common physical properties. Amyloid fibrils are always unbranched, 5-10nm in diameter, variable in length and polymorphic (*3*). Studies using electron microscopy (EM) and scanning transmission electron microscopy (STEM) indicate that fibrils are normally made up of protofilaments which often left-handed coiled together (Figure 1-1) (*4*). The diameter of individual protofilaments are around 5

nm (*5*). STEM mass-per-length analysis of IAPP fibrils indicate that about 2.6 molecules are packed in 1 nm of protofibril length *(6)*. A characteristic feature of amyloid fibrils is the cross β-sheet structure in which β-sheets extend over the length of fibrils and the individual β-strands are aligned perpendicular to the fibril axis which gives rise to extensive hydrogen bonding between β-strands along the axis of the fibril (Figure 1-1) (*7-9*).

The highly ordered fibrillar structures of amyloids can bind to histological dyes such as Congo red and thioflavin-T. Thioflavin-T has been widely used for characterizing the presence of amyloid fibrils and following kinetics of amyloid formation (Figure 1-2). Thioflavin-T has very low quantum yield in solution and its quantum yield increases significantly when it binds to fibrillar structures (*10*). There is no structure of thioflavin-T bound to any amyloid fibrils, but the dye is believed to bind to grooves on the surface of amyloid fibrils. In the cross-β structure, side chains in consecutive strands will form a ridge and a set of side chains at positions n and n+2 will lead to two ridges separated by a groove (Figure 1-2). These grooves likely account for the specificity of the dye's binding interactions with amyloid fibrils (*11*).

Various studies have focused on the mechanism of amyloid formation. But the exact mechanism of amyloid formation is not known. Experimental evidence suggests that peptides form amyloid fibrils in a nucleation-dependent manner which can be affected by seeding (*12-14*). The nucleation dependent model is always characterized by a lag phase in which no fibers are detected. During the lag phase, the monomers associate

into oligomers and then the oligomers slowly convert to fiber nucleus. The lag phase is followed by a rapid growth phase in which fibers are formed. After the growth phase, the fibrillization reaction reaches a plateau in which the fibrils are in equilibrium with soluble peptide (Figure 1-3) (*15*). The limiting step in the process is the formation of seeds to direct further aggregation (*14*). The transition from the lag phase to the growth phase is sharp and the sharp transition is not predicted by simple nucleation polymerization models. The sharp transition is thought to be caused by secondary nucleation. Seconday nucleation cn happen because of breakage of fibrils or by the growth of new fibrils off the surface of existing fibrils. Amyloid formation can be substantially accelerated by the addition of preformed seeds. The lag phase is generally diminished by providing preformed fibers as seed.

1.2 Islet amyloid polypeptide (IAPP)

1.2.1 Pancretic synthesis of IAPP

IAPP is a member of the 'calcitonin peptide family', and is similar to calcitonin gene-related peptide (CGRP) in sequence and shares some actions and receptor binding affinities with CGRP (*16*). Islet amyloid polypeptide (IAPP, also known as amylin) is a 37-residue polypeptide which is co-processed and co-secreted with insulin in pancreatic β-islet cells in a roughly of 1:100 ratio of IAPP: insulin (*17-19*). The physiological roles of IAPP remain unclear. It is thought to be important for maintaining glucose homeostasis by suppressing insulin-mediated glucose uptake (*20-21*). It is believed that it

plays a role in inhibition of gastric emptying, promotion of satiety and suppression of glucagon release from isolated islets (*21-23*).

IAPP is initially synthesized as a 89 precursor (preproIAPP) (*24-25*). The signal sequence is removed proteolytically to produce the 67 residue pro hormone, proIAPP. proIAPP is further processed in secretory granule by proprotein convertase enzymes PC1, PC2, and PC3. PC(1/3) is responsible for processing at the C-terminal dibasic site while PC2 favors cleavage at the N-terminal dibasic site (*26*). Normal processing of proIAPP occurs at two well-conserved dibasic sites: Lys10-Arg11 at the N-terminus and Lys50-Arg51 at the C-terminus (*25-26*). Following this reaction, the remaining residue at the C-terminus are removed by carboxypeptidase E and mature IAPP is formed by removal of glycine and amidation of the Tyr-37 by peptidylglycine alpha-amidating monooxygenase (PAM). Formation of the disulfide bond between cysteine residues at positions 2 and 7 in the mature peptide is required for full biological activity of mature IAPP. The primary sequences of proIAPP and mature IAPP and the location of cleavage sites are shown in Figure 1-4.

1.2.2 Type 2 diabetes and amyloid formation by IAPP

There are two major types of diabetes in human, type 1 diabetes and type 2 diabetes. Type 2 diabetes develops in mostly over 40-years old individuals and is a mutifactorial disease, including family history, aging and several causes of insulin resistance. Type 2 diabetes is characterized by deficiency of insulin secretion from islet

β-cells and insulin resistance. Amyloid deposition is a characteristic feature of the islets in type 2 diabetes and IAPP is the major component of the pancreatic amyloid deposits associated with type 2 diabetes (*17*) and the extent of amyloid deposition correlates with severity of the disease in humans (*27-29*). Islet amyloid deposits may play an important role in β-cell mass loss and decrease in insulin secretion characteristic of type 2 diabetes.

The IAPP sequence varies from species to species although 80% of the sequence is conserved and not all species form islet amyloid. The ability to form amyloid is different because of the different amino acid sequence, for example, humans, primates, cats, dogs and monkeys develop islet amyloid, and while IAPP derived islet amyloid does not found in rat or mice. Synthetic full length human IAPP forms amyloid fibrils easily *in vitro*, while synthetic rat IAPP does not form amyloid (*30-31*). The sequence of rat IAPP differs from that of human IAPP in 6 out of 37 residues, and 3 of these residues are prolines which are known to be β-sheet breaking residues. They are located in the region between residues 20-29 (Figure 1-5) (*32*). Moreover, the decapeptide sequence human IAPP 20-29 does form amyloid with β-structure and rat IAPP 20-29 does not aggregate into amyloid. Therefore, the amino acid constitution of sequence 20-29 has been implicated to play an important role for the amyloidogenic propensity of full length IAPP. Ashburn and Lansbury studied the human F23L IAPP 20-29 and S29P IAPP20-29 peptides, both peptides affect the rate and stability of amyloid formation by human IAPP 20-29 which suggest that residues F23 and S29 are important for the kinetics of human IAPP20-29 amyloid formation and stability of the fibrils (*33*). The importance of each

residue of human IAPP 20-29 was studied by performing proline scanning 20-29 region (*34*). All of the substitutions affect amyloidogenicity, while mutation at positions N22, I26, L27 and S28 had the most dramatic effects and they did not form amyloid and has no beta structure was seen. However, the primary sequence in the 20 to 29 region can not be the only factor. Biophysical studies were performed to test how critical the 20-29 region is for IAPP amyloid formation by studying a variant which is identical to the human peptide in the 20-29 segment but contains three prolines outside of this region (*35*). Studies showed that the IAPP variant reduces its amyloid forming ability and suggested that there is not a single short amyloidogenic domain within the IAPP amino acid sequence.

1.2.3 Causes of IAPP amyloid formation

The factors that affect IAPP amyloid formation remain unclear. Some studies suggest that impaired processing of proIAPP by islet cells may contribute to IAPP amyloid formation. ProIAPP and proinsulin are processed by the same prohormone convertase enzyme, PC1 and PC2, and stored in secretory granules (*36-39*). It is known that some incorrect processing of insulin occurs during type 2 diabetes. Both recombinant and synthetic proIAPP can form amyloid although the rate of amyloid formation is slower than mature IAPP peptide (*40-41*). Immunohistochemical investigations of islet amyloid deposits found the presence of the proIAPP N-terminal flanking region in islet amyloid deposits but not the C-terminal flanking region, suggesting that N-terminal

region of proIAPP has been improperly process (*42-43*). This is caused by loss or defective processing by PC2 (*44*). Abnormal processed N-terminal flanking region of proIAPP has been found in islet amyloid deposits from type 2 diabetic patients, suggesting that N-terminal region of proIAPP may play a role in islet amyloid formation. Verchere and coworkers have shown that the N-terminal region of proIAPP contains a heparan sulfate proteoglycan (HSPG) binding domain (*45*). The heparin/heparan binding sites in the proIAPP sequence have been mapped by using a series of overlapping peptides (*46*). HSPG is a component of extracellular basement membranes and has been implicated in almost all the amyloidoses (*47-52*). The HSPG perlecan is also a found in islet amyloid deposits and has been proposed as a factor for amyloid assembly. These observations suggest that secretion of proIAPP processing intermediates could accumulate by binding to HSPG and form a seed for IAPP aggregation.

Other workers have postulated that IAPP membrane interactions are important for amyloid formation. Lipid membrane IAPP interactions have been shown to promote the aggregation of IAPP and generate potentially toxic forms of IAPP (*53-55*). Some studies have shown that IAPP disrupts membrane integrity and to permeabilize membranes (*56-58*). But many of the *in vitro* studies used non-physiological concentration of anionic lipids and the relevance of these studies to the *in vivo* situation is not clear.

Glycation of protein is another charteristic feature of the hyperglycemia of type 2 diabetes (*59*). *In vitro* studies suggest that modification of the IAPP peptide by advanced

glycosylation end products (AGEs) enhance peptide aggregation. AGE-IAPP seeds can also accelerate IAPP amyloid formation by abolish the nucleation which is required for the polymerization of unseeded IAPP (*60*). However, IAPP amyloid deposits are also observed when the glucose concentration is low and glycation is minimal. This suggests that glycation of IAPP is not important for IAPP aggregation. AGE-IAPP formation may occur after IAPP amyloid is formed.

Serum amyloid P (SAP) and apolipoprotein (Apo) E are also components of amyloid deposits (*61-62*). The role of apoE and SAP in islet amyloid is not very clear. Studies indicate that SAP can not promote amyloid formation, but it protects amyloid from dissaggregation and may play an important role in protecting pancreatic amyloid deposits from removal and degradation (*63*). ApoE may play a role in lipid metabolism disorder and no correlation has been found between apoE and the degree of islet amyloid in type 2 diabetes (*64*).

1.2.4 Cytotoxicity of IAPP

Amyloid forming proteins can adopt a number of conformations, oligomers, protofibrils and fibrils. There is a lively debate on what constitutes the toxic species in the amyloid diseases (*65*). In early studies, applying human IAPP or rat IAPP to cultured human islet cells gave different results, human IAPP but not rat IAPP cause β cell apoptosis. This work suggested that amyloid fibrils or their precursors are toxic and contribute to the progression of the systemic amyloidoses (*66*). However, recent studies

have not support this conclusion (*67-68*). Apoptosis does not appear to be induced by adding amyloid fibrils to islet cells in culture and viable cells decorated with amyloid fibrils are observed by using electron microscopy (*67*). In contrast, apoptosis is reproducibly induced by adding a freshly prepared aqueous solution of hIAPP to islet cells in culture and the cell membrane is damaged. Electron microscopy reveals the presence of small nonfibrillar hIAPP oligomers under these conditions. These studies indicate the soluble, partially structured oligomers which are early intermediates in the fibrillation pathway, may be the toxic entities (*65, 69-71*).

1.2.5 Structural models of IAPP amyloid fibrils

The exact structure model of the IAPP monomer in its fibrillar state has not determined yet. One model of the IAPP amyloid fibril suggests a parallel β-serpentine structure. In this model, each polypeptide forms three β-strands which are residues 12-17, 22-27 and 31-37 (Figure 1-6) (*3*). The 4.0-4.5nm protofilament diameter and 0.47nm axis rise per molecule which are predicted in this model are in agreement with the results observed by electron microscopy and scanning transmission electron microscopy. The serpentines are stacked along axis direction and fibril has the cross β-structure. The first 11 residues at the N-terminus, which contain a disulfide-bonded loop, are not compatible with extending the serpentine. For this reason, the first 11 residues are not included in the serpentine core. The serpentine core includes many apolar residues and is stabilized by Asn ladders which are formed from the stacking of Asn-22,

Asn-31 and Asn-35 in successive molecules. This model is also consistent with fluorescence probe studies which show the residue Tyr-37 is in proximity with residues Phe-15 and Phe-23. In addition, this model can provide explanation for mutation studies (*72*). However, the model was not based on any atomic level structural constraints.

By using STEM with one and two dimentional solid state NMR techniques, Tycko and coworkers purposed a different structure model of the IAPP protofilament. Each protofilament contains four layers of parallel β-sheets which are formed by two symmetric layers of IAPP molecules (Figure 1-7) (*73*). In this model, individual polypeptides take on a U-shaped fold made of two β-strands which span from residues 8-17 and 28-37 and separated by a segment comprised of residues 18-27 as predicted by solid state NMR. Both hydrophobic and polar side chains are contained in the core of the IAPP protofilament. Hydrophobic residues 23-27 interact favorably with hydrophobic residues 15-17 and 32. While, hydrophilic residues 28-31 in one molecular layer interact with the same residues in the other molecular layer. This model is also consistent with fluorescent probe studies of the C-terminal Tyr-37 packing and with the proximity at Tyr-37 to Phe-15 and predicts a mass-per-length for the protofilament of 20 kDa/nm which agrees with the STEM data (*12*).

1.3 Beta Amyloid and Alzheimers's Disease

Alzeheimer's disease (AD) is characterized by progressive deposition of the amyloid-β peptide (Aβ) in senile plaques, oxidative neuronal damage, and loss of

synaptic and neuronal degeneration. AD is one of the most extensively studied amyloid-related disorders because of lack of effective treatments. Aβ peptides, i.e. $A\beta_{40}$ and $A\beta_{42}$, are the most common amyloid deposits in AD and they are generated by cleavage of the amyloid precursor protein (APP) by the β-amyloid precursor cleaving enzyme β-secretase (32, 33) and followed by cleavage of the C-terminal fragment of APP by gamma-secretase (34). Although the physiological role of Aβ is not clearly known, monomeric Aβ is not toxic to the cells and the deposition of Aβ fibrils is believed to associate with AD. The formation of oligomers and fibrils is considered to be a critical step in the pathology of AD. Recent studies suggest that oligomers which are intermediates during amyloid formation are the most neurotoxic species (*70, 74*). Therefore, inhibiting oligomers and fibrils formation is a promising therapeutic strategy.

1.4 Inhibition of Amyloid Formation

The design of inhibitors is a very active research area both because of their therapeutic potential, but also because they can provide powerful tools for mechanistic studies. There is a large body of work on inhibitors of the beta amyloid peptide (Aβ) and fewer studies on the IAPP peptide. A large number of synthetic organic compounds and short peptide inhibitors have been designed and developed to inhibit amyloid formation and toxicity. Many polyphenol compounds are inhibitors of amyloid formation, including resveratrol, Garlic acid, pomegranate, EGCG and curcumin. The red wine compound resveratrol has been shown to be an inhibitor of IAPP amyloid formation and it can also

inhibit lipid membrane-induced IAPP fibrillogenesis (*75-76*). EGCG inhibits the *in vitro* amyloid formation of several natively unfolded polypeptides including Aβ, α-synuclein, polyglutamine and κ-casein peptides (*77-79*). Several sulfonated small molecule compounds are reported to be effective inhibitor of amyloid formation by certain proteins. Tramiprosate (3-amino-1-propane sulfonic acid) has been shown to be an effective inhibitor of *in vitro* amyloid formation by Aβ and reduces the amyloid burden in TgCRND8 mice, while eprodisate (1, 3-propanedisulfonic acid) has been tested as a potential therapeutic agent for AA amyloidosis (*80-83*).

A range of short peptide inhibitors have also been designed and developed to inhibit amyloid formation and toxicity. Peptides which contain the β-sheet breaker residue, proline, N-alkylated amino acids, or ester functionalities have been shown to inhibit amyloid formation in IAPP as well as other amyloidogenic proteins (*84*). A double N-methylated variant of IAPP has been shown to inhibit IAPP fibrillogenesis, dissociation of cytotoxic aggregates and reduce cytotoxicity of IAPP aggregates (*85*). The addition of bulky groups or charged amino acids to peptide ends which also have β-sheet breaking effects can lead to the inhibition of amyloid formation (*86-87*). A diverse range of small organic compounds have also been shown to act as aggregation inhibitors (*88-89*). Small fragments of IAPP can be inhibitors. A series of overlapping hexapeptides spanning 8-20 domain of human IAPP indicate that one particular peptide, ANFLVH, could inhibit the amyloid formation of human IAPP *in vitro* and in human islet cultures leading to a increase in islet cell viability (*90*).

Recent studies suggest the formation of a helical intermediate in the lag phase and helix-helix associations promotes the formation of multimeric species (*54, 91*). A peptidomimetic α-helix which targets helix-helix interactions was reported to inhibit IAPP myloid formation catalyzed by lipid bilayers and reduce IAPP-induced toxicity in cell culture (*92*). Rat IAPP which differs from the human polypeptide at six positions, three of them are prolines and localized between residues 20 and 29, has been reported as an effective inhibitor by formation of an early helical intermediate in the N-terminal region of IAPP (*93*). Conformational restriction of peptides via cyclization can prevent β-structure formation and lead to compounds that act as inhibitor of amyloidogenesis (*94*). Despite the large amount of work, almost all known inhibitors of fibril formation by IAPP are only effective in significant molar excess, thus further design of inhibitors is required.

Inhibitors can target different steps of amyloid formation. A large number of inhibitors have no effect on the lag phase but decrease the amount of amyloid formed. Some inhibitors lengthen the lag phase and have no effect on the total amount of amyloid formed. The kinetic profiles of the different inhibitors on amyloid formation are illustrated in Figure 1-8.

Protein or Peptide	Disease	Affected Tissure
Islet amyloid polypeptide (IAPP, amylin)	Type 2 diabetes	Pancreas
Beta amyloid (Aβ)	Alzheimers's disease	Brain
Prion protein	Transmissible spongeiform encephalopathies	Brain
α-synuclein	Parkinson's disease	Brain
Huntingtin	Huntington's disease	Brain
Human lysozyme	Familial or hereditary amyloidosis	Liver, Kidney
Transthyretin	Familial amyloid polyneuropathy	Peripheral nerve
Immunoglobulin light chain	Primary amyloidosis	Kidney, lung,heart
Apolipoprotein A1	Familial or hereditary amyloidosis	Heart
Desmin	Desmin-related cardiac amyloidosis	Heart
Stefin B	Myoclonus epilepsy type 1	Brain

Table 1-1: Amyloid formation associated diseases (*95*).

A B

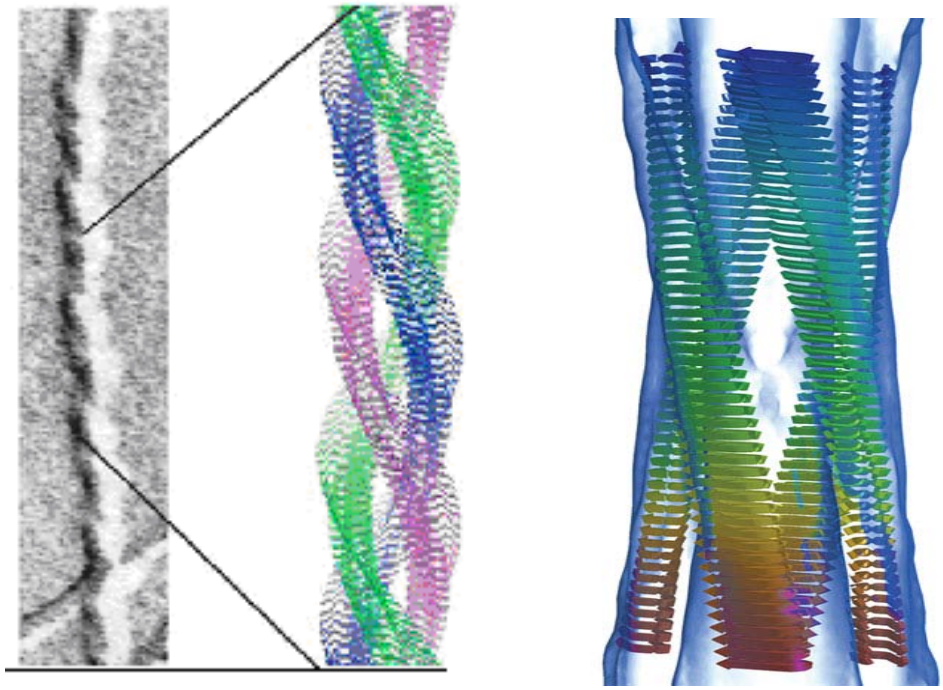

Figure 1-1: (A) Left: TEM micrograph of amyloid fibrils. Right: Model of Amyloid fibril in which 3 protofilaments coil around each other. Figure is adapted from reference (*3*). (B) Cross-β amyloid fibril structure obtained by cryo-electron microscopy modeled into the electron density map. Each protofibril consists of two long β-sheets. Polypeptide β-sheets run perpendicular to the fibrils axis. Figure is adapted from reference (*9*).

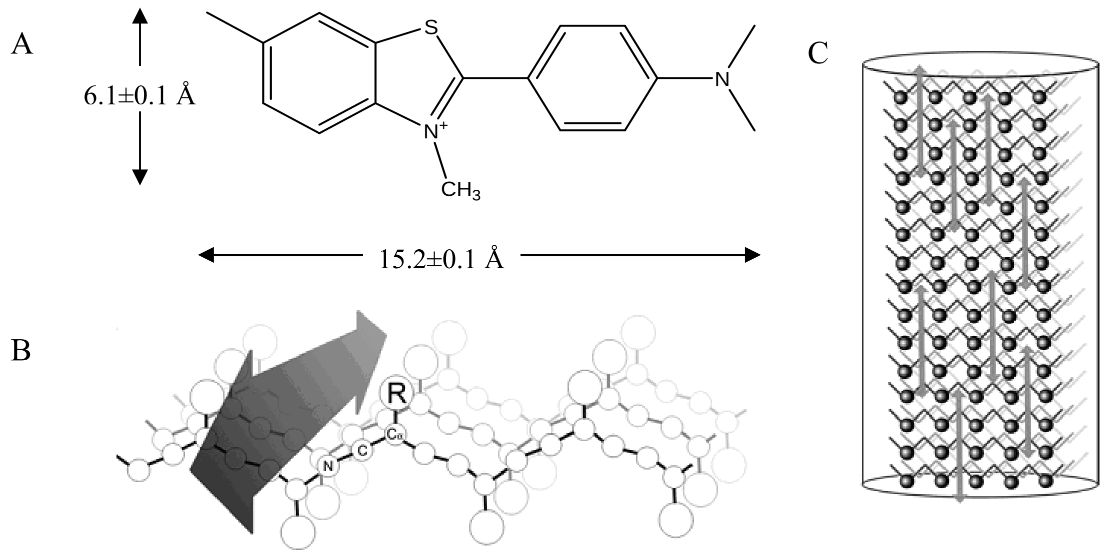

Figure 1-2: Schematic representation of thioflavin-T binding to the β-sheet structure of amyloid fibrils. Figures are adapted from reference (*11*). (A) The structure of thioflavin-T. It is 6.1 ± 0.1Å high and 15.2 ±0.1Å long. (B) Model of thioflavin-T binding within a β-sheet channel formed by aligned rows of surface sidechains. The backbone atoms (N, C, and Cα) and sidechain (R) for one residue are shown. The double-headed arrow indicates one thioflavin-T molecule with its long axis parallel to the long axis of the arrow. It is likely that only one face of the sheet would be accessible to the solvent. (C) Schematic representation of thioflavin-T binding with a protofilament which is composed of three β-sheets. Individual β-strands are shown by zig-zag lines in black, dark gray and light grey. Black circles indicate the side chains which are accessible to the solvent and point out of the plane of the paper. Dye molecules are represented by double-headed arrows.

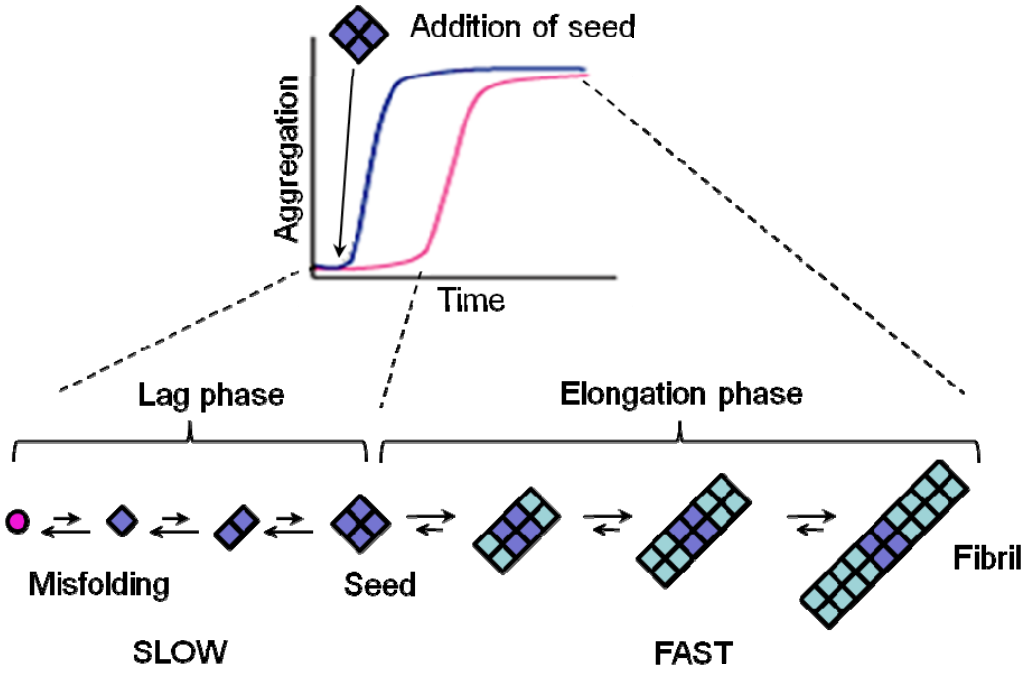

Figure 1-3: Model of the nucleation-polymerization pathway of amyloid formation. Figure is adapted from reference (*15*). Amyloid formation consists of two observable phases: lag phase which involves misfolding of peptide and formation of seeds and elongation phase where fibrils are formed.

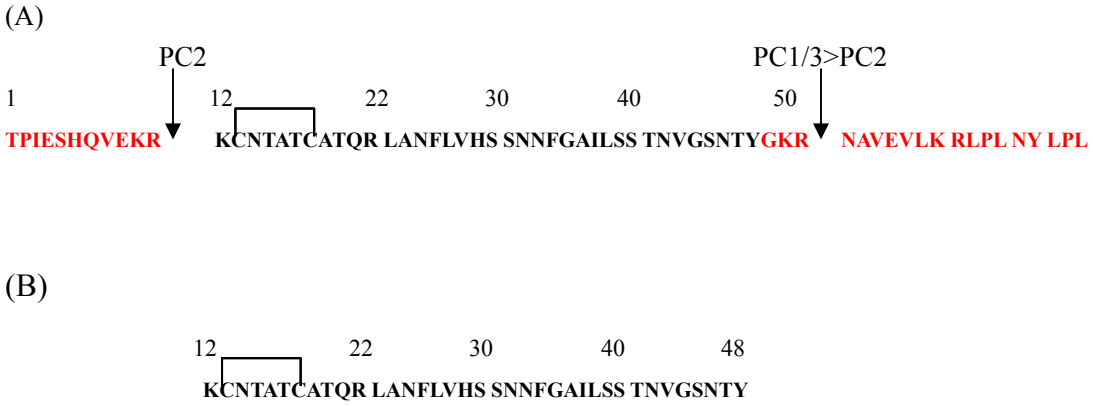

Figure 1-4: (A) The primary sequence of the 67-residue proIAPP peptide. The N-terminal and C-terminal flanking regions of proIAPP are shown in red, and the mature IAPP sequence is shown in black. Cleavage of proIAPP occurs at the two dibasic sites at (Lys-10, Arg-11) and at (Lys-50, Arg-51) which are indicated by black arrows. Cleavage at the N-terminus is initiated by PC2. Processing at the C-terminus is favored by PC1 and PC3 but can also be cleaved by PC2. (B) The primary sequence of the 37-residue mature IAPP. The disulfide bond is formed between residues 2 and 7 in the mature sequence.

	1 10	11 19	20 29	30 37
Human	**KCNTATCATQ**	**RLANFLVHS**	**SNNFGAILSS**	**TNVGSNTY**
Monkey	----------	-------R-	-----T----	-----D--
Pig	---M------	H-----DR-	R---T-F-P	-K------
Cat	----------	------IR-	---L-----P	--------
Cougar	----------	------IR-	---L-----P	--------
Dog	----------	-------RT	---L-----P	--------
Rat	----------	-------R-	---L-PV-PP	--------
Mouse	----------	-------R-	---L-PV-PP	--------
Hamste	----------	----------	N--L-PV-PP	--------
Guinea Pig	----------	--T----R-	-H-L--A-LP	-D------
Degu	----------	--T----R-	-H-L--A-PP	-K------
Rabbit	----------	------I--	-------F-P	PS------
Hare	----------	------I--	-------F-P	P-------

Figure 1-5: The primary sequences of IAPP from difference species.

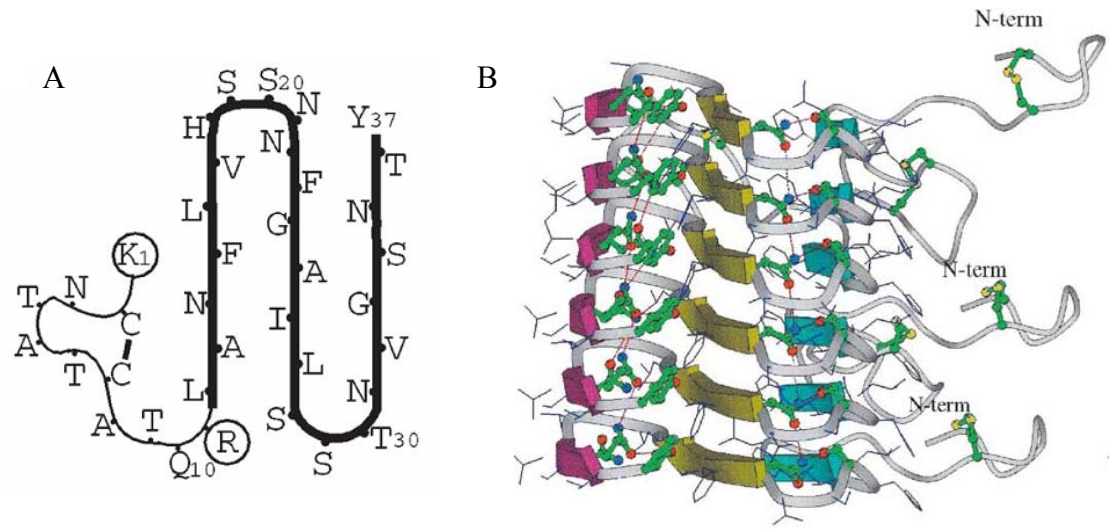

Figure 1-6: The β-serpentine model of fibrillar IAPP. Figures are adapted from reference (*3*). (A) The model has three β-strands for each peptide. The first 11 residues are not involved in the β-strands because of the disulfide bonds. The circled residues are charged. (B) View of the protofilament model of fibrillar IAPP. The three β-strands of the serpentine are marked by blue, yellow and purple colored arrows. The N terminuses protrude from the core of the protofilament.

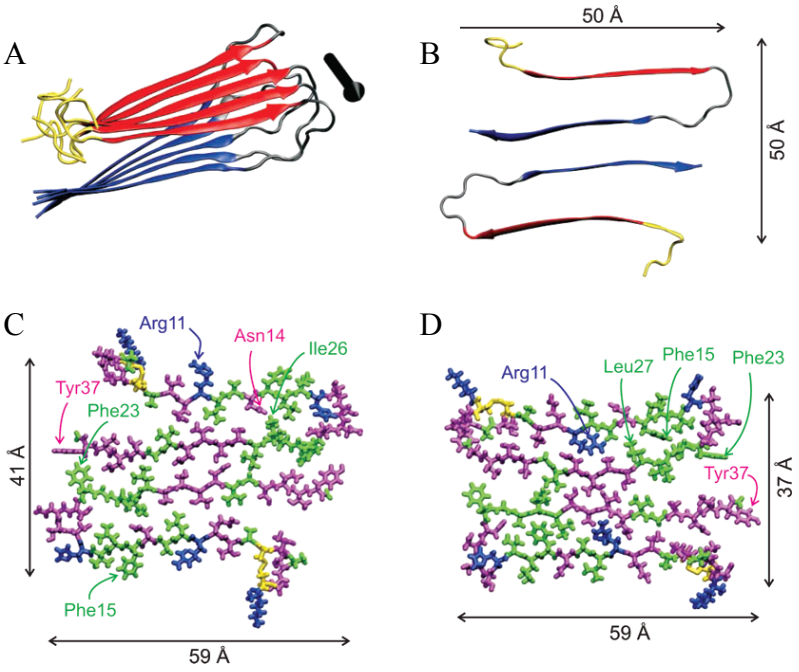

Figure 1-7: Structural model for the protofilament in IAPP fibrils. Figures are adapted from reference (*73*). (A) View of one cross-β-molecular layer model of IAPP; N-terminal β-strand (red), C-terminal β-strand segments (blue). The black arrow indicates the fibril axis. (B) View of two IAPP molecules in the protofilament. (C and D) All-atom representations of two possible models showing contacts between residues; hydrophobic residues (green), polar residues (magenta), positively charged residues (blue), and disulfide-linked cysteine residues (yellow). The main differences in the C and D models are different sets of side chain contacts between β-sheet layers in residues 19-21, 24 and 25.

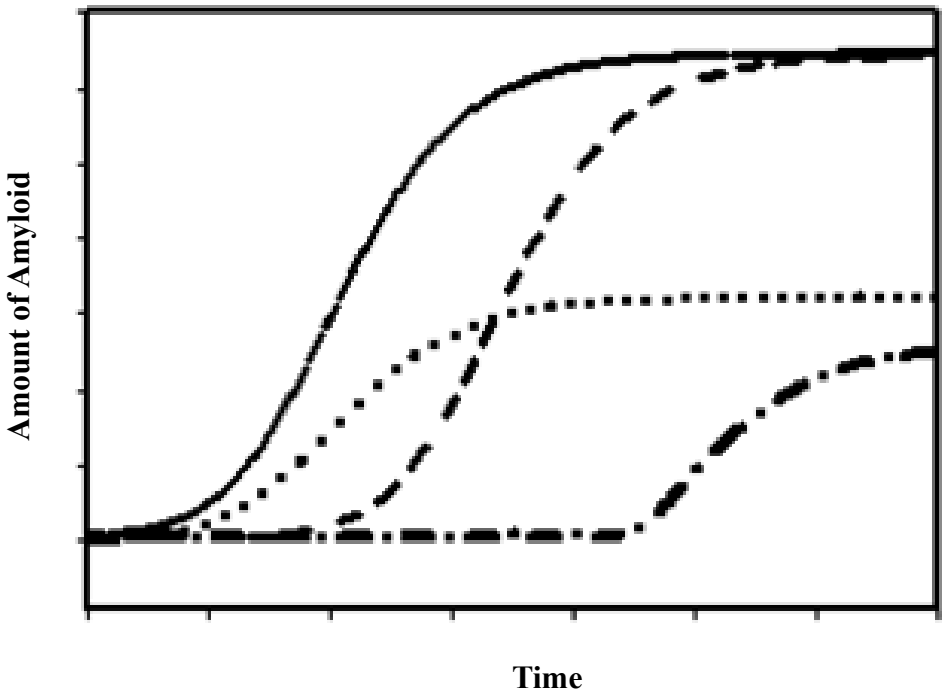

Figure 1-8**:** Kinetic profiles of different inhibitors of amyloid formation. The solid curve indicates the kinetic of amyloid formation by amyloidgenic proteins or peptides. An inhibitor which can lengthen the lag phase, but has no effect of the amount of amyloid is indicated by the dashed curve. The dotted curve shows the kinetic curve for an inhibitor which decreases the amount of amyloid formed, but does not alter the lag phase. An inhibitor which both alters the lag phase and decreases the amount of amyloid formed leads to the dotted dash curve.

2. Amyloid formation by pro-Islet amyloid polypeptide processing intermediates: examination of the role of protein heparan sulfate interactions and implication for islet amyloid formation in type 2 diabetes.

Abstract

Amyloid formation has been implicated in a wide range of human diseases including Alzheimer's disease, Parkinson's disease and type 2 diabetes. In type 2 diabetes, islet amyloid polypeptide (IAPP, also known as amylin) forms cytotoxic amyloid deposits in the pancreas and these are believed to contribute to the pathology of the disease. The mechanism of islet amyloid formation is not understood, however recent proposals have invoked a role for incompletely processed proIAPP. In this model, incompletely processed proIAPP containing the N-terminal pro region is excreted and binds to heparan sulfate proteoglycans (HSPGs) of the basement membrane thereby establishing a high local concentration which can act as a seed for amyloid formation. In this chapter, I describe biophysical proof of principle experiments designed to test the viability of this model. The model predicts that interactions with HSPGs should accelerate amyloid formation by the proIAPP processing intermediate and this is indeed what is observed. Interaction with heparan sulfate leads to the rapid formation of an intermediate state with partial helical content which then converts, on a slower time scale,

to amyloid fibrils. TEM shows that fibrils formed by the proIAPP processing intermediate in the presence and in the absence of heparan sulfate have the classic features of amyloid. Fibrils formed by the proIAPP processing intermediate are competent to seed amyloid formation by mature IAPP. The seeding experiments support a second major premise of the model; namely that fibrils formed by the processing intermediate are capable of seeding amyloid formation by the mature peptide.

NOTE: The material presented in this chapter has been published (Fanling Meng, Andisheh Abedini, Benben Song and Daniel P. Raleigh. "Amyloid Formation by pro-Islet Amyloid Polypeptide Processing Intermediates: Examination of the Role of Protein Heparan Sulfate Interactions and Implication for Islet Amyloid Formation in Type 2 Diabetes" (2007) *Biochemistry* **46** 12091-12099). This chapter contains direct excerpts from the manuscript which was written by me with suggestions and revisions from Professor Daniel P. Raleigh.

2.1 Introduction

Amyloid deposition is a characteristic component of many human diseases, including Alzheimer's disease, Parkinson's disease and type 2 diabetes (*1, 96*). Human islet amyloid polypeptide (IAPP), also called amylin, is a 37 residue peptide that is responsible for pancreatic amyloid formation in type-2 diabetes (*17, 29, 97-99*). Synthetic amyloid fibrils are toxic to the insulin-producing β-cells indicating that islet amyloid could contribute to the loss of β-cell mass and function in type 2 diabetes (*17, 27-29, 99-100*). The extent of amyloid deposition correlates with the severity of the disease, offering further evidence for a relationship between IAPP amyloid formation and type 2 diabetes (*100*). IAPP is synthesized in the pancreatic β-cells where it is stored with insulin in the insulin secretory granules (*25*). The normal physiological role of soluble IAPP is not entirely clear, but it is thought to act as an antagonist of insulin and is believed to play a role in gastric emptying, suppression of food intake and glucose homeostasis (*21-23, 101-102*).

The mechanism of islet amyloid formation is not well understood. IAPP secretion is co-regulated with insulin secretion and is elevated in type 2 diabetes. However, over production of IAPP alone does not trigger amyloid formation, nor, with one exception, have mutations in the IAPP gene been implicated in islet amyloid formation (*16-17*). It has recently been proposed that defects in the processing of proIAPP could play a critical role in triggering islet amyloid deposition (*45-46, 103-105*). IAPP is initially synthesized as a 89 precursor (preproIAPP) (*25*). The signal sequence is removed proteolytically to

produce the 67 residue pro hormone, proIAPP. ProIAPP is further processed to yield the mature 37 residue hormone. Posttranslational processing of proIAPP occurs at two conserved dibasic sites and involves the same prohormone convertases that process proinsulin, PC(1/3) and PC2 (*44, 104-106*). PC(1/3) is responsible for processing at the C-terminal dibasic site while PC2 favors cleavage at the N-terminal dibasic site(*44, 106-108*). Normal processing of proIAPP is a two stage process that is initiated by cleavage at the C-terminal site either in the trans-Golgi network or secretory granule, while N-terminal cleavage occurs in the β-secretory granule. Additional post translation modifications include amidation of the C-terminus and formation of the intramolecular disulfide.

A portion of the secreted insulin is incompletely processed in type 2 diabetes suggesting that the same could be true for IAPP. Immunohistochemical studies of islet amyloid have indicated the presence of the N-terminal region of proIAPP but not the C-terminal region thus demonstrating the presence of a processing intermediate which contains the N-terminal prosequence (*42-43*). This intermediate corresponds to the first 48 residues of proIAPP and is designated $proIAPP_{1-48}$. Abnormal processing of proIAPP has been proposed to play an important role in islet amyloid formation and correlate with cell death (*46, 103, 105*). One hypothesis is that incorrectly processed proIAPP interacts with heparan sulfate proteoglycans (HSPGs) of the basement membrane(*45*). HSPGs are found in islet amyloid deposits and appear to be a general feature of amyloid plaques (*47-50, 52, 109-112*). The proteoglycan perlecan has been implicated in virtually all

human amyloid diseases. HSPGs are ubiquitously expressed and have been proposed to serve as scaffolds for amyloid, stabilizing and possibly inducing amyloid formation. Peptide fragments derived from the N-terminal region of the $proIAPP_{1-48}$ processing intermediate have been shown to bind glycosaminoglycans (GAGs) (*45-46*), suggesting that interactions between HSPGs and $proIAPP_{1-48}$ might play a role in amyloid deposition in type 2 diabetes. In particular, Verchere and coworkers have proposed that improperly processed N-terminal extensions of proIAPP could bind to HSPGs upon secretion to the extracellular space and provide a seed for the formation of amyloid deposits *in vivo (45)*. This model predicts that peptide GAG interactions should promote amyloid formation by the $proIAPP_{1-48}$ intermediate and also predicts that fibrils formed by the interaction of $proIAPP_{1-48}$ with GAGs should be competent to seed amyloid formation by mature IAPP. In this work, we report biophysical proof-of-principle studies of this proposal.

2.2 Material and methods

2.2.1 Peptide synthesis and purification.

Peptides were synthesized on a 0.25 mmol scale using an applied Biosystems 433A peptide synthesizer, using 9-fluornylmethoxycarbonyl (Fmoc) chemistry as described. Pseudoprolines were incorporated to facilitate the synthesis (*113*). The 5-(4'-fmoc-aminomethyl-3',5-dimethoxyphenol) valeric acid (PAL-PEG) resin was used to afford an amidated C-terminal. Standard Fmoc reaction cycles were used. The first residue attached to the resin, β-branched residues, residues directly following β-branched

residues and pseudoprolines were double coupled. Crude peptides were oxidized by dimethyl sulfoxide (DMSO) for 24 hours at room temperature. The peptides were purified by reverse-phase HPLC using a Vydac C18 preparative column. A two-buffer system was utilized. Buffer A consists of H_2O and 0.045% HCl (v/v). Buffer B consists of 80% acetonitrile, 20% H_2O, and 0.045% HCl (v/v). The gradient used was 0-70% buffer B in 70 minutes. The pure peptide eludated out at 52 minutes, which is 52% buffer B. Analytical HPLC were used to check the purity of the peptides before each experiment. The identity of the pure peptides was conformed by mass spectrometry using a Bruker MALDI-TOF MS ($proIAPP_{1-48}$, expected is 5209.7, observed is 5209.2. For IAPP, expected is 3904.3, observed is 3904.5).

2.2.2 Sample preparation

A 1.58 mM peptide solution was prepared in 100% hexafluoroisopropanol (HFIP) and stored at -20^{o}C. Heparan sulfate, dermatan sulfate and chondroitin sulfate were obtained from Sigma-Aldrich. 2mg/2.2ml GAG solutions were prepared by dissolving GAGs in 20mM Tris-HCl buffer at pH 7.4. For the seeding experiments, preformed proIAPP/HSPG seeds were produced by diluting 34 μL of filtered stock solution and 70 μL of heparan sulfate solution into 20 mM Tris-Hcl buffer which gave a final concentration 32 μM proIAPP/ 2.7 μM heparan sulfate in 2% HFIP. The solution was incubated with stirring for 80 minutes at 25^{o}C to obtain solutions of fibrils which were used within 8 hours for the seeding experiment.

2.2.3 Thioflavin-T fluorescence

All fluorescence experiments were performed on on a Jobin Yvon Horiba fluorescence spectrophotometer at an excitation wavelength of 450 nm and emission wavelength of 485 nm. The excitation and emission slits were set at 5 and 10 nm respectively. A 1.0cm cuvette was used and each point was averaged for 1 minute. All solutions for these studies were prepared by diluting filtered stock solution (0.45μm filter) into a Tris-HCl buffer (pH =7.4) and thioflavin-T solution immediately before the measurement. The final concentration was 32μM peptide and 32 μM Thioflavin-T in 2% HFIP for all $proIAPP_{1-48}$/ GAGs experiments. The final concentration of seeds for the heparan sulfate and $proIAPP_{1-48}$/HSPG complex seeding experiments were 0.16μM heparan sulfate and 2 μM proIAPP/0.16μM heparan sulfate respectively in 2.2% HFIP. All solutions were stirred during the fluorescence experiments.

2.2.4 Circular Dichroism (CD) experiments

CD experiments were measured on an Aviv Model 62A DS circular dichroism spectrometer. CD experiments used exactly the same stock solutions as the thioflavin-T fluorescence measurements. The final concentration of peptide was 32μM peptide. Some samples contained 2.7 μM heparan sulfate. Spectra were recorded from 190 to 250 nm at 1 nm intervals in a 0.1 cm pathlength quartz cuvette at $15^{o}C$.

2.2.5 Transmission Electron Microscopy (TEM)

TEM was performed at Life Science Microscopy Center at the State University of New York at Stony Brook. Solutions that had been used for the fluorescence measurements were used so that samples could be compared under as similar conditions as possible. 15 uL of peptide solution was placed on a carbon-coated Formvar 300 mesh copper grid for 1 min and then negatively stained with saturated uranyl acetate for 1 min.

2.3 Results and discussion

2.3.1 Amyloid formation by proIAPP$_{1-48}$ is slower than wildtype IAPP but is accelerated by heparan sulfate

The sequence of proIAPP, the proIAPP$_{1-48}$ processing intermediate and mature IAPP are shown in Figure 2-1. The locations of the prohormone cleavage sites are also indicated. The N-terminal extension of proIAPP$_{1-48}$ contains a pair of basic residues immediately adjacent to the first residue of the mature peptide which are important for heparan sulfate binding (*46*). Fibril formation was initiated by diluting stock solutions of peptide in HFIP into Tris-HCl buffer and was monitored by thioflavin-T fluorescence. Fluorescence detected thioflavin-T binding provides a convenient probe of the time course of fibril formation (*10*). Since the quantum yield of the dye increases significantly upon binding to amyloid fibrils. The proIAPP processing intermediate, proIAPP$_{1-48}$, is capable of amyloid formation in the absence of any added heparan sulfate but it forms amyloid more slowly than mature IAPP with a lag phase five to six fold longer under the

conditions of our studies (Figure 2-2). ProIAPP$_{1-48}$ has a lag phase on the order of 140 minutes under the conditions of these experiments while IAPP has a lag phase of 25 minutes. The slower rate of amyloid formation by proIAPP$_{1-48}$ is not surprising considering that the N-terminal extension is rich in polar and charged residues. Transmission electron microscopy (TEM) images of the end product of the reaction reveals that it consists of fibril material with dimensions typical of *in vitro* amyloid deposits.

GAG heparan sulfate is used as a model for HSPGs interactions since it has been employed in other investigations of the interaction of HSPGs with IAPP and proIAPP. The addition of heparan sulfate to a sample of proIAPP$_{1-48}$ accelerates amyloid formation (Figure 2-2). The results are quite interesting and somewhat surprising. Addition of heparan sulfate at 20 minutes after initiation of the fibrilization action lead to a very rapid increase in thioflavin-T fluorescence but the fluorescence intensity is less than that of wild type fibrils. The rapid initial rise is followed by an intermediate plateau and then a subsequent rapid growth phase which ultimately lead to a final fluorescence similar to wildtype. The final fluorescence intensity at the end of the reaction is essentially identical for the seeded and non-seeded samples. The results are not an artifact caused by substoichiometric addition of heparan sulfate. Increasing the amount of heparan sulfate three-fold leads to the same behavior. The results are reproducible having been observed with several different samples. The unusual time course is not a consequence of waiting 20 minutes to add the heparan sulfate. Similar behavior is observed if the reaction is

seeded at time equal zero. In that case a rapid raise in fluorescence is once again observed leading to an intermediate plateau. The intermediate plateau persists for on the order of 30 minutes before a rapid increase to a final value that is similar to the level achieved by unseeded peptide (Figure 2-3).

In order to follow the reaction in more detail, CD spectra were collected at the various time points indicated in Figure 2-2. For the proIAPP$_{1-48}$ plus heparan sulfate sample, the first spectrum was collected at 8 minutes which corresponds to a time point prior to the addition of heparan sulfate. The spectrum was similar to that expected for a largely unstructured peptide (Figure 2-4). Heparan sulfate was added at 20 minutes. The CD spectrum collected 4 minutes after the addition of heparan sulfate (total time 24 minutes) indicates a mixture of α-helix and β-sheet structure. The dramatic change in the CD spectrum confirms that binding to heparan sulfate causes a significant change in the conformational ensemble of proIAPP$_{1-48.}$ Binding to heparan sulfate induces an intermediate which is partially helical. At 82 minutes, which corresponds to a time point in the growth phase, the ensemble has converted into β-sheet rich structure. β-sheet structure continues to develop and the CD spectrum recorded at the end of the reaction (200 minutes) is typical of those observed for IAPP amyloid. It is natural to inquire if the conformational transitions observed after the addition of heparan sulfate are due to the binding of proIAPP$_{1-48}$ to heparan sulfate or if they are rather necessary steps in the amyloid formation pathway that are promoted by interactions with heparan sulfate. CD spectra as a function of time for a sample of proIAPP$_{1-48}$ without any GAG was collected

in order to distinguish between these possibilities (Figure 2-5). The spectrum collected at time = 24 minutes is similar to the spectrum collected for the proIAPP$_{1-48}$ plus heparan sulfate prior to addition of GAG (i.e. the 8 minute time point in Figure 2-4A). A spectrum collected during the lag phase of the proIAPP$_{1-48}$ sample (time= 82 minutes) is consistent with the development of partial helical structure. A spectrum recorded in the growth phase region of the reaction (Figure 2-5C) shows the conversion of the partially helical ensemble into β-sheet structures. The time dependent CD studies show that interactions with heparan sulfate are not required for the formation of the intermediate but do promote its rapid formation. CD, particularly of heterogeneous systems is best used viewed as a semi-qualitative technique and we do not wish to imply that structural ensembles of the two samples are identical. TEM studies confirm that the addition of heparan sulfate induces significant changes and promotes aggregation. Aliquots from both samples were removed at 24 minutes, blotted onto TEM grids and imaged (Figure 2-6). The sample of proIAPP$_{1-48}$ alone shows modest amounts of stained material but no obvious fibrils or large aggregates. The micrograph of the proIAPP$_{1-48}$ plus GAG sample is dramatically different, exhibiting dense mats of standard material. TEM images of the final products confirm the presence of amyloid in both the proIAPP$_{1-48}$ sample and in the proIAPP$_{1-48}$ plus heparan sulfate sample although there are some apparent minor differences (Figure 2-6). ProIAPP$_{1-48}$ formed long fibrils in the presence of heparan sulfate, while in the absence of heparan sulfate it formed a mixture of long fibrils and small short fibrils.

2.3.2 ProIAPP$_{1-48}$ fibrils can seed amyloid formation by wild type IAPP

Having demonstrated that heparan sulfate can promote amyloid formation by the proIAPP$_{1-48}$ processing intermediate, we next sought to determine if these fibrils could efficiently seed fibril formation by fully processed wildtype IAPP. It has been suggested that complexes formed by improperly processed proIAPP$_{1-48}$ and heparan sulfate could promote amyloid formation by mature IAPP (*46*). The data presented in Figure 2-7 demonstrates that the proIAPP$_{1-48}$/ heparan sulfate fibrils are indeed capable of seeding amyloid formation by mature IAPP. Addition of the seeds to the reaction mixture abolished the lag phase (Figure 2-7). The effect is not simply due to interactions of mature IAPP with heparan sulfate since addition of heparan sulfate alone has only a very small effect upon the kinetics of amyloid formation by mature IAPP under these conditions. TEM measurements clearly demonstrate that amyloid is formed in both the seeded and unseeded reactions (Figure 2-7). The images of the amyloid formed by unseeded mature IAPP and by mature IAPP seeded with proIAPP1-48/ heparan sulfate fibrils are similar in appearance and have the classical amyloid morphology.

2.3.3 Demonstration of specificity in proIAPP$_{1-48}$ GAG interactions

The interaction of proIAPP$_{1-48}$ with two other GAGs was examined in order to test if the interactions we observed with heparan sulfate are generic or if there is any specificity. Chondroitin sulfate and dermantan sulfate were used for these control studies. Chondroitin sulfate induced effects which were similar to those observed with heparan

sulfate, namely an initial rapid increase in thioflavin-T fluorescence followed by an intermediate plateau that lead to a second rapid growth phase and than a final plateau. TEM images collected from this sample at the end of the reaction reveal the presence of extensive amyloid fibrils while the CD spectrum is consistent with significant β-sheet structure (Figure 2-8). The situation is very different when dermatan sulfate is used. In this case, the rapid rise in thioflavin-T fluorescence is observed upon addition but the subsequent behavior is significantly different. There is a gradual decrease in thioflavin-T fluorescence leading to a final apparent steady state value (Figure 2-9). We fail to observe the second growth phase that was detected with the two other GAGs even though the proIAPP$_{1-48}$/dermatan sulfate sample was followed for a significantly longer time, 600 minutes *vs* 200 minutes, for the other samples. TEMs of the reaction mixture collected after the completion of the time course are very different from those of the proIAPP$_{1-48}$/heparan sulfate or proIAPP$_{1-48}$/chondroitin sulfate samples. A large amount of aggregated densely stained material is present but no fibrils are detected. The image is qualitatively similar to the one recorded of the proIAPP$_{1-48}$/heparan sulfate sample just after the addition of the GAG. CD spectra of this sample also differ significantly from the other GAG/proIAPP$_{1-48}$ samples; the spectrum appears noticeablely more helical (Figure 2-8).

2.4 Conclusions

We have demonstrated that amyloid formation by the proIAPP$_{1-48}$ processing

intermediate is promoted by its interaction with heparan sulfate and chondroitin sulfate. Heparan sulfate peptide interactions likely enhance proIAPP$_{1-48}$ amyloid formation by promoting a high local concentration of the peptide. The GAG binding site has previously been shown to be located in the N-terminal half or two thirds of the molecule (*45-46*). Binding to this region would leave the C-terminal region free to play a role in peptide self association. The C-terminal portion of IAPP is very prone to aggregation and amyloid formation (*54*). Along these lines, it is interesting to note that a fragment comprised of the first thirty residues of proIAPP$_{1-48}$, which lacks the C-terminal region, also interacts strongly with heparan sulfate but is far less prone to form amyloid in the presence of heparan sulfate (*45*).

The control experiments with chondroitin sulfate and dermatan sulfate demonstrate that the effects are not specific to heparan sulfate but they also indicate that there is some specificity in the polypeptide GAG interaction. It is interesting that interaction with dermatan sulfate appears to trap the peptide in a state which is not able to undergo the final self assembly into β-sheet fibrils, or at the very least slows it significantly. It may be that interactions with dermatan sulfate induce a conformation which is not competent to undergo the conversion to β-structure. Alternatively, the conformation of the peptide could be similar to that adopted with the other GAGs, but the interactions might be stronger with dermatan sulfate than with the other GAGs and this could trap the intermediate. A detailed structure function study will be required to sort out all of the details of proIAPP$_{1-48}$ GAGs interactions. This is beyond the scope of the

present study but is clearly an interesting topic for further exploration.

One interesting feature of the seeding experiments is the observation of a partial helical intermediate. Although this may seem counterintuitive given that the final fibril structure is rich in β-sheet, there is a precedent for helical intermediates in amyloid formation. Partial helical structure is induced when IAPP interacts with model vesicles and helical structure has been postulated to play a role in the membrane mediated association of IAPP (*55*). In addition Teplow and coworkers have present compelling evidence implicating an on pathway helical intermediate in Aβ amyloid formation (*114-115*).

Importantly, fibrils formed by proIAPP$_{1-48}$/heparan sulfate are competent to promote amyloid formation by mature IAPP. Models of islet amyloid formation that involve a critical role for interactions between proIAPP processing intermediates and the HSPGs components of the extracellular matrix assume that such complexes can promote amyloid formation by mature IAPP (*46*). The work presented here provides the first direct evidence that this is indeed the case. Our observations provide *in vitro* proof of principles studies in support of the mechanism of amyloid formation initially proposed by Verchere and colleagues (*46*). A schematic diagram depicting the proposed mechanism is shown in Figure 2-10. ProIAPP$_{1-48}$ binds to HSPGs in the extracellular matrix leading a high local concentration of aggregation prone peptide. This acts as a seed for further recruitment of proIAPP$_{1-48}$ and mature IAPP thus promoting amyloid formation.

Peptides and HSPGs interactions are thought to play a general role in amyloidosis

and they may modulate cytotoxicity by mediating the interaction of amyloid fibrils with the cell membrane. Peptide HSPGs interactions have been proposed as potential drug targets (*116*). There is an emerging view in the amyloid field that non-fibrillar oligomers or pre-fibrillar aggregates may be the toxic species in amyloid diseases. While the current study has not addressed the toxicity of the intermediate species observed, it is possible that conformational transitions induced in $proIAPP_{1-48}$ by interaction with GAGs could result in more toxic aggregates. The work reported here demonstrates the importance of interactions between proIAPP processing intermediates and GAGs, at least *in vitro*, suggesting that targeting proIAPP HSPGs interactions may be an interesting strategy for inhibiting amyloid formation (*117*). The development of inhibitor of GAG mediated amyloid formation is discussed in chaper 6.

(A) ProIAPP:

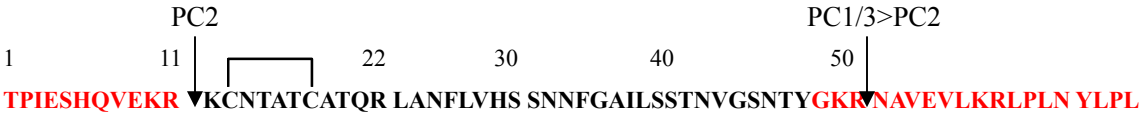

(B) ProIAPP$_{1-48}$:

(C) IAPP:

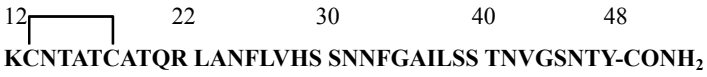

Figure 2-1: (A) The primary sequence of the 67 residue human proIAPP polypeptide. The N-terminal and C-terminal flanking regions of proIAPP are shown in red, and the black sequence corresponds to mature IAPP. Cleavage of proIAPP occurs at the two dibasic sites (Lys_{10}-Arg_{11}) and (Lys_{50}-Arg_{51}) indicated by the arrows. Further processing occurs at the C-terminus to yield amidated mature IAPP. (B) The primary sequence of the proIAPP$_{1-48}$ processing intermediate. (C) The primary sequence of mature IAPP. All three peptides have an intramolecular disulfide and an amidated C-terminus. The numbering system used corresponds to that of the complete pro sequence.

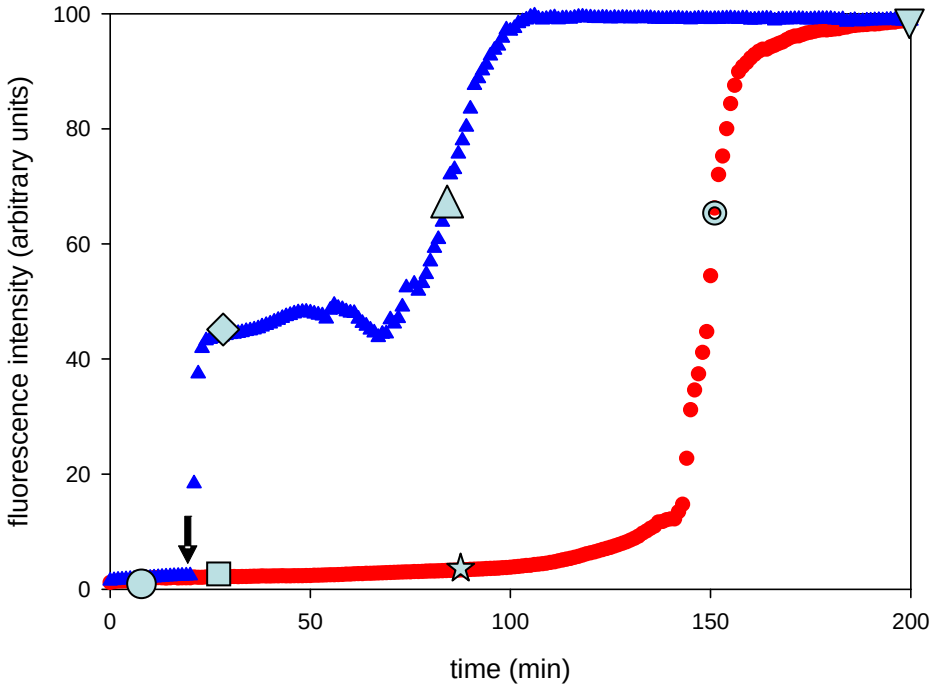

Figure 2-2: Effect of heparan sulfate upon amyloid formation by proIAPP$_{1-48}$. Heparan sulfate was added at 20 minutes as indicated by the arrow (↓). The red curve corresponds to a solution of 32 μM proIAPP$_{1-48}$. The blue curve corresponds to a solution of 32 μM proIAPP$_{1-48}$ in the presence of 2.7μM heparan sulfate (added at 20 minutes). The pH of the solutions was 7.4. The solutions contained 2% HFIP by volume and were continually stirred at 15^{o}C. The symbols indicate the time points at which CD spectra were recorded (Figure 2-3 and Figure 2-4).

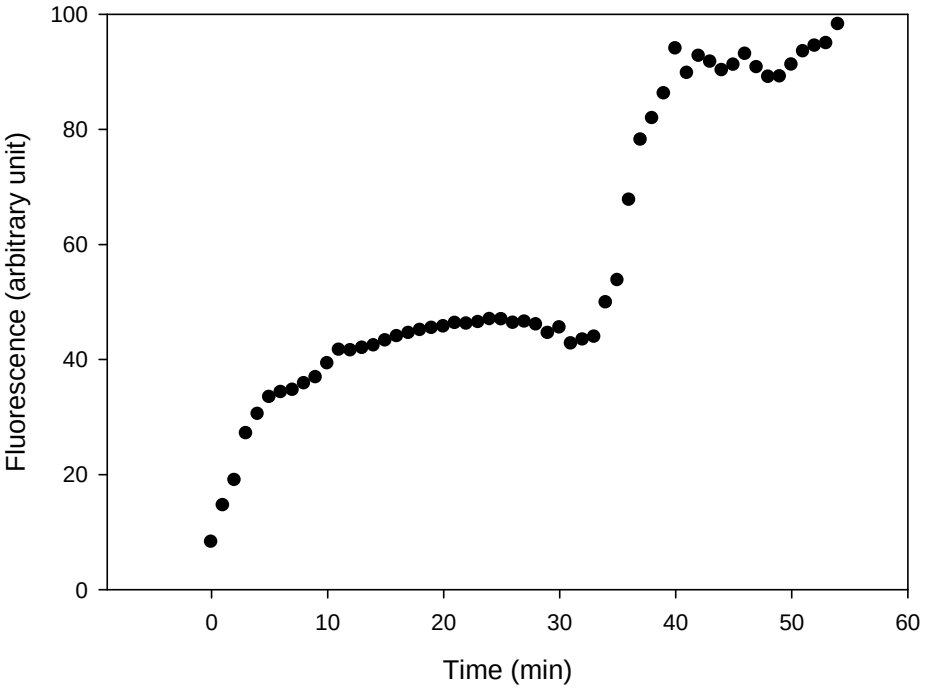

Figure 2-3: Effects of heparan sulfate upon amyloid formation by proIAPP$_{1-48}$. The experiment was performed as described in the caption of Figure 2-2 with the exception that heparan sulfate was present at the start of the reaction. ProIAPP$_{1-48}$ was prepared as a stock solution as described in the experimental procedures and aggregation initiated by dilution into buffer containing heparan sulfate. Final conditions were 32 μM proIAPP$_{1-48}$, 2.7 μM heparan sulfate, pH 7.4 and 2% HFIP by volume at 15 ^{o}C. Samples were continually stirred.

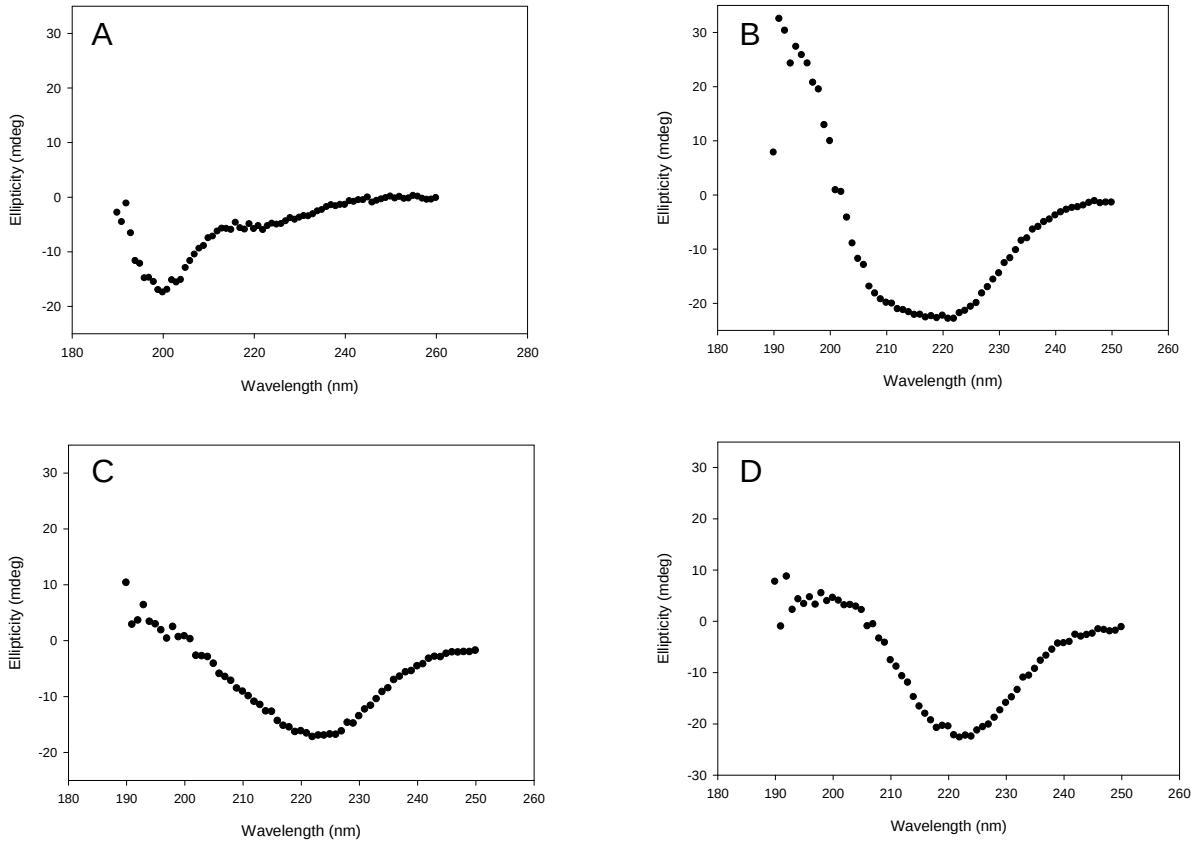

Figure 2-4: Far UV CD spectra of proIAPP$_{1-48}$ collected at four different time points after the initiation of the fibrilization reaction. Heparan sulfate was added at 20 minutes. The time points correspond to the times indicated in the kinetic trace displayed in figure 2-2. (A) corresponds to the time at (○) 8-minutes, (B) corresponds to the time at (◇) 24-minutes, which corresponds to 4 minutes after the addition of heparan sulfate, (C) corresponds to the time at (Δ) 82 minutes and (D) corresponds to the time at the end of reaction (▽) 200 minutes. The sample used for the CD measurements was exactly the same as that used for the fluorescence experiment.

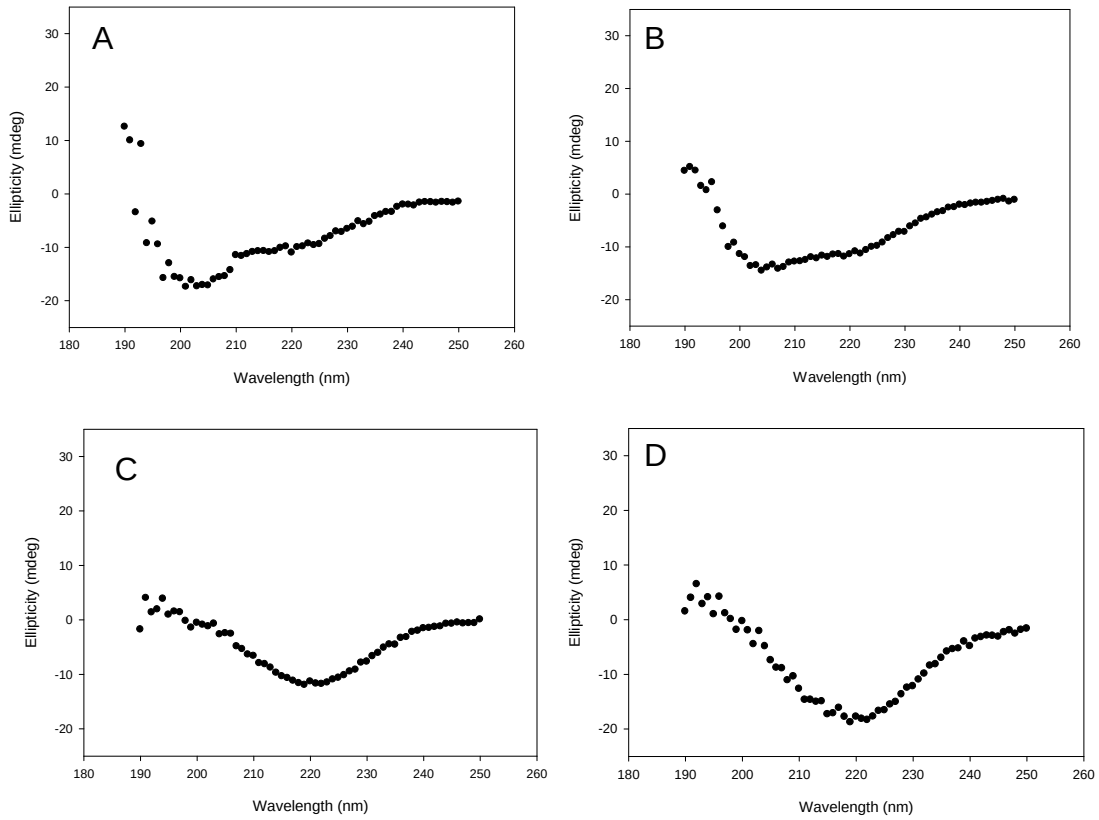

Figure 2-5: Far UV CD spectra of proIAPP$_{1-48}$ collected at four different time points after the initiation of the fibrilization reaction. No heparan sulfate was added. The time points correspond to the times indicated in the kinetic trace displayed in figure-2. (A) corresponds to the time at (□) 24-minutes, (B) corresponds to the time at (☆) 82-minutes, (C) corresponds to the time within the growth phase (◎) 150 to 165 minutes and (D) corresponds to the time at the end of reaction (▽) 200 minutes. The sample used for the CD measurements was exactly the same as that used for the fluorescence experiment.

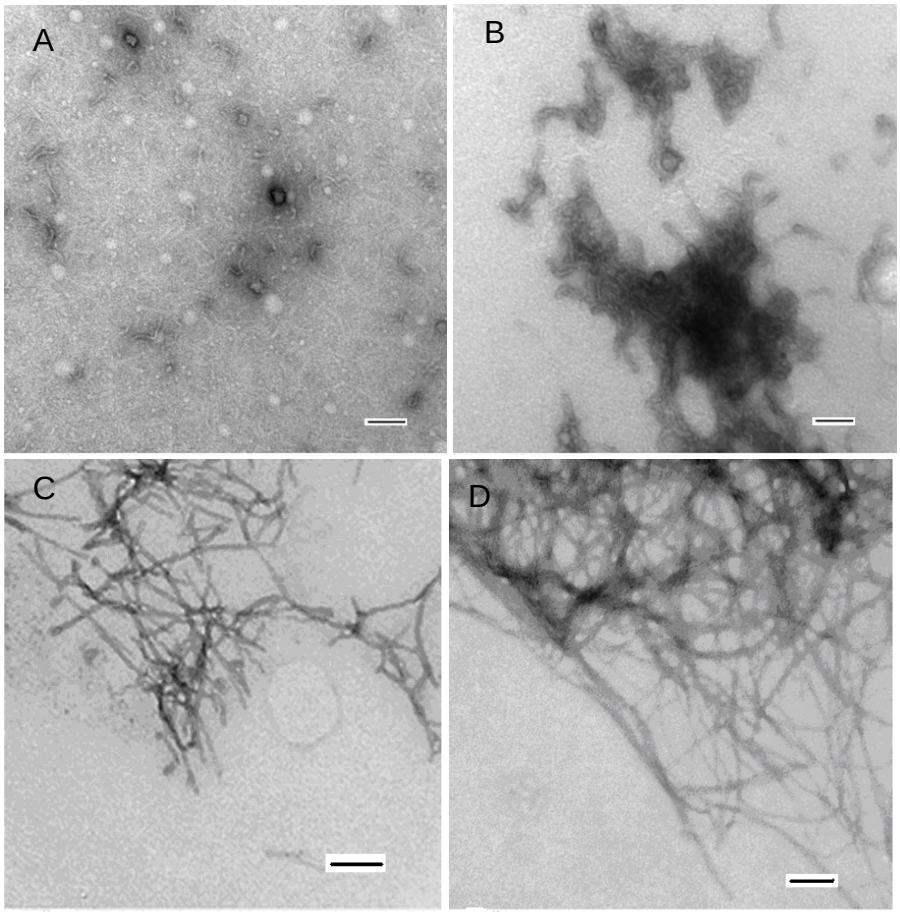

Figure 2-6: Transmission Electron Microscopy of $ProIAPP_{1-48}$ aggregates formed in the presence and absence of heparan sulfate. (A) $ProIAPP_{1-48}$ alone collected at 24 minutes. (B) $ProIAPP_{1-48}$ plus heparan sulfate collected at 24 minutes. (C) $ProIAPP_{1-48}$ alone collected after 200 minutes (D) $ProIAPP_{1-48}$ plus heparan sulfate collected after 200 minutes. Scale bars represent 100nm.

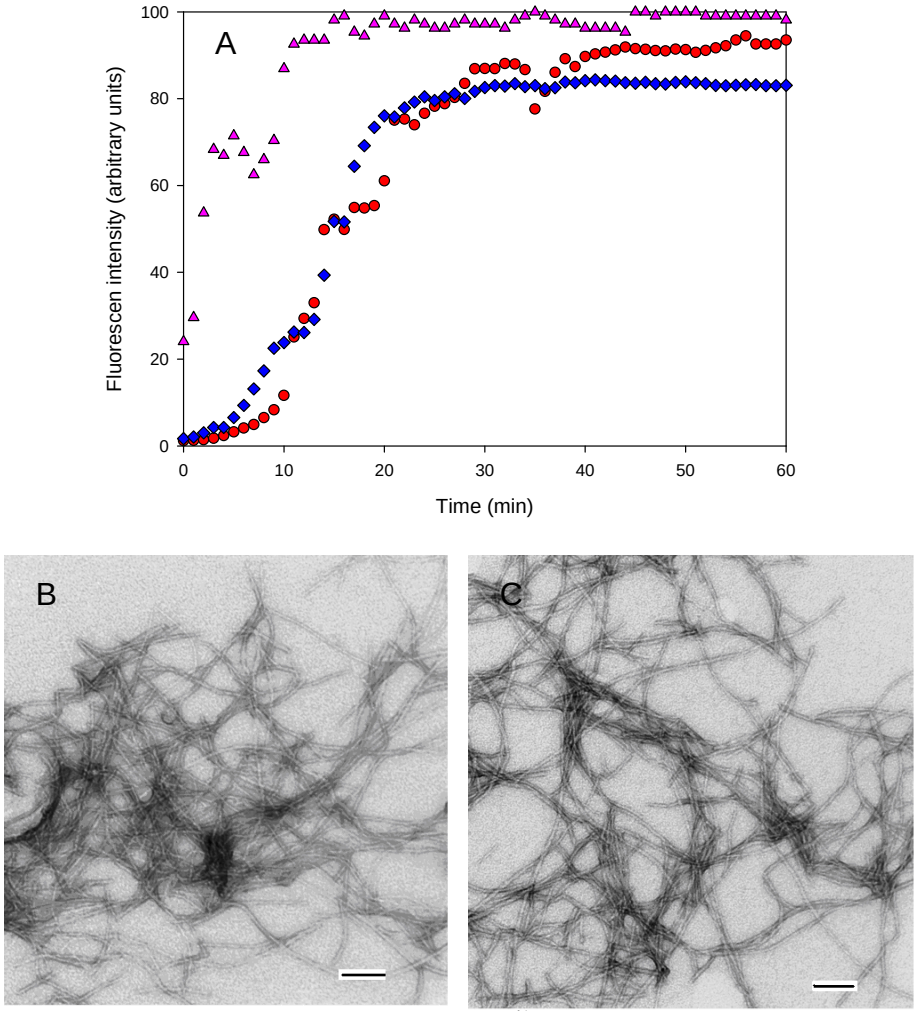

Figure 2-7: (A) Thioflavin-T monitored aggregation of mature IAPP and the effects of seeding. Mature IAPP alone (●), Mature IAPP seeded by proIAPP/ heparan sulfate (▲) and mature IAPP with heparan sulfate added at time zero (♦). The seeds were added at 0 minutes. (B) TEM image of amyloid fibrils formed by mature IAPP in the absence of seeds. (C) TEM image of amyloid fibrils formed by mature IAPP in the presence of proIAPP$_{1\text{-}48}$/heparan sulfate seeds. Solutions used for TEM were identical to those used for the seeding studies. The pH of the solutions was 7.4. The solutions contained 2.2% HFIP by volume and were continually stirred at 25^{o}C. The scale bars in the TEM figures represent 100nm.

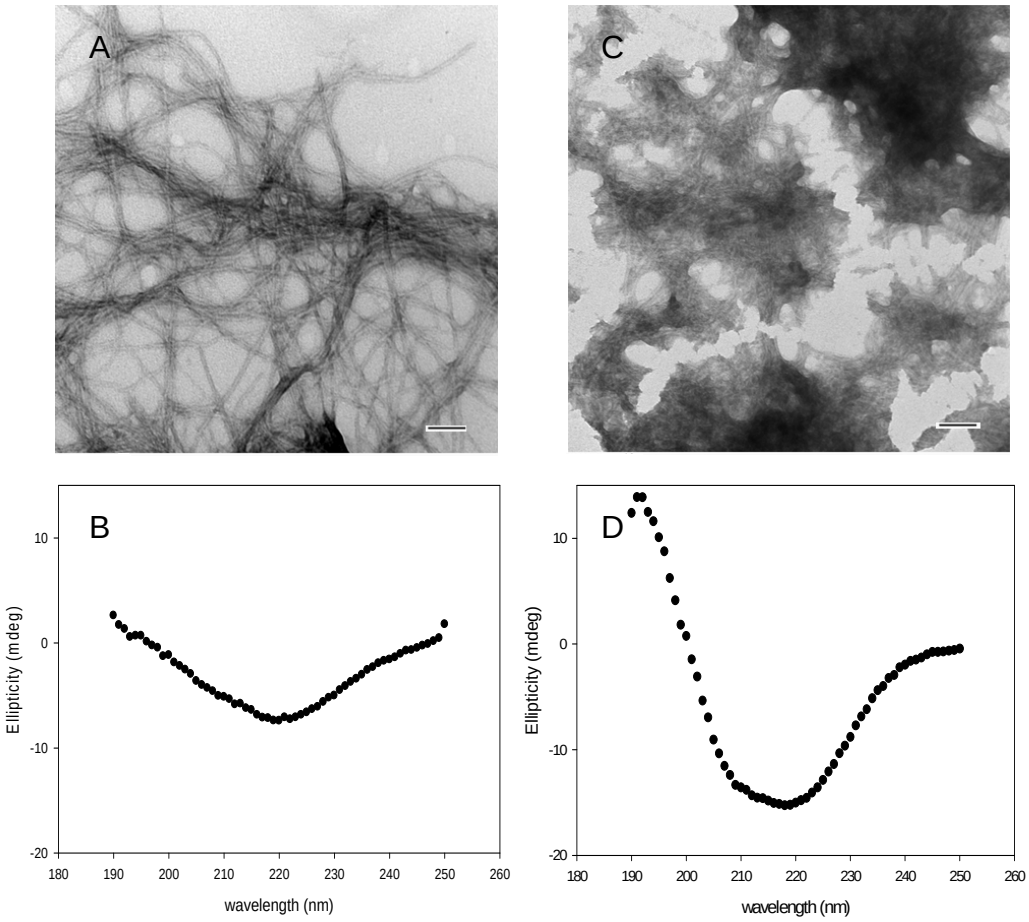

Figure 2-8: Comparison of the effects of the addition of chondroitin sulfate and dermatan sulfate to a solution of proIAPP$_{1-48}$. (A) TEM of the proIAPP$_{1-48}$/ chondroitin sulfate sample after 200 minutes. (B) CD spectrum of proIAPP$_{1-48}$/ chondroitin sulfate sample after 200 minutes incubation. (C) TEM of the proIAPP$_{1-48}$/ dermatan sulfate sample after 600 minutes. (D) CD spectrum of proIAPP$_{1-48}$/ dermatan sulfate sample after 600 minutes incubation.

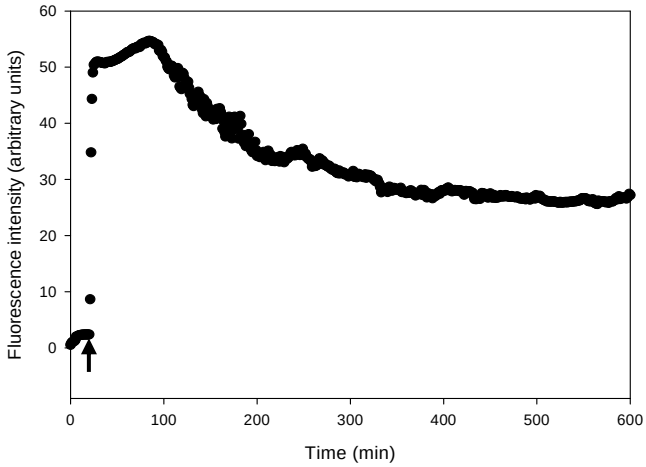

Figure 2-9: Effects of dermatan sulfate upon amyloid formation by proIAPP$_{1-48}$ as monitored by thioflavin-T fluorescence. Dermatan sulfate was added at 20 minutes as indicated by the arrow (↓). The pH of the solutions was 7.4. The solutions contained 2% HFIP by volume and were continually stirred at 15^{o}C.

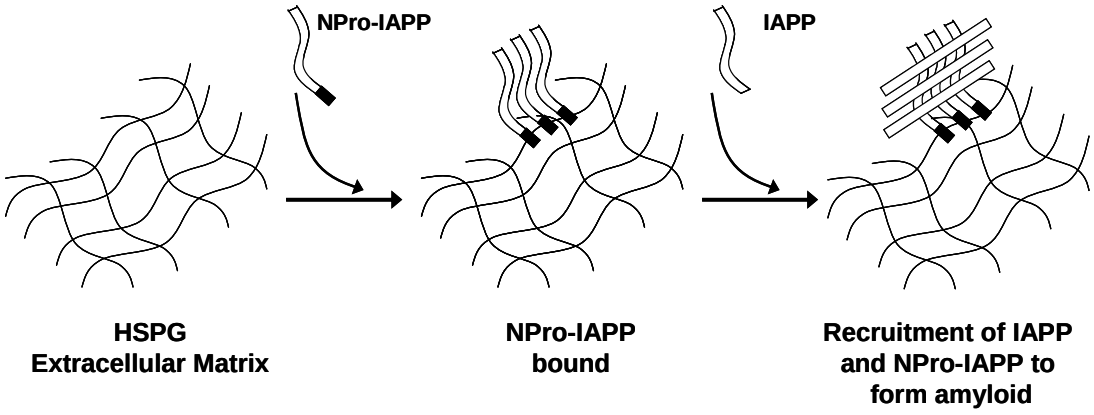

Figure 2-10: Schematic representation of how an increase in the production of incorrectly processed IAPP (Npro-IAPP) could contribute to amyloid formation. Polypeptides with an uncleaved N-terminal extension (shaded) are able to bind to HSPGs in the extracellular matrix resulting in a high local concentration of peptide. This in turn could act as a seed for amyloid formation.

3. Rifampicin does not prevent amyloid fibril formation by human islet amyloid polypeptide but does inhibit fibril thioflavin-T interactions: implications for mechanistic studies of β-cell death.

Abstract

The development of inhibitors of amyloid is a topic of considerable interest, both because of their potential therapeutic applications and because they are useful mechanistic probes. Recent studies have highlighted the potential use of rifampicin as an inhibitor of amyloid formation by a variety of polypeptides, however, there are conflicting reports on its ability to inhibit amyloid formation by islet amyloid polypeptide (IAPP). IAPP is the cause of islet amyloid in type 2 diabetes. In this chapter, I describe that rifampicin does not prevent amyloid formation by IAPP and does not disaggregate preformed IAPP amyloid fibrils; instead it interferes with standard fluorescence based assays of amyloid formation. Rifampicin is unstable in aqueous solution and is readily oxidized. However, the effects of oxidized and reduced rifampicin are similar, in that neither prevents amyloid formation by IAPP. Furthermore, use of a novel p-cyanoPhe analog of IAPP shows that rifampicin does not significantly affect the kinetics of IAPP amyloid formation. The implications for the development of amyloid inhibitors are discussed as are the implications for studies of the toxicity of islet amyloid. The work

also demonstrates the utility of p-cyanoPhe IAPP for the screening of inhibitors.

NOTE: The material presented in this chapter has been published (Fanling Meng, Peter Marek, Kathryn J. Potter, C. Bruce Verchere and Daniel P. Raleigh. "Rifampicin does not Prevent Amyloid Fibril Formation by Human Islet Amyloid Polypeptide but does Inhibit Fibril Thioflavin-T Interactions: Implications for Mechanistic Studies of Beta-cell Death" (2008) *Biochemistry*, 47 6016-6024.). This chapter contains direct excerpts from the manuscript which was written by me with suggestions and revisions from Professor Daniel P. Raleigh and Professor C. Bruce Verchere. Cell toxicity experiments were performed by Kathryn J. Potter at the University of British Columbia in Professor Verchere's laboratory. They are included in this chapter for completeness.

3.1 Introduction

There is considerable interest in developing inhibitors of amyloid formation, both because of their obvious therapeutic potential but also because they can provide powerful tools for mechanistic studies (*85, 118-121*). In particular, there is a lively debate on what constitutes the toxic species in the amyloid diseases. Early work focused on the potential toxicity of the fibrils themselves and fibril deposits certainly contribute to the progression of the systemic amyloidoses (*122*). In recent years, however, considerable attention has focused on oligomeric intermediate species and their potential toxicity, although there is also evidence that fibrils can be toxic (*65, 67, 69-70, 123-127*). Molecules which inhibit fibril formation but not the formation of intermediates are attractive mechanistic probes since they will inhibit toxicity if fibrils are the only toxic entity but will not inhibit toxicity if intermediates are the key player (*69, 128*).

Epidemiological investigations have shown that leprosy patients have a statistically lower probability of senile dementia provided they have been treated with rifampicin or dapsone suggesting that the drug might prevent Aβ amyloid formation (*129-131*). *In vitro* studies showed that rifampicin did indeed inhibit fibril formation by $A\beta_{1-40}$ and reduced its toxicity to cultured rat PCL2 cells (*131*). Rifampicin has been reported to inhibit *in vitro* amyloid formation by a number of proteins (*128, 131-137*). More recently, rifampicin has been used to probe the mechanism of IAPP-induced cell death (*128, 138*). However, the IAPP literature is confusing since some reports argue that rifampicin is an inhibitor of fibril formation and does not inhibit toxicity (*128*) while

others claim that it does not inhibit amyloid formation but inhibits the toxicity of pre-aggregated IAPP fibrils (*137, 139*). Rifampicin has also been reported to inhibit the membrane disrupting activity of IAPP but not its ability to form amyloid(*139*). Further complicating the issue, Fink and colleagues, in a series of careful studies, showed that rifampicin inhibits fibrillization of α-synuclein but found that an oxidation product of the drug is actually the most potent inhibitory compound (*135*). The conflicting reports on the effects of rifampicin on IAPP toxicity and fibril formation and the importance of these studies for understanding the origin of cellular toxicity prompted us to reexamine the effects of the drug on the *in vitro* fibrillization of IAPP using transmission electron microscopy (TEM) and fluorescence detected thioflavin-T binding assays as well as newly developed fluorescent analogs of IAPP. We show that rifampicin does not prevent amyloid fibril formation by IAPP and does not disaggregate preformed IAPP amyloid but does interfere with thioflavin-T assays.

3.2 Material and Methods

3.2.1 Reagents

Rifampicin was purchased from Sigma (Lot #R3501), ascorbic acid from Fisher Scientific and Thioflavin-T from Aldrich Chemical Company.

3.2.2 Peptide synthesis and purification

Peptides were synthesized on a 0.25 mmol scale using an applied Biosystems 433A

peptide synthesizer, using 9-fluornylmethoxycarbonyl (Fmoc) chemistry as described (44). Pseudoprolines were incorporated to facilitate the synthesis. The 5-(4'-fmoc-aminomethyl-3',5-dimethoxyphenol) valeric acid (PAL-PEG) resin was used to afford an amidated C-terminal. Standard Fmoc reaction cycles were used. The first residue attached to the resin, β-branched residues, residues directly following β-branched residues and pseudoprolines were double coupled. Crude peptides were oxidized by dimethyl sulfoxide (DMSO) for 24 hours at room temperature (*113, 140*). The peptides were purified by reverse-phase HPLC using a Vydac C18 preparative column. A two-buffer system was utilized. Buffer A consists of H_2O and 0.045% HCl (v/v). Buffer B consists of 80% acetonitrile, 20% H_2O, and 0.045% HCl (v/v). The gradient used was 0-70% buffer B in 70 minutes. The pure peptide eludated out at 50 minutes, which is 50% buffer B. Analytical HPLC was used to check the purity of the peptides before each experiment. The identity of the pure peptides was confirmed by mass spectrometry using a Bruker MALDI-TOF MS.

3.2.3 Sample preparation

A 1.58 mM peptide solution was prepared in 100% hexafluoroisopropanol (HFIP) or DMSO and stored at -20^{o}C. A 20 mM rifampicin stock solution was prepared by dissolving rifampicin in DMSO. For the antioxidant experiments, ascorbic acid was dissolved in Tris-HCl buffer and adjusted to pH 7.4 to give a 100 mM ascorbic acid stock solution. The stability of rifampicin in Tris-HCl buffer and ascorbic acid solutions was

tested by UV-Vis absorbance at 483 nm (*141-142*).

3.2.4 Thioflavin-T fluorescence

All fluorescence experiments were performed with a Jobin Yvon Horiba fluorescence spectrophotometer or with an Applied Phototechnology Fluorescence Spectrophotometer. An excitation wavelength of 450 nm and emission wavelength of 485 nm was used for the thioflavin-T studies. The excitation and emission slits were set at 5 nm. A 1.0 cm cuvette was used and each point was averaged for 1 minute. All solutions for these studies were prepared by diluting filtered stock solution (0.45μm filter) into a Tris-HCl buffered (20mM, pH 7.4) thioflavin-T solution immediately before the measurement. The final concentration was 32 μM peptide and 25 μM thioflavin-T with or without rifampicin in 2% HFIP. Some experiments made use of DMSO stock solutions. For these studies, the final conditions were 32 μM peptide and 25 μM thioflavin-T in 20 mM Tris-HCl buffer (pH 7.4) 2% DMSO. The final concentration of ascorbic acid used in antioxidant experiments was 83 μM. All solutions were stirred during the fluorescence experiments. P-cyanoPhe fluorescence was excited at 240 nm and detected at 296 nm, with both excitation and emission slits of 10 nm.

3.2.5 Transmission electron microscopy (TEM)

TEM was performed at the Life Science Microscopy Center at the State University of New York at Stony Brook. The same solutions that were used for the fluorescence

measurements were used so that samples could be compared under as similar conditions as possible. 15 μL of peptide solution was placed on a carbon-coated Formvar 300 mesh copper grid for 1 min and then negatively stained with saturated uranyl acetate for 1 min.

3.2.6 Alamar Blue viability assay

Alamar Blue (Biosource, Camarillo, CA) reduction was used as a measure of cell viability. Rat (INS-1) insulinoma cells were seeded at a density of 20,000 cells per well. After 24 hours culture in RPMI (11 mM glucose) plus 10% fetal bovine serum, HEPES (0.5 M), L-glutamine (102 mM), sodium pyruvate (50 mM), β-mercaptoethanol (50 μM), penicillin (50 U/ml) and streptomycin (50 μg/ml), culture media was removed and replaced with fresh media and the appropriate amount of rifampicin, freshly dissolved human IAPP (Bachem, Torrance, CA), and/or DMSO vehicle. The final DMSO concentration did not exceed 0.1% and viability was not reduced in control cells treated with 0.1% DMSO. After 24 hour incubation, media was replaced with fresh media containing 10% Alamar Blue and incubated for 3 hours. Fluorescence was measured using a Fluoroskan Ascent microplate reader (Labsystems, Fischer Scientific, Pittsburgh, PA) using excitation and emission wavelengths of 530 and 590 nm, respectively.

3.3 Results and discussion

3.3.1 Rifampicin does not inhibit the cytotoxicity of IAPP.

The IAPP sequence is shown in Figure 3-1. There are apparently conflicting

reports on the effects of rifampicin on IAPP-induced toxicity, however the discrepancy maybe due to the different nature of the studies. Tomiyama and colleagues (*137*) showed that rifampicin inhibited the toxicity of preformed fibril aggregates of IAPP while Meier and coworkers (*128*) examined the effects of treating cells with initially soluble IAPP and rifampicin. The second study demonstrated that rifampicin had no effects on toxicity with this protocol. Thus the two studies, while seemingly at variance, need not be contradictory since different conditions were examined. Given the importance of the toxicity results we reexamined the effect of added rifampicin on IAPP induced cytotoxicity.

INS-1 cell viability assays. Treatment of INS-1 cells for 24 hours with 20 or 40 μM human IAPP reduced cell viability by 39.7% and 91.1% respectively ($p < 0.05$ and $p < 0.001$, respectively; Figure 3-2). Rifampicin alone (1.5 – 6.0 μM) had no impact on cell viability (Figure 3-2), nor did treatment of control cells with the maximal concentration of 0.1% DMSO vehicle (data not shown). Addition of rifampicin to media containing human IAPP failed to protect INS-1 cells from human IAPP-induced death. Even at the maximal concentration of rifampicin used (6.0 μM), the reduction in cell viability induced by human IAPP was not significantly different between control cells and cells treated with rifampicin (20 μM human IAPP: 64.8 ± 12.6% versus 57.4 ± 7.0%, p = NS; 40 μM human IAPP: 12.1 ± 5.0% versus 10.4 ± 3.3%, p = NS).

3.3.2 Rifampicin interferes with thioflavin-T assays but does not prevent amyloid

formation by IAPP

We monitored the apparent time course of fibril formation of IAPP in the presence and in the absence of rifampicin using thioflavin-T assays. Thioflavin-T is a small dye molecule which has proven enormously useful in studies of amyloid formation. Thioflavin-T has a low fluorescence quantum yield in solution which increases significantly when bound to fibrils (*10*). There is no structure of thioflavin-T bound to any amyloid fibrils but the dye is believed to bind to grooves on the surface of amyloid fibrils. Amyloid is made up of a cross-β structure in which individual β-strands are aligned perpendicular to the fibril axis. In such a structure, side chains in consecutive strands will form a ridge and a set of side chains at positions n and n+2 will lead to two ridges separated by a groove. These grooves are the likely binding sites.

Samples were 32 μM in IAPP and contained either no rifampicin or 15 μM rifampicin. The ratio of drug to IAPP is higher than that reported to inhibit IAPP fibrillization (*128*). The data collected in the absence of rifampicin is typical of IAPP fibrillization experiments. A lag phase is observed followed by a growth phase with a rapid change in thioflavin-T fluorescence leading to a final plateau where the bound thioflavin-T fluorescence reaches a steady state value (Figure 3-3). TEM images collected of samples corresponding to the end point of the reaction display the classic features of amyloid (Figure 3-3). The results of the experiment in the presence of rifampicin are strikingly different. No significant change in thioflavin-T fluorescence is observed over the entire time course of the reaction. Taken alone, the thioflavin-T

fluorescence experiment would argue that rifampicin is a potent inhibitor of fibrillization. However, the drug could instead be a competitive inhibitor of thioflavin-T binding to IAPP fibrils or it might quench the fluorescence of the bound thioflavin-T without preventing amyloid formation. Consequently, we recorded TEM images of aliquots of each reaction mixture collected at a time point corresponding to 100 minutes after initiation of the reaction. This is much longer than the time required for IAPP to form amyloid fibrils. The images reveal numerous fibrils with the classic morphology associated with *in vitro* IAPP fibrils for both samples, indicating that rifampicin did not prevent amyloid formation by IAPP. Not all of the grids displayed fibrils and qualitatively they appeared somewhat less abundant for the samples which contain rifampicin than for the samples of IAPP in the absence of rifampicin. Nonetheless, the key conclusion is that rifampicin, when present at the start of the fibrillization reaction, leads to false negatives in the thioflavin-T assay. The experiments were repeated at lower rifampicin concentration, examining solutions which were 5 μM or 2.5 μM rifampicin. The final fluorescence intensity is higher than observed in the 15 μM rifampicin experiment but is considerably lower than the value observed in the absence of rifampicin (Figure 3-4, Figure 3-5). The final thioflavin-T fluorescence intensity is often used as a measurement of the amount of amyloid formation and by this measure the drug would still be classified as a fibrillization inhibitor. However TEM images recorded at the end of the reaction show that extensive fibrils are formed (Figure 3-4, Figure 3-5). Thus the conclusion that rifampicin inhibits thioflavin-T fluorescence but not amyloid formation is independent of

the range of rifampicin tested.

All of these experiments were conducted using stock solutions prepared in HFIP which is the standard protocol for biophysical studies of IAPP fibril formation. The result of initially solubilizing IAPP in DMSO was tested since DMSO stock solutions are sometimes used in studies of IAPP. An IAPP stock solution was prepared in 100% DMSO and fibrilization initiated by dilution into aqueous buffer (final DMSO concentration 2% by volume). The choice of co-solvent does not affect the conclusions. Rifampicin inhibits thioflavin-T fluorescence but not amyloid formation (Figure 3-6). Thus our results are not an artifact of the choice of co-solvent.

Next the effect of adding rifampicin to preformed fibrils was investigated. Such an experiment is often performed to test a compound's ability to disaggregate fibrils. In this case, a compound which eliminated the fluorescence of bound thioflavin-T but did not dissociate fibrils would be incorrectly scored as having the ability to disaggregate fibrils: i.e. it would generate a false positive. It is possible that rifampicin only interferes with thioflavin-T binding to IAPP if it is present in the initial reaction mixture. This seems unlikely since the dye generally does not bind to species populated in the lag phase but it is important to test. Figure 3-7 displays the result of an experiment in which rifampicin is added to the plateau region of the reaction (indicated by the arrow). Addition of the drug leads to a rapid loss of thioflavin-T fluorescence. TEM images of a sample collected before the drug is added (Figure 3-7) confirm that abundant fibrils had formed. Strikingly TEM images collected after the drug was added also display numerous

amyloid fibrils (Figure 3-7). Once again, the drug interferes with the thioflavin-T fluorescence response but does not disaggregate IAPP fibrils.

3.3.3 Rifampicin does not prevent IAPP amyloid formation in the presence of antioxidants

The naphthohydroquinone ring in rifampicin is easily oxidized to the quinone form and aqueous solutions of rifampicin are not stable. Under basic conditions they break down to the rifampicin quinone form and under acidic conditions, 3-formyl rifampicin is produced (*135, 141-142*). Fink and coworkers have shown that the oxidation product is a more potent inhibitor of α-synuclein fibril formation (*135*). The experiments described in the previous subsection were conducted in the absence of antioxidants, thus rifampicin will be present as a mixture of the oxidized and reduced form. We conducted our first set of studies under those conditions because they were used in all reported studies of rifampicin IAPP interactions. We repeated the studies in the presence of the same antioxidant used by Fink and coworkers, ascorbic acid, to test if our results were dependent on the oxidation state of the drug. The breakdown of rifampicin can be easily monitored by following changes in its absorption spectrum. In particular, the intensity at 483 nm is significantly decreased if a sample of rifampicin is incubated in aqueous buffer at physiological pH due to oxidation (*141-142*). Control experiments showed that no significant change in the absorbance of rifampicin at 483 nm for at least 1000 minutes in the presence of ascorbic acid. In contrast, a steady decrease is observed in the absence of

ascorbic acid.

The results are not affected by the presence of the antioxidant; rifampicin still inhibits thioflavin-T fluorescence but does not prevent amyloid formation by IAPP. A sample of IAPP in the presence of 83μM ascorbic acid yields a typical kinetic curve as monitored by thioflavin-T fluorescence (Figure 3-8), and TEM confirms that fibrils were formed. Addition of rifampicin to the reaction mixture at time zero leads to a flat curve with no significant change in the thioflavin-T fluorescence. A sample was removed from this reaction mixture after 100 minutes (Figure 3-8) and TEM images were recorded. They revealed abundant amyloid fibrils. We also repeated the experiment in which rifampicin was added to preformed fibrils. Again we observed the same results in the presence and absence of ascorbic acid. Addition of rifampicin eliminated the thioflavin-T fluorescence but did not dissociate fibrils (Figure 3-9). We also examined the effect of oxidized rifampicin by testing samples which had been preincubated in aqueous solutions under conditions which promote oxidation of the drug. A sample of rifampicin was incubated in aqueous solution for 35 days prior to testing its inhibitory potential. This is, of course, a highly unlikely experimental protocol for any therapeutic studies but it is useful for testing the properties of breakdown products of the drugs. The material interfered with thioflavin-T fluorescence measurements, but failed to prevent amyloid formation although the resulting fibrils appeared to be somewhat thinner than those formed with unoxidized rifampicin (Figure 3-10).

3.3.4 Use of a novel IAPP fluorescent analog allows the kinetics of amyloid formation to be monitored in the presence of rifampicin

The intrinsic fluorescence of p-cyanoPhenylalanine (p-cyanoPhe) can be used to follow the time course of amyloid formation by IAPP (*143*). P-cyanoPhe fluorescence is large in aqueous solution but the fluorescence is significantly reduced in a hydrophobic environment (*144*). An analog of IAPP in which the C-terminal tyrosine is replaced by p-cyanoPhe (IAPP $Y37F_{CN}$) forms amyloid at the same rate as wildtype and the morphology of the resulting fibrils are identical as judged by TEM. Furthermore, the time course of the change in p-cyanoPhe fluorescence describes the same kinetic trace as the thioflavin-T fluorescence, thus p-cyanoPhe fluorescence can be used to follow fibrillization of IAPP. Figure 3-11 compares the time course of the fluorescence of IAPP $Y37F_{CN}$ in the presence and absence of rifampicin. The time courses of fibril formation are very similar in the presence and in the absence of the drug. Quantitative analysis of the data shows that the t_{50} time (the time for the reaction to reach 50% of the maximum fluorescence intensity) is 19 minutes when rifampicin is present and 18 minutes when it is absent. The respective growth phase, here defined as the time for the reaction to go from 10% to 80% completion are also very similar; 7 minutes in the presence of the drug and 6 minutes in its absence.

3.4 Conclusions

The studies described here demonstrate that rifampicin does not prevent amyloid

formation by human IAPP, furthermore the results are not an artifact of the choice of co-solvent or of failing to control the oxidation state of the drug. One important lesson from these studies is that the thioflavin-T based assay can lead to false positives in tests of fibrillization inhibitors. It is impossible to say how general this effect may be but there are undoubtedly other small molecules which inhibit thioflavin-T binding or compromise its fluorescence response. This is very important since thioflavin-T binding is widely used, particularly for high throughput screens of fibril inhibitors. The p-cyanoPhe analog of IAPP used here overcomes these difficulties and should be a generally useful tool for the screening of inhibitors. The data presented here have important implications for studies which seek to define the toxic species in IAPP fibrillization by studying the effects of fibril inhibitors on cell death (*138*). In particular, studies which have used rifampicin will need to be reexamined, since the data presented here clearly demonstrates that rifampicin does not prevent amyloid formation by IAPP. Thus the observation of toxicity in the presence of rifampicin (*128*) does not prove that IAPP fibrils are non-toxic.

(A) IAPP:

(B) Rifampicin:

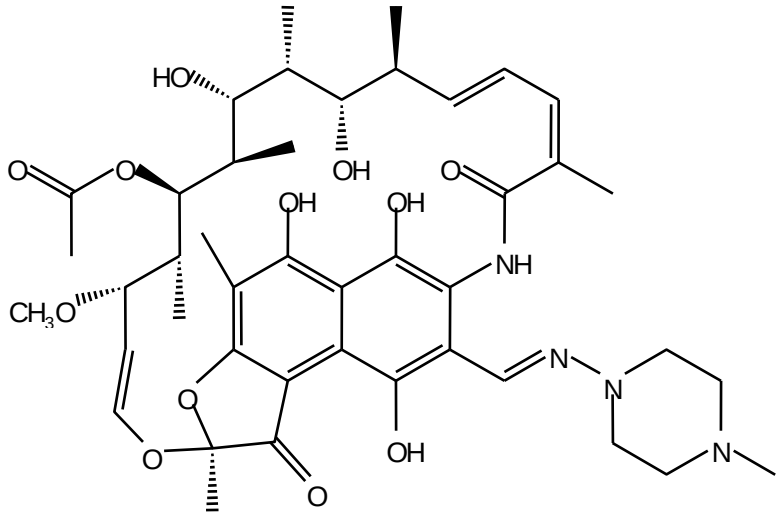

Figure 3-1: (A) The primary sequence of human IAPP. The peptide contains a disulfide bridge between Cys-2 and Cys-7 and has an amidated C-terminus. (B) The structure of the drug rifampicin. The naphthohydroquinone ring can be oxidized to the quinone form in aqueous buffer.

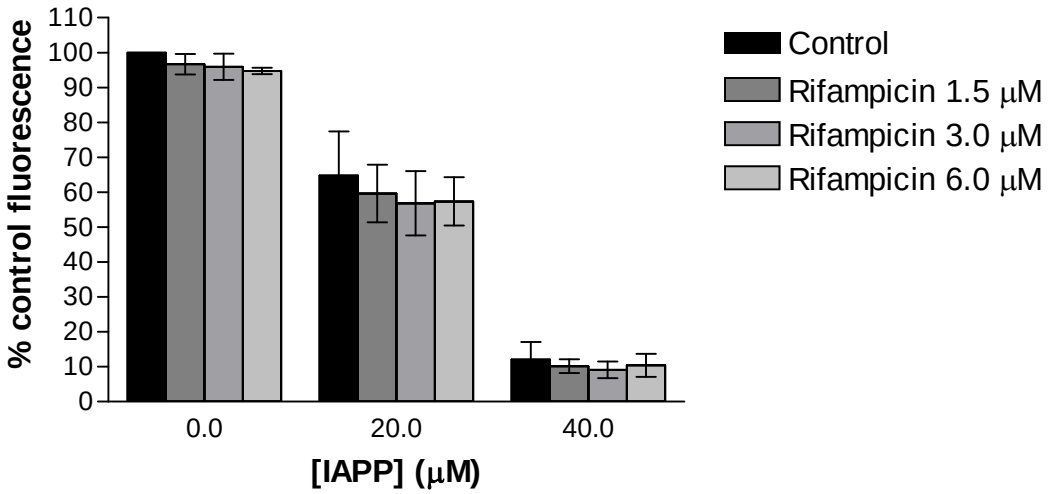

Figure 3-2: Rifampicin does not inhibit the cytotoxicity of human IAPP. Alamar blue fluorescence assays monitored INS-1 cell viability. Cells were treated for 24 hours with human IAPP alone or in the presence of varying concentrations of rifampicin. Bars indicate means ± standard error. P values were determined using one-way ANOVA and significant differences ($p < 0.05$) were determined using Tukey's multiple comparison post-hoc test. Asterisk indicates significant difference from untreated cells. There were no significant differences between control and rifampicin-treated cells at any concentration in the presence of 0, 20 μM and 40 μM human IAPP. Cell toxicity assays were performed by Kathryn J. Potter at the University of British Columbia in Professor Verchere's laboratory.

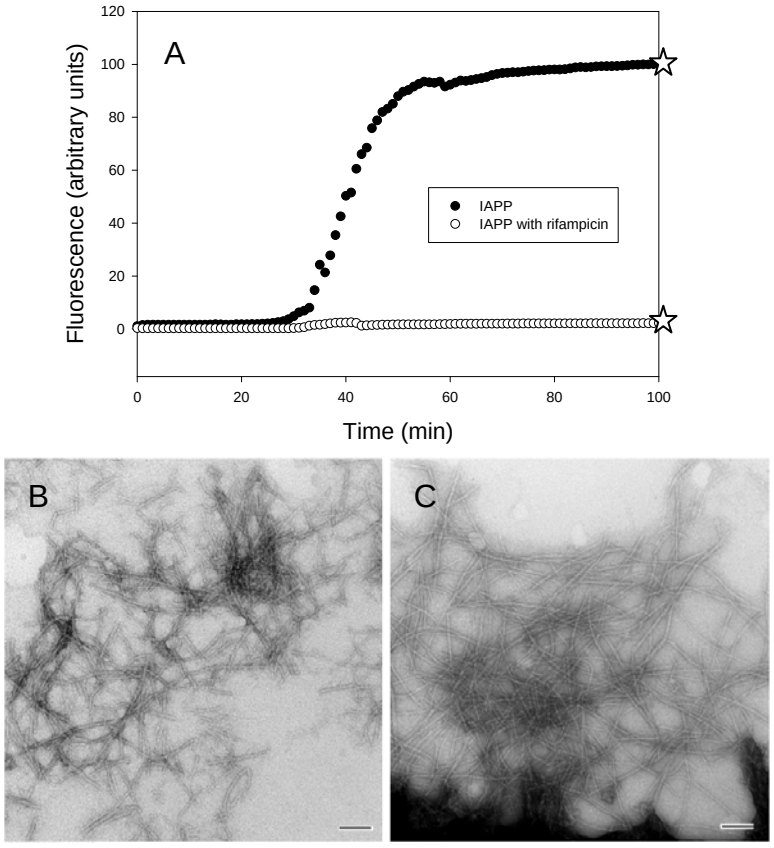

Figure 3-3: Rifampicin does not prevent amyloid formation by human IAPP. (A) Thioflavin-T fluorescence monitored assays of fibril formation. The closed circles (●) represent the experiment conducted in the absence of rifampicin. Open circles (○) correspond to an experiment conducted in the presence of 15 μM rifampicin. The stars (☆) indicated the time points at which aliquots were removed for TEM. (B) TEM images of the fibrillization reaction product for IAPP without rifampicin. (C) TEM image of a sample of 32 μM peptide and 15 μM rifampicin collected at 100 minutes after the start of the fibrillization reaction. Reactions were conducted at 25 ºC, pH 7.4, 32 μM IAPP, 25 μM thioflavin-T in 2% HFIP. Scale bar is 100 nm.

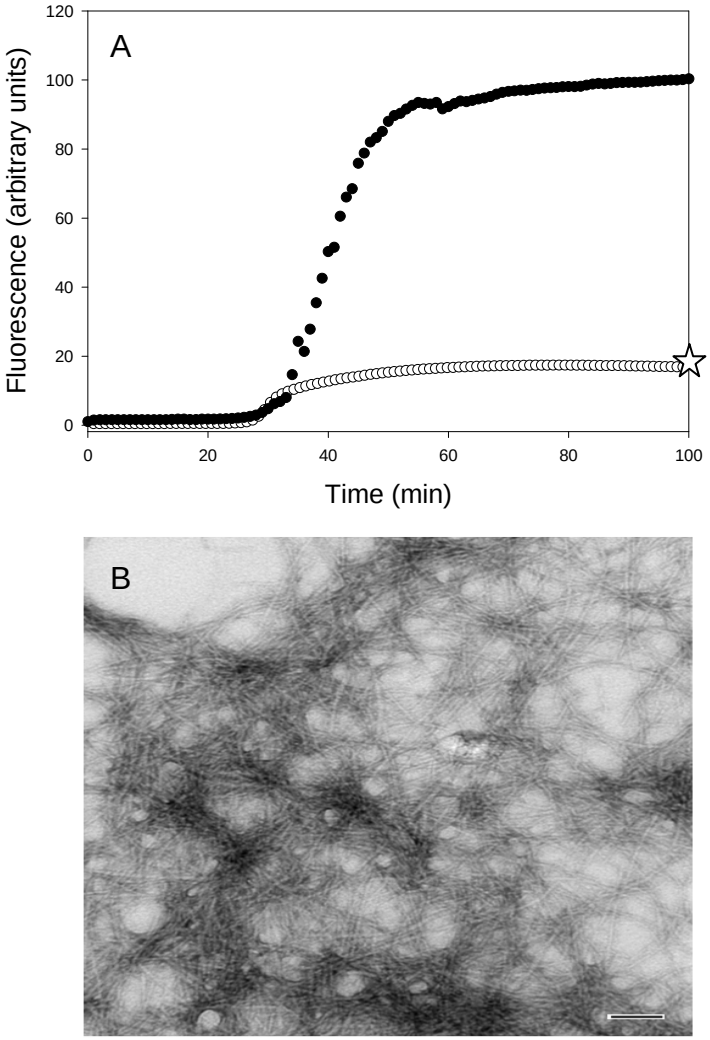

Figure 3-4: Effects of 5 μM rifampicin on the thioflavin-T monitored time course of human IAPP fibril formation. (A) Open circles (○) correspond to thioflavin-T fluorescence monitored time course of IAPP fibril formation with 5 μM rifampicin. Closed circles (●) represent an experiment conducted in the absence of rifampicin. Samples were 32 μM IAPP, 25 μM thioflavin-T in 2% HFIP, 25 ºC, pH 7.4. (B) TEM image of a sample collected at the indicated time point (☆). Scale bar is 100 nm.

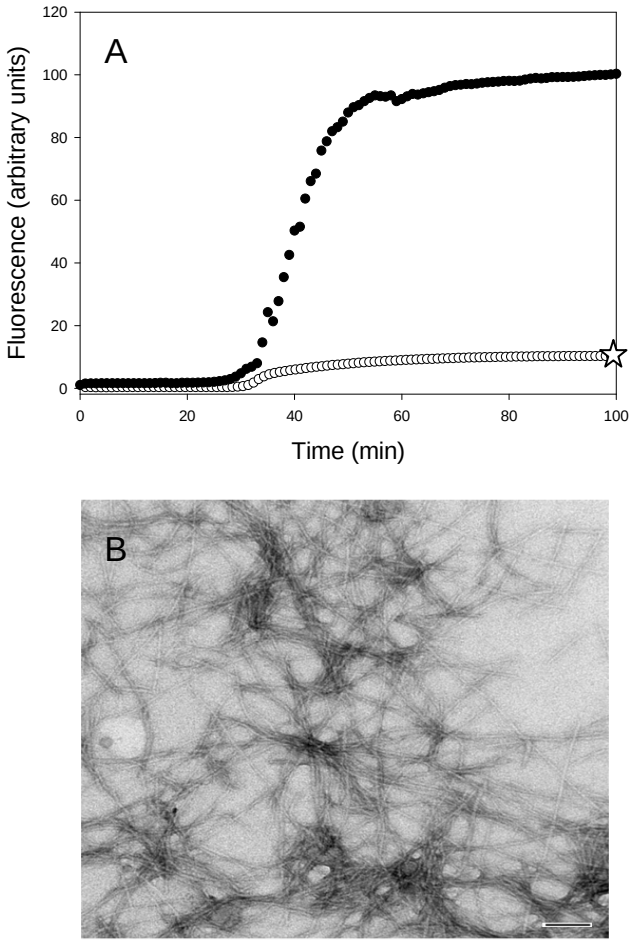

Figure 3-5: Effects of 2.5 μM rifampicin on the thioflavin-T monitored time course of human IAPP fibril formation. (A) Open circles (○) correspond to thioflavin-T fluorescence monitored time course of IAPP fibril formation with 2.5 μM rifampicin. Closed circles (●) correspond to an experiment conducted in the absence of rifampicin. Samples were 32 μM IAPP, 25 μM thioflavin-T in 2% HFIP, 25 ºC, pH 7.4. (B) TEM image of a sample collected at the indicated time point (☆). Scale bar is 100 nm.

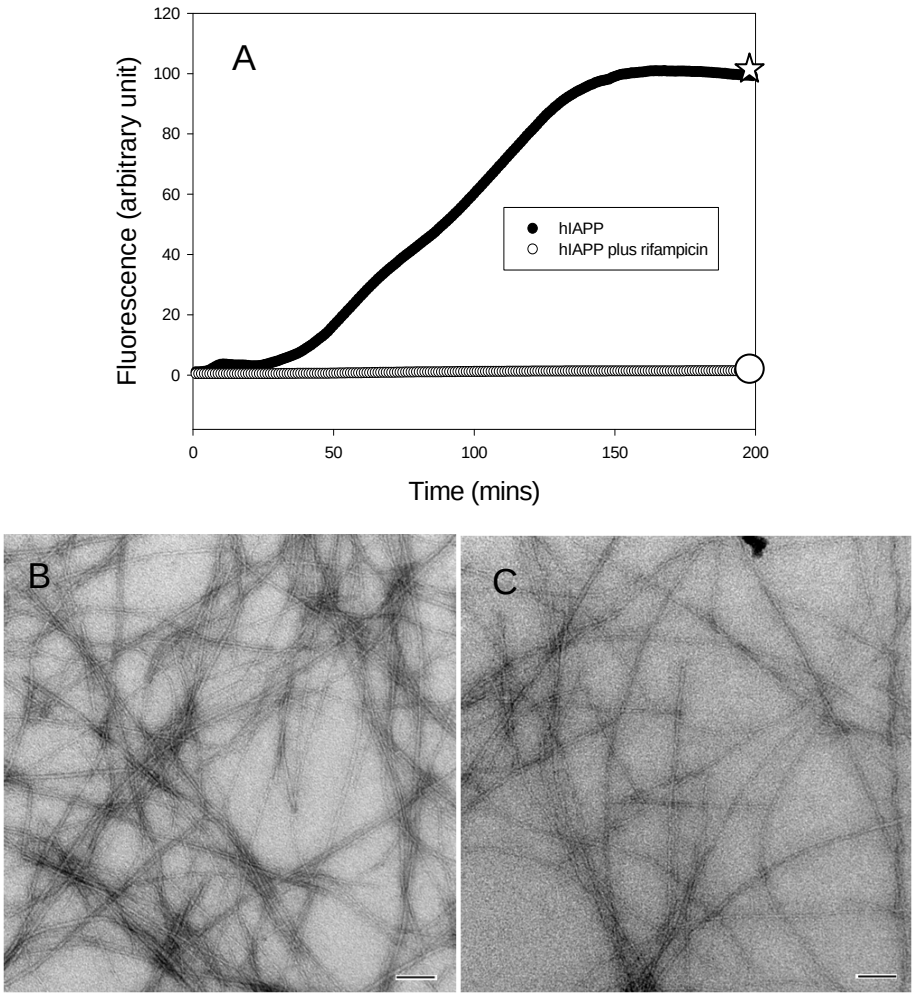

Figure 3-6: The method used to prepare IAPP stock solutions does not affect the results. Analysis of the effects of preparing stock solution in DMSO. (A) Thioflavin-T fluorescence monitored time course of human IAPP fibril formation with or without rifampicin. The closed circles (●) represent the experiment conducted in the absence of rifampicin. Open circles (○) correspond to an experiment conducted in the presence of 15μM rifampicin. All samples were 32 μM IAPP, 25 μM thioflavin-T in 2% DMSO, 25 ºC, pH 7.4. (B) TEM image of a sample collected at the indicated time point (☆) for a sample of IAPP without rifampicin. (C) TEM image of a sample collected at the indicated time point (○) for a sample of IAPP plus rifampicin. Scale bar is 100 nm. Stock solutions of IAPP were prepared in 100% DMSO and amyloid formation was initiated by diluting into buffer. Scale bar is 100 nm.

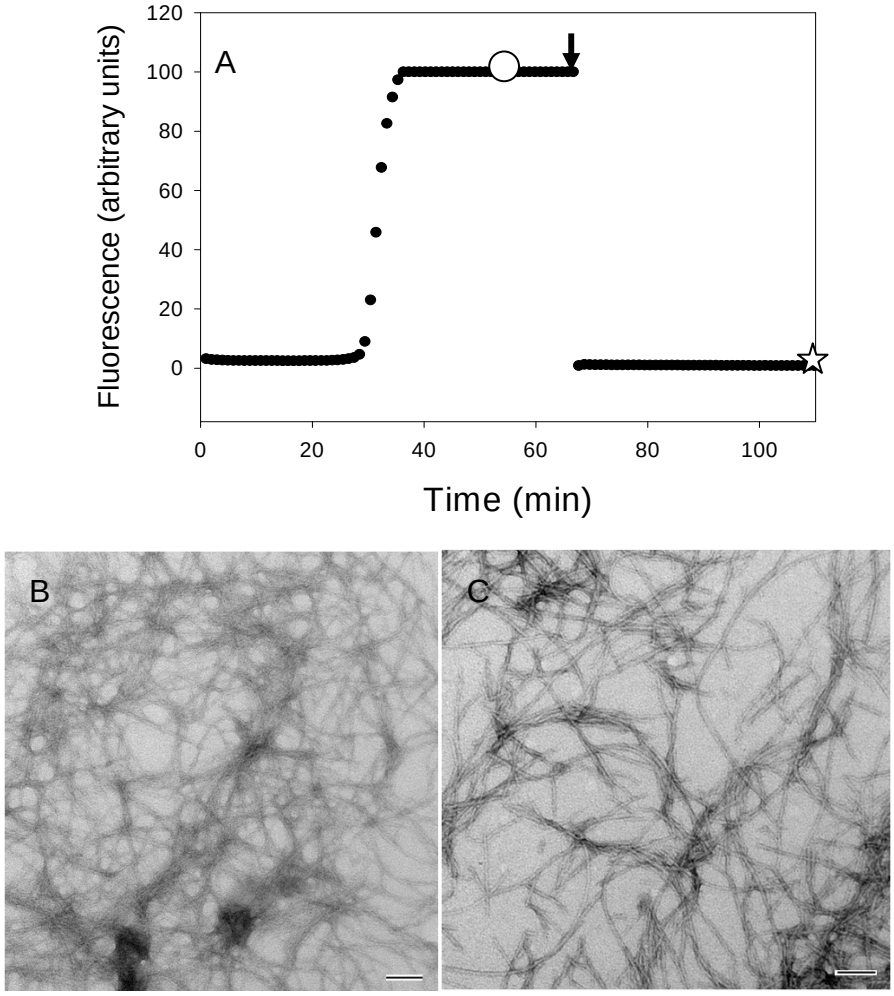

Figure 3-7: Effects of adding rifampicin to human IAPP fibrils. (A) Thioflavin-T fluorescence monitored time course of IAPP fibril formation. Rifampicin was added at the point indicated by the arrow (↓). (B) TEM image recorded before the drug was added at a time indicated by the (○). (C) TEM image recorded 35 minutes after addition of the drug, indicated by the (☆). All samples were 32 μM IAPP, 25 μM thioflavin-T in 2% HFIP, 25 ºC, pH 7.4. Scale bar is 100 nm.

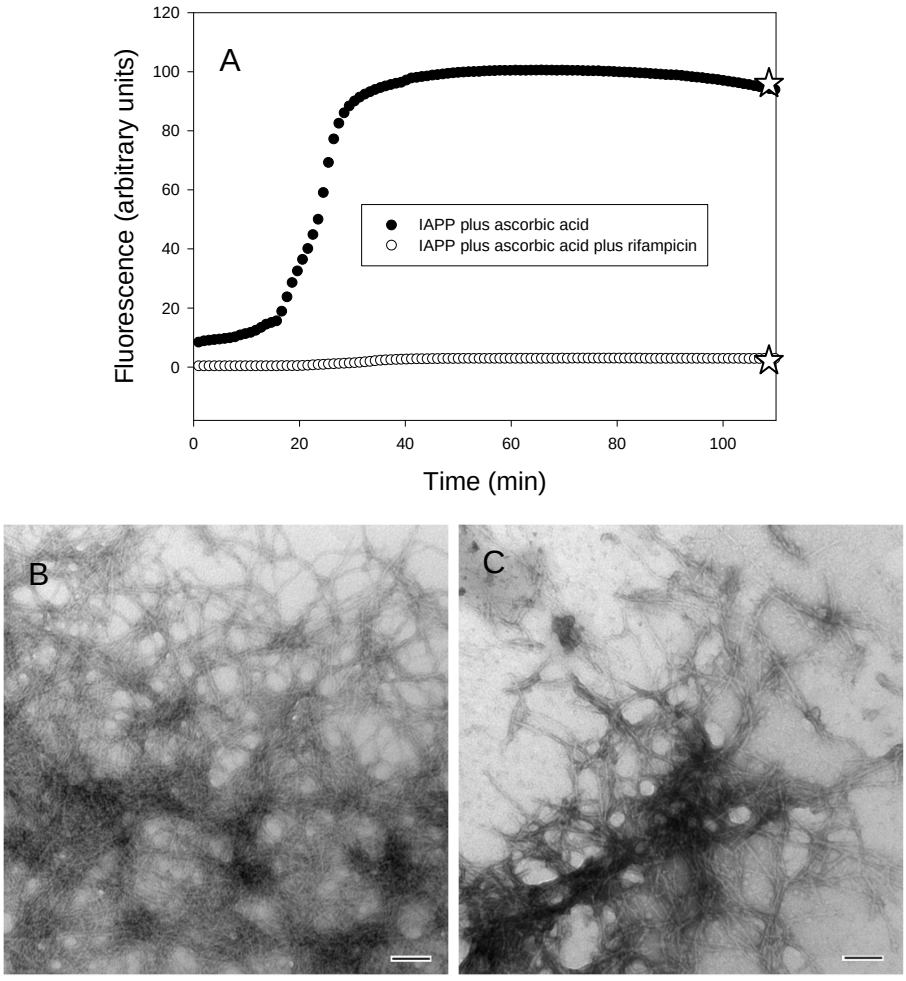

Figure 3-8: Rifampicin fails to prevent amyloid formation by human IAPP in the presence of antioxidants. (A) Thioflavin-T fluorescence monitored assays of fibril formation. The closed circles (●) represent the experiment conducted in the absence of rifampicin. Open circles (○) correspond to an experiment conducted in the presence of 15μM rifampicin. The stars (☆) indicated the time points at which aliquots were removed for TEM. (B) TEM images of the product of the fibrillization reaction for IAPP without rifampicin. (C) TEM image of a sample of 32μM peptide and 15μM rifampicin collected at 110 minutes after the start of the fibrillizatoin reaction. Reactions were conducted at 25 ºC, pH 7.4, 32 μM IAPP, 83 mM ascorbic acid, 25 μM thioflavin-T in 2% HFIP. Scale bar is 100 nm.

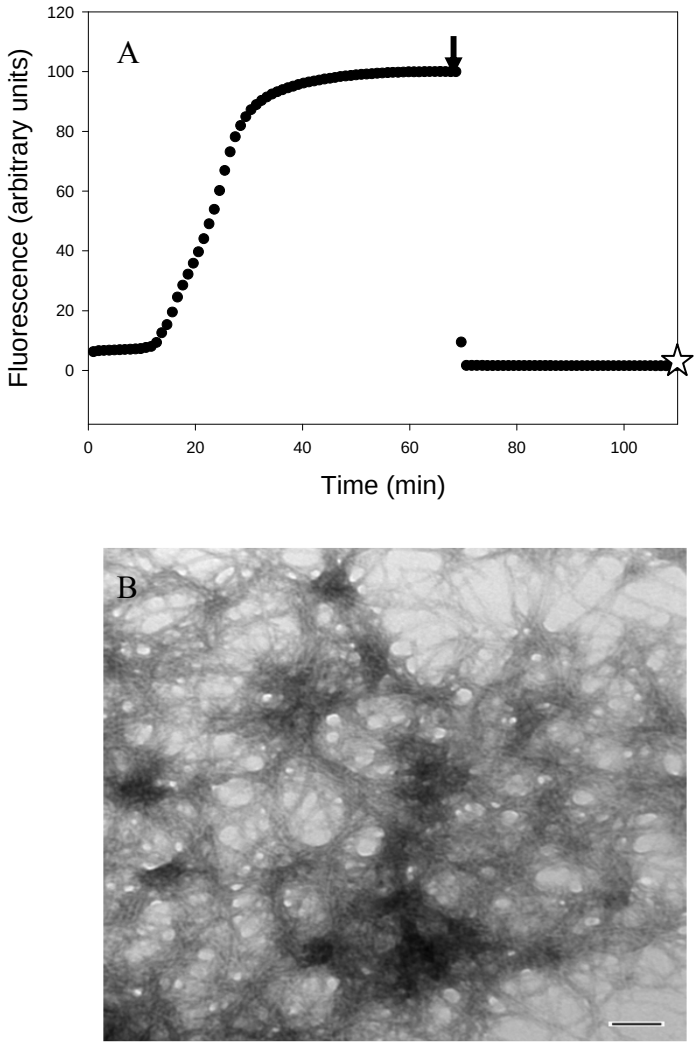

Figure 3-9: Effects of adding rifampicin to human IAPP fibrils in the presence of antioxidant. (A) Thioflavin-T fluorescence monitored time course of human IAPP fibril formation. Rifampicin was added at the point indicated by the arrow (↓). (B) TEM image recorded 35 minutes after addition of the drug, indicated by the (☆). All samples were 32 μM IAPP, 83 mM ascorbic acid, 25 μM thioflavin-T in 2% HFIP, 25 ºC, pH 7.4. Scale bar is 100 nm.

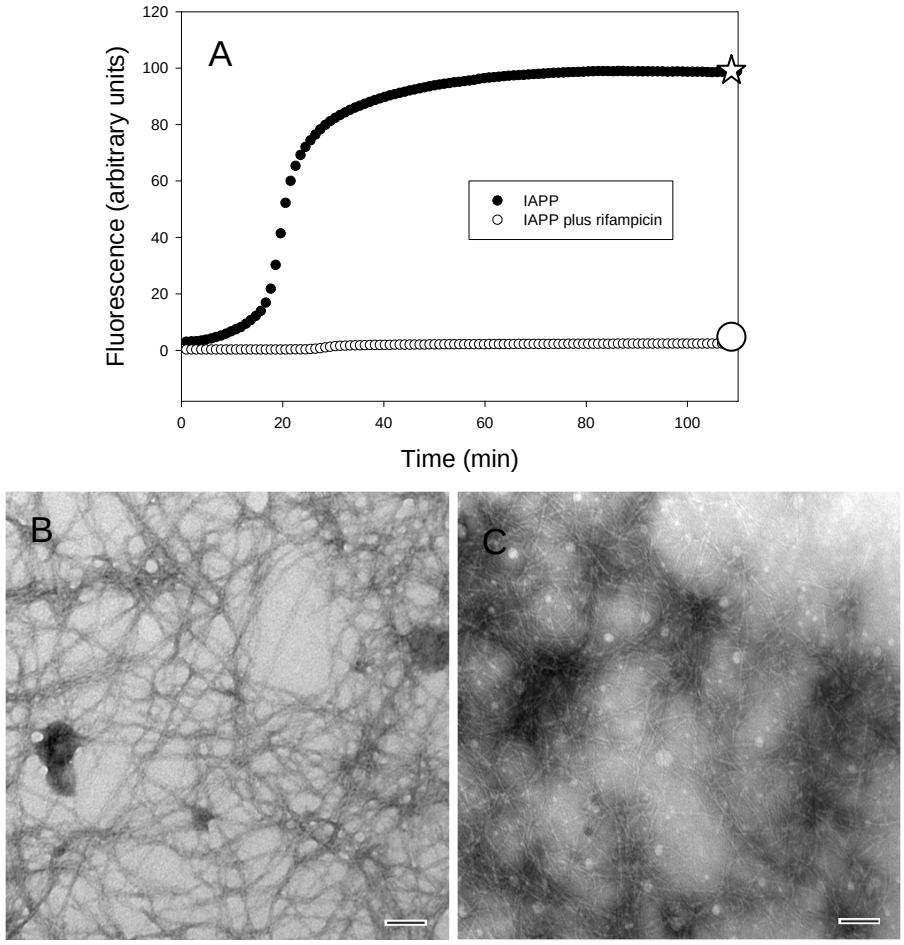

Figure 3-10: (A) Thioflavin-T fluorescence monitored time course of human IAPP fibril formation with or without rifampicin. The closed circles (●) represent the experiment conducted in the absence of rifampicin. Open circles (○) correspond to an experiment conducted in the presence of 15μM rifampicin. Rifampicin in Tris-HCl buffer, pH 7.4 was incubated for 35 days at room temperature before the start of the experiment. All samples were 32 μM IAPP, 25 μM thioflavin-T in 2% HFIP, 25 ºC, pH 7.4. (B) TEM image of a sample collected at the indicated time point (☆) for a sample of IAPP without rifampicin. (C) TEM image of a sample collected at the indicated time point (○) for a sample of IAPP plus rifampicin. Scale bar is 100 nm.

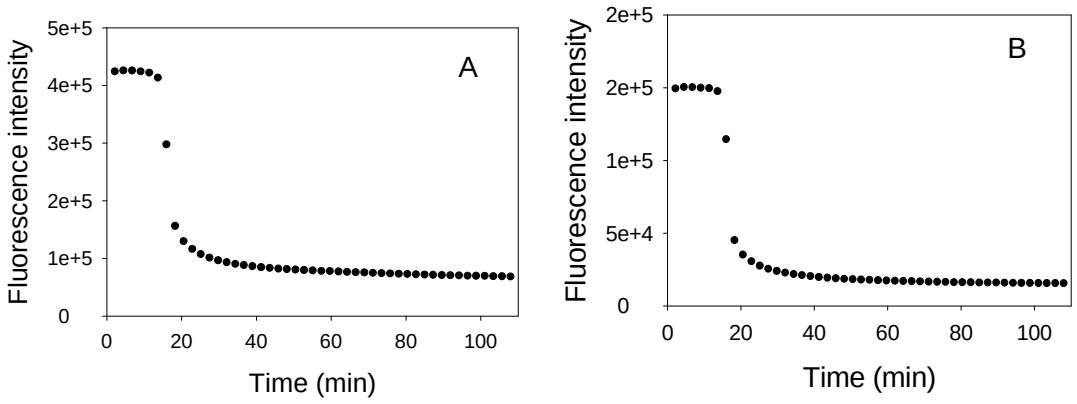

Figure 3-11: P-cyanoPhe fluorescence detected kinetics of IAPP $Y37F_{CN}$ in the absence of rifampicin (A) and in the presence of rifampicin (15 μM) (B). All samples were 32 μM peptide, 25 μM thioflavin-T in 2% HFIP, 25 ºC, pH 7.4. Excitation was at 240 nm and the emission was monitored at 296 nm. The difference in the maximum fluorescence intensity is likely due to inner filter effects.

4. The combination of kinetically selected inhibitors *in trans* leads to the highly effective inhibition of amyloid formation.

Abstract

Amyloid formation plays a role in over twenty five human disorders. A range of strategies have been applied to the problem of developing inhibitors of amyloid formation, but unfortunately, many inhibitors are effective only in molar excess and typically either lengthen the time to the onset of amyloid formation, (the lag time), while having modest effects on the total amount of amyloid fibrils produced, or decrease the amount of amyloid without significantly reducing the lag time. We demonstrate that a single point mutation converts the highly amyloidogenic human IAPP into a potent fibrillization inhibitor and a general strategy whereby two moderate inhibitors of amyloid formation can be rationally selected via kinetic assays and combined *in trans* to yield a highly effective inhibitor which dramatically delays the time to the appearance of amyloid and drastically reduces the total amount of amyloid formed. A key feature is that the selection of the components of the mixture is based on their effect on the time course of amyloid formation rather than on just the amount of amyloid produced. The approach is validated using inhibitors of amyloid formation by islet amyloid polypeptide, the causative agent of amyloid formation in type 2 diabetes and the Alzheimer's disease Aβ peptide.

NOTE: The material presented in this chapter has been submitted for publication to *Journal of the American Chemical Society* (Fanling Meng, Daniel P. Raleigh and Andisheh Abedini "The Combination of Kinetically Selected Inhibitors *in Trans* Leads to the Highly Effective Inhibition of Amyloid Formation."). This chapter contains direct excerpts from the manuscript which was written by me with suggestions and revisions from Professor Daniel P. Raleigh and Dr. Andisheh Abedini.

4.1 Introduction

Amyloid fibril formation plays a role in at least 20 different diseases, including Alzheimer's disease, Parkinson disease and type-2 diabetes (*2, 65, 69, 145-147*). The design of inhibitors of amyloid formation is an extremely active area of research (*71, 85, 148-150*). The process of amyloid formation is complex, involving multiple steps and both primary and secondary nucleation processes. Phenomologically the process typically exhibits a lag phase in which little or no fibril material is generated followed by a more rapid growth phase that leads to a final steady state in which amyloid fibrils are in equilibrium with soluble monomers and/or soluble oligomer species (*66*). Early work focused on the amyloid fibril since it was believed to be the toxic entity. However work in the last few years has lead to the suggestion that prefibril species may be the toxic forms (*69-70, 123*). This in turn has motivated the research for inhibitors which can intervene earlier in the self assembly process. Inhibitors of amyloid formation are also powerful mechanistic probes. For example, inhibitors which rigorously blocked the final assembly in the amyloid structure but did not inhibit the formation of prefibril oligomers could be used to test if fibrils were toxic in a particular case.

A wide range of strategies have been applied to the search for amyloid inhibitors. These include the screening of small molecules typically based upon a parent structure thought to bind to fibrils or known to already have inhibitory activity, the use of so called "β-breaker" peptides which incorporate residues such as proline or modifications such as N-methylation on one face of a putative β-strand (*85*). Unfortunately, many of the

inhibitors reported to date are effective only in excess and typically either reduce the apparent total amount of amyloid formed without having a major effect on the lag time or length the lag phase while only having modest effects on the total amount of amyloid fibrils ultimately produced. Improved inhibitors are needed but, given the considerable effort expanded to date, it is not obvious what strategy will be generally applicable. The approach is demonstrated islet amyloid polypeptide, (IAPP, also known as Amylin), which is the causative agent of islet amyloid in type 2 diabetes (*17, 29, 66, 97-98, 100, 151*) and the A $\beta_{1\text{-}40}$ peptide of Alzheimer's disease (Figure 4-1). The development of effective inhibitors of amyloid formation by IAPP is a challenging test case since the polypeptide is extremely amyloidogenic and aggregates even faster than the Aβ peptide *in vitro*. Considerably less work has been reported on the development of IAPP inhibitors than has been reported on the development of Aβ inhibitors. Here, we rationally designed peptide based inhibitors based on proposed mechanism of IAPP amyloid formation (Figure 4-2). IAPP 14-19 region is important for self-association and may serve as the molecular recognition motif for the full length IAPP (*152*). Previous proline scanning studies 20 to 29 region of IAPP suggest that mutation both at positions G24 and I26 affects amyloidogenicity of 20-29 fragment (*34*). Peptide-based inhibitors have been designed using the 20 to 29 fragment as the basic unit and rat IAPP which has multiple proline substitutions within this region also inhibit amyloid formation by IAPP (*85, 93*). I demonstrate that the point mutation I26P, (I26P-IAPP) and G24P point mutant, (G24P-IAPP), convert IAPP into a moderately effective inhibitor of amyloid formation

by wild type IAPP (*121*). More importantly, I also demonstrate a striking synergy when the two inhibitors are combined in *trans*. I show that the combination is also a potent inhibitor of amyloid formation by the $A\beta_{1-40}$ peptide.

4.2 Material and Methods

4.2.1 Peptide synthesis and purification

Peptides were synthesized on a 0.25 mmol scale using an applied Biosystems 433A peptide synthesizer, using 9-fluornylmethoxycarbonyl (Fmoc) chemistry. Pseudoprolines were incorporated to facilitate the synthesis of IAPP as described (*113*). 5-(4'-fmoc-aminomethyl-3',5-dimethoxyphenol) valeric acid (PAL-PEG) resin was used to afford an amidated C-terminal. Standard Fmoc reaction cycles were used. The first residue attached to the resin, β-branched residues, residues directly following β-branched residues and pseudoprolines were double coupled. Crude IAPP was oxidized by dimethyl sulfoxide (DMSO) for 24 hours at room temperature (*140*). $A\beta_{1-40}$ was also prepared using Fmoc chemistry. Pseudoprolines were incorporated at Asp7-Ser8 and Gly24-Ser25. Preloaded Val-wang resin was used to provide a free C-terminus. The first residue attached to the resin, β-branched residues, residues directly following β-branched residues and pseudoprolines were double coupled. The peptides were purified by reverse-phase HPLC using a Vydac C18 preparative column. A two-buffer system was utilized. Buffer A consists of H_2O and 0.045% HCl (v/v). Buffer B consists of 80% acetonitrile, 20% H_2O, and 0.045% HCl (v/v). The gradient used was 0-70% buffer B in

70 minutes. The pure IAPP peptide eludated out at 50 minutes, which is 50% buffer B. The pure I26P-IAPP and G24P-IAPP peptide eludated out at 48 minutes, which is 48% buffer B. Analytical HPLC were used to check the purity of the peptides before each experiment. The identity of the pure peptides was confirmed by mass spectrometry using a Bruker MALDI-TOF MS. Wild type IAPP expected 3904.6, observed 3904.8; G24P-IAPP expected 3942.9, observed 3942.8; I26P-IAPP expected 3888.3, observed 3888.2; G24P, I26P-IAPP expected 3924.5, observed 3923.9; $A\beta_{1\text{-}40}$, expected 4329.8, observed 4328.9.

4.2.2 Thioflavin-T fluorescence

All fluorescence experiments were performed on a Photon Technology International fluorescence spectrophotometer at an excitation wavelength of 450 nm and emission wavelength of 485 nm. Both the excitation and emission slits were set at 6 nm. A 1.0 cm cuvette was used and each time point was averaged for 1 minute. Solutions for the IAPP studies were prepared by diluting filtered stock solutions (0.45μm filter) into a Tris-HCl buffer (pH 7.4), thioflavin-T solution immediately before the measurement. The IAPP stock solutions were prepared in 100% hexafluoroisopropanol (HFIP) and stored at 4^{o}C. The final concentration of IAPP was 16 μM. Inhibitors when present were at a total concentration of 16 μM. Thus the 1:0.5:0.5 mixture contained 16 μM IAPP, 8 μM I26P-IAPP plus 8 μM G24P-IAPP. All samples contained 25 μM thioflavin-T, 20 mM Tris-HCl (pH 7.4) in 2% HFIP. All solutions were stirred during the fluorescence

experiments.

Samples for the experiments with the $A\beta_{1-40}$ peptide were prepared as follows: 1.0 mg $A\beta_{1-40}$ peptide was dissolved in 400 μL 100 mM Tris-HCl (pH 7.4). The solution was vortexed for 10 sec and then centrifuged for 4 min at 17,200 g. The supernatant was immediately withdrawn and peptide concentration was determined from the absorbance at 280 nm. This supernatant was used for the amyloid assays. Aliquots of the $A\beta_{1-40}$ supernatant were diluted into 100 mM Tris-HCl (pH 7.4) to initiate the reactions in the presence or absence of inhibitors. The final concentration of $A\beta_{1-40}$ was 24 μM. Inhibitors when present were at a total concentration of 24 μM. Aliquots were withdrawn at different time points and diluted into Tris-HCl buffered (100mM, pH 7.4), thioflavin-T solution before the measurement. The final concentration of thioflavin-T was 24 μM.

4.2.3 Transmission electron microscopy (TEM)

TEM was performed at the Life Science Microscopy Center at the State University of New York at Stony Brook. 15 μL aliquots of the samples used for the kinetic studies were removed at the end of the reaction, placed on a carbon-coated Formvar 300 mesh copper grid for 1 min and then negatively stained with saturated uranyl acetate for 1 min. Aliquots were removed after 600 minutes for the IAPP studies and after 20 hours for the $A\beta_{1-40}$ studies.

4.2.4 Circular dichroism (CD) spectra of the reaction endpoint

CD experiments were conducted with an Applied Photophysics Chirascan circular dichroism spectrometer. CD experiments used the same solutions as the thioflavin-T fluorescence measurements. Spectra were recorded from 190 or 195 to 250 nm at 1 nm intervals in a 0.1 cm path length quartz cuvette at 25^{o}C.

4.3 Results and discussion

4.3.1 A single point mutation converts human IAPP into a fibrillization inhibitor

Thioflavin-T fluorescence monitored kinetic assays of the time course of amyloid are shown in Figure 4-3A. The data obtained for wild type IAPP in the absence of inhibitor displays the classic sigmoidal curve expected for amyloid formation. Both I26P and G24P show only a very modest increase in thioflavin-T fluorescence under conditions where the wild type rapidly self assembles to form amyloid (Figure 4-4). TEM images confirm neither the G24P variant nor the I26P variant form amyloid (Figure 4-4). A 1:1 molar mixture of wild type IAPP with either inhibitor behaves very differently than does the wild type peptide in the absence of inhibitor. The I26P point mutant is a potent inhibitor of wild type IAPP fibrillization. The lag time for a 1:1 mixture of I26P and wildtype hIAPP was increased by 6 to 7 fold relative to wild type IAPP, and the final fluorescence intensity of the mixture was significantly reduced. The intensity of the thioflavin-T fluorescence in the plateau region at the end of the reaction is a factor of 2 lower for the 1:1 mixture than for wild type IAPP alone. Like the I26P peptide, the G24P mutant is also an inhibitor of amyloid formation. It lengthens the lag phase by 25 fold

relative to wild type IAPP and decreases the value of final thioflavin-T fluorescence intensity, but it does not completely abolish amyloid formation by IAPP. We have observed some experiment to experiment variability for the effects of the G24P peptide on the wild type IAPP, but the same trend relative to I26P is always observed. The G24P mutant always has a larger effect on the lag phase of wild type then does the I26P mutant. In contrast, the G24P peptide always has a smaller effect on the final value of the thioflavin-T fluorescence of the 1:1 mixture. The general features of the kinetic assays are robust and similar results have been obtained by different investigators using different preparations of peptides.

4.3.2 Two moderate inhibitors can be combined *in trans* to yield a highly effective inhibitor

The two inhibitors I26P and G24P clearly have different relative affects on the lag phase and on the final fluorescence signal, suggesting that the two molecules target different steps in the pathway of amyloid fibril formation with different efficiencies. We reasoned, based upon their differential effects upon the kinetics, that a combination of the two inhibitors would prove much more effective than the individual inhibitors. The results of combining the two inhibitors *in trans* are striking; the combination is a far more effective inhibitor than either mutant alone and no change in thioflavin-T fluorescence is observed over the time course of the entire experiment (Figure 4-3A). The dramatic effect of the mixture is not due to an increase in the total amount of inhibitor since experiments

were conducted with the total inhibitor concentration, (single inhibitor or combination), held constant.

We confirmed the results of the thioflavin-T studies by recording TEM images of the end points of the kinetic experiments (Figure 4-3B-E). TEM images were recorded of aliquots removed 600 minutes after the start of the reaction. This corresponds to a time that is 20-fold longer than that required for IAPP to form amyloid under these conditions. The images collected for the sample of wild type IAPP in the absence of inhibitor display numerous amyloid fibers with the morphology commonly observed for IAPP-derived amyloid (Figure 4-3B). The TEM images of the 1:1 molar mixtures of IAPP with either point mutant are very different (Figure 4-3C, Figure 4-3D). Significantly fewer fibers are observed, and those which are detected have a distinctly thinner appearance compared to the wild type fibers. The TEM image of the 1:0.5:0.5 mixture of wild type IAPP with G24P-IAPP and I26P-IAPP is very different from the images of the binary mixtures and no fibers were detected on the grid (Figure 4-3E). Far UV circular dichroism (CD) spectra were also recorded 600 minutes after the start of the reaction and provide a third independent probe of the effects of the various inhibitors. The CD spectrum of IAPP indicates considerable β-structure. In contrast, the spectrum of the 1:0.5:0.5 mixture of IAPP with the G24P-IAPP and I26P-IAPP point mutants shows no evidence of β–structure. The spectra of the binary mixtures of IAPP with a single point mutant are intermediate (Figure 4-5).

4.3.3 The combination is also a potent inhibitor of amyloid formation by the $A\beta_{1-40}$ peptide.

We tested the generality of the synergistic effects by examining the ability of the combination of inhibitors to inhibit amyloid formation by other polypeptides. There has been at least one report of a peptide based inhibitor of IAPP amyloid formation inhibiting amyloid formation by the $A\beta_{1-40}$ Alzheimer's polypeptide (*153*). Thus we examined the ability of the G24P and I26P IAPP points mutants to inhibit amyloid formation by $A\beta_{1-40}$. Thioflavin-T monitored kinetic assays reveal that each peptide is a moderate inhibitor of amyloid formation by $A\beta_{1-40}$ and show that the two IAPP point mutants exert different relative effects on the lag phase and the final thioflavin-T fluorescence intensity (Figure 4-6A). The combination of the two inhibitors again proved to much more effective than either inhibitor alone even thought the total inhibitor concentration was kept constant. TEM images collected of aliquots removed at the end of kinetic experiments, (20 hours), are fully consistent with the thioflavin-T studies. Dense mats of fibers are observed for the $A\beta_{1-40}$ sample in the absence of inhibitors, while a 1:1 mixtures of $A\beta_{1-40}$ with either point mutant leads to much shorter aggregates (Figure 4-6B, C, D). Fewer aggregates are observed in the 1:0.5:0.5 mixture of $A\beta_{1-40}$ with G24P-IAPP and I26P-IAPP (Figure 4-6E). CD measurements show that the mixture inhibits β-sheet formation (Figure 4-7).

It is natural to ask why the combination of the two inhibitors is more effective than a single inhibitor. The kinetic data strongly suggest that the different inhibitors target different stages of the amyloid fibril formation pathway. In this scenario one inhibitor

may preferentially bind to species which are populated early and inhibit their progression to the next stage, while the second inhibitor may target structures which are formed latter and whose production was slowed by the first inhibitor, or which formed from molecules that escaped the first inhibitor. Alternatively, amyloid formation may proceed by parallel pathways and the two inhibitors may target separate pathways. The process of amyloid formation has yet to be defined at high resolution for any system, and in the absence of a residue specific description of the kinetic mechanism of amyloid formation, it is impossible to deduce exactly what stages the two inhibitors target. Irrespective of the mechanistic details, the data presented here is very striking, and clearly illustrates strong synergistic effects with the combination strategy.

4.4 Conclusions

In this study, we used peptide based inhibitors to illustrate a powerful combination approach for inhibiting amyloid formation and we have provided a second example of an IAPP inhibitor which exerts strong inhibitory effects on amyloid formation by the Aβ peptide.

The concept is generalizable to non-peptide inhibitors. The key feature of the approach is that the selection is based upon assays which monitor the time course of amyloid formation and not just the total amount of amyloid produced. These real time measurements allow one to select molecules which have different effects on different aspects of the self-assembly reaction. In contrast, traditional assays which rely on the

read out of a single time point, such as the final thioflavin-T fluorescence, are unable to select such combinations. The approach outlined here has the potential to greatly expand the number of hits for a given set of compounds and is well suited for high throughput screens since thioflavin-T based assays are readily conducted in microtiter plates (*154*).

(A) **KCNTATCATQRLANFLVHS SNNFGAILSSTNVGSNTY-CONH$_2$**

(B) **DAEFRHDSGY EVHHQKLVFF AEDVGSNKGA IIGLMVGGVV**

Figure 4-1: (A) The primary sequence of human IAPP. The C-terminus is amidated. (B) The primary sequence of the 1-40 isoform of the Aβ polypeptide.

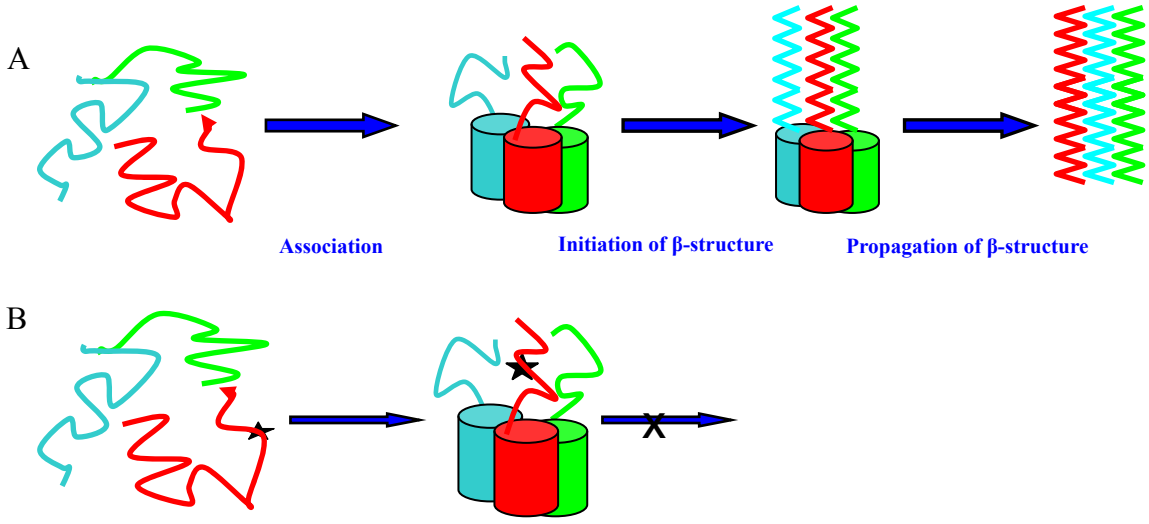

Figure 4-2: Proposed mechanism of IAPP amyloid formation and inhibition of IAPP amyloid formation by IAPP proline mutant. (A) IAPP monomers associate with each other which brings C-terminal region together resulting in formation of β-structure. (B) Monomeric IAPP can bind to IAPP mutant recognized by recognition region. IAPP proline mutant could block further progreesion towards amyloid because the proline mutant inhibits beta-sheet assembly.

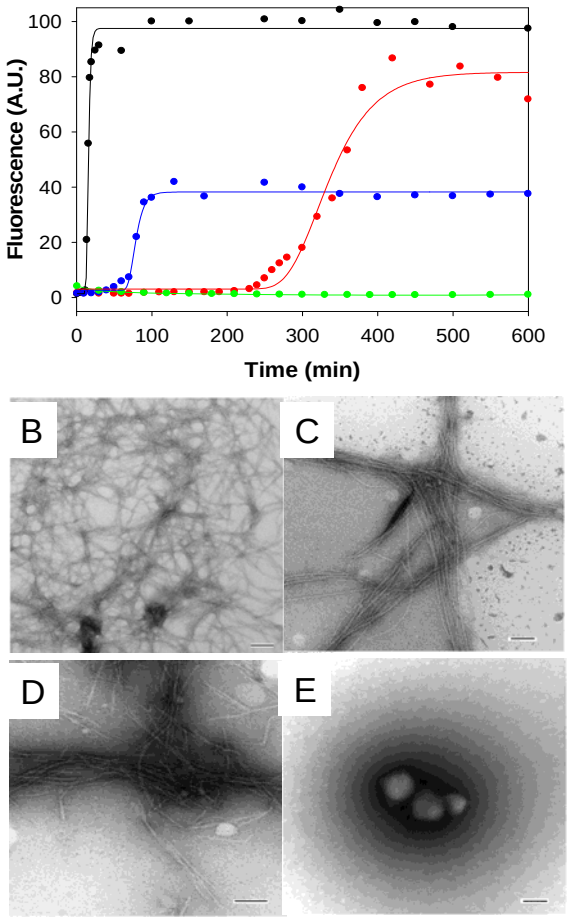

Figure 4-3: Inhibition of amyloid formation by IAPP. (A) The results of fluorescent detected thioflavin-T binding assays are displayed. Black, wild type IAPP; Red, a 1:1 mixture of wild type IAPP with G24P-IAPP; Blue, a 1:1 mixture of wild type IAPP with I26P-IAPP; Green, a 1:0.5:0.5 mixture of wild type IAPP with G24P-IAPP and I26P-IAPP. (B) TEM image of wild type IAPP alone. (C) TEM image of a1:1 mixture of wild type IAPP and G24P-IAPP. (D) TEM image of a1:1 mixture of wild type IAPP and IAPP-I26P. (E) TEM image of a 1:0.5:0.5 mixture of wild type IAPP, G24P-IAPP and I26P-IAPP. Scale bars represent 100 nm. Aliquots were removed from the kinetic experiments 600 minutes after amyloid formation was initiated and TEM images collected. The kinetic assays depicted in panel (A) were carried out in 20 mM Tris-HCl (pH 7.4), 2% HFIP (v/v) with continuous stirring at 25^{o}C. The total concentration of inhibitor was the same in the 1:1 mixtures and in the 1:0.5:0.5 mixtures, and was equal to 16 μM. Wild type IAPP was at 16 μM.

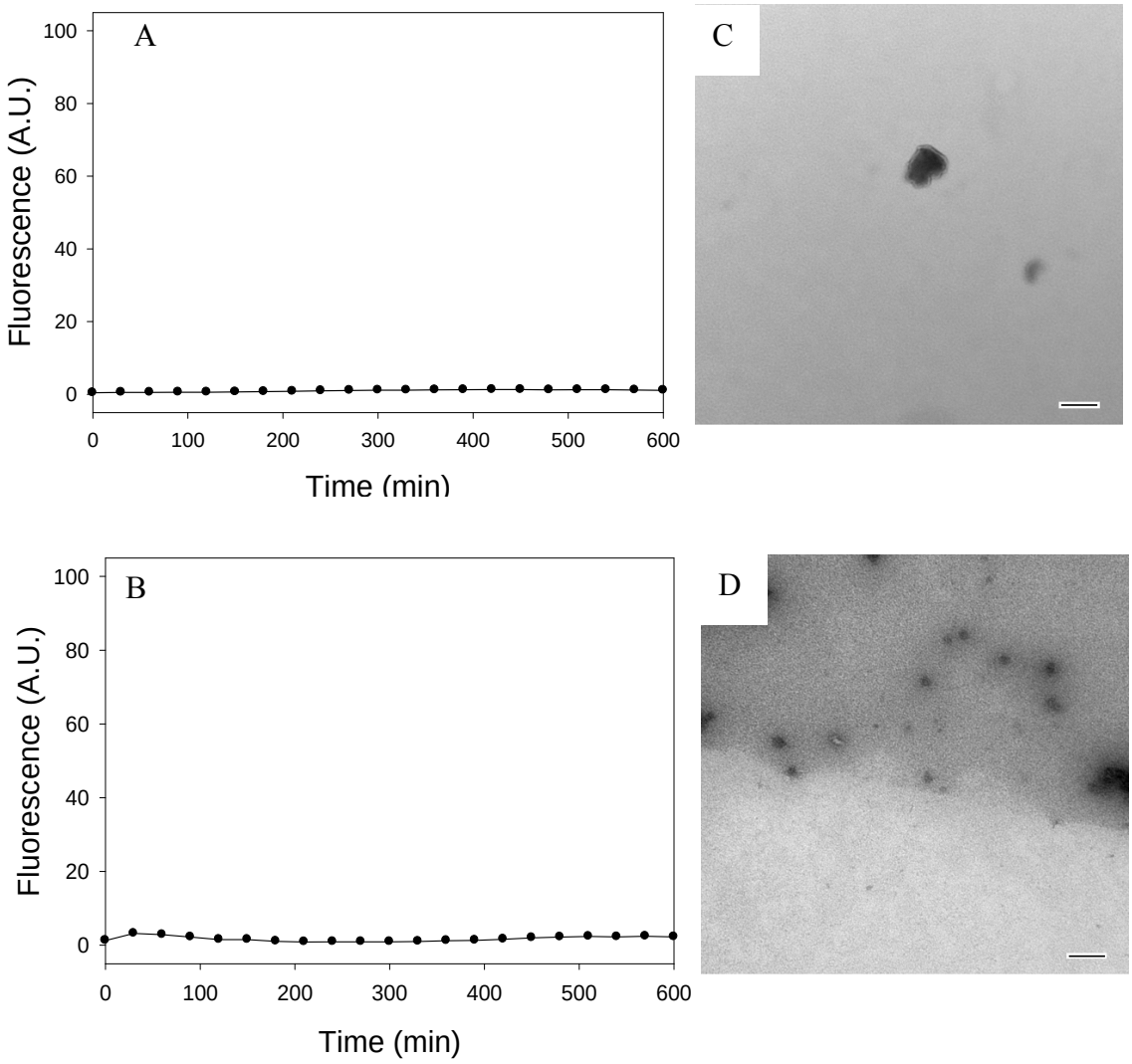

Figure 4-4: G24P-IAPP and I26P-IAPP do not form amyloid. Thioflavin-T kinetic assays for (A) G24P-IAPP, (B) I26P-IAPP. TEM images collect from aliquots removed at the end of the reaction. (C) G24P-IAPP, (D) I26P-IAPP. The scale bar is 100 nm.

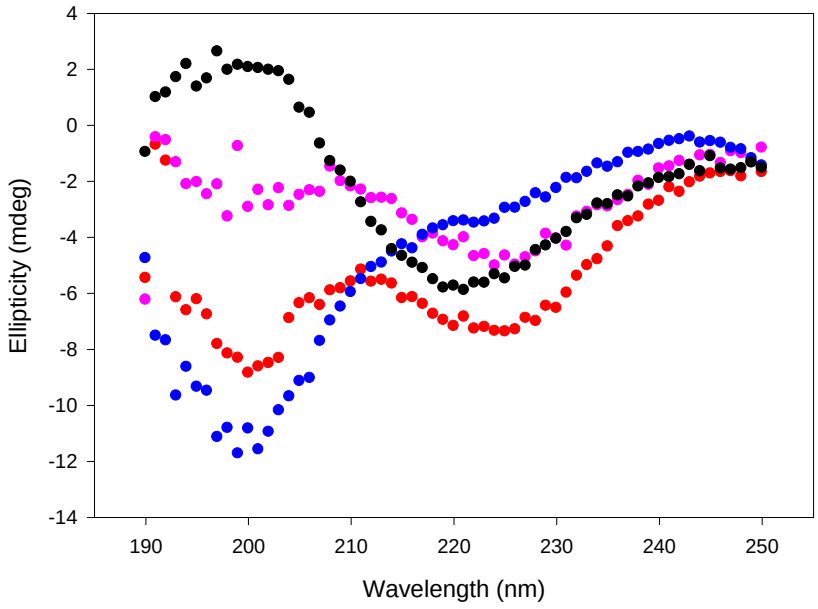

Figure 4-5: CD spectra of mixtures of the different inhibitors with wildtype hIAPP. Aliquots were removed at the end of the various thioflavin-T monitored kinetic experiments displayed in Figure 4-2. wildtype hIAPP alone (black), 1:1 mixture of wildtype hIAPP with the G24P hIAPP (pink), 1:1 mixture of wildtype hIAPP with the I26P hIAPP (*155*), 1:0.5:0.5 mixture of wildtype hIAPP with the G24P hIAPP and I26P hIAPP (blue). The total concentration of inhibitor was the same in the 1:1 mixtures and in the 1:0.5:0.5 mixture and was equal to 16 μM wild type. Wild type hIAPP, when present, was also at 16 μM.

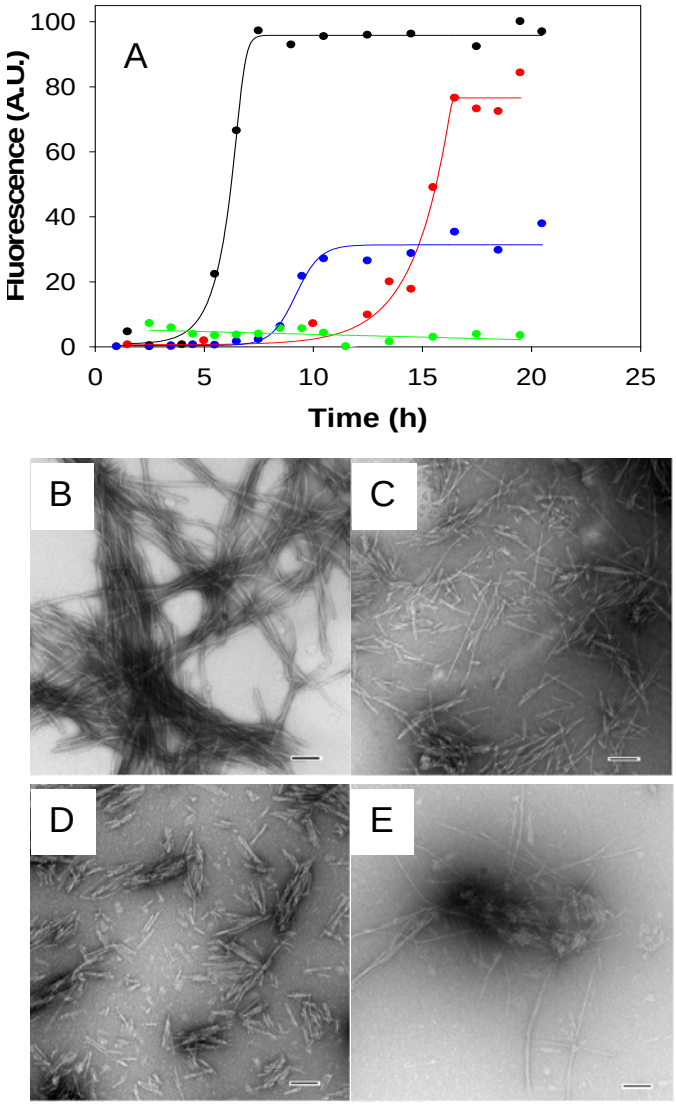

Figure 4-6: Inhibition of amyloid formation by the $A\beta_{1-40}$ polypeptide. (A) The results of fluorescent detected thioflavin-T binding assays are displayed. Black, $A\beta_{1-40}$; Red, a 1:1 mixture of $A\beta_{1-40}$ with G24P-IAPP; Blue, a 1:1 mixture of $A\beta_{1-40}$ with I26P-IAPP; Green, a 1:0.5:0.5 mixture of $A\beta_{1-40}$ with G24P-IAPP and I26P-IAPP. (B) TEM image of $A\beta_{1-40}$ alone. (C) TEM image of a 1:1 mixture of $A\beta_{1-40}$ and G24P-IAPP. (D) TEM image of a 1:1 mixture of $A\beta_{1-40}$ and I26P-IAPP. (E) TEM image of a 1:0.5:0.5 mixture of $A\beta_{1-40}$, G24P-IAPP and I26P-IAPP. Scale bars represent 100 nm. Aliquots were removed from the kinetic experiments 20 hours after amyloid formation was initiated and TEM images collected. The kinetic assays depicted in panel (A) were carried out in 100 mM Tris-HCl (pH 7.4) with continuous stirring at 25°C. The total concentration of inhibitor was the same in the 1:1 mixtures and in the 1:0.5:0.5 mixtures and was equal to 24 μM. $A\beta_{1-40}$ was at 24 μM.

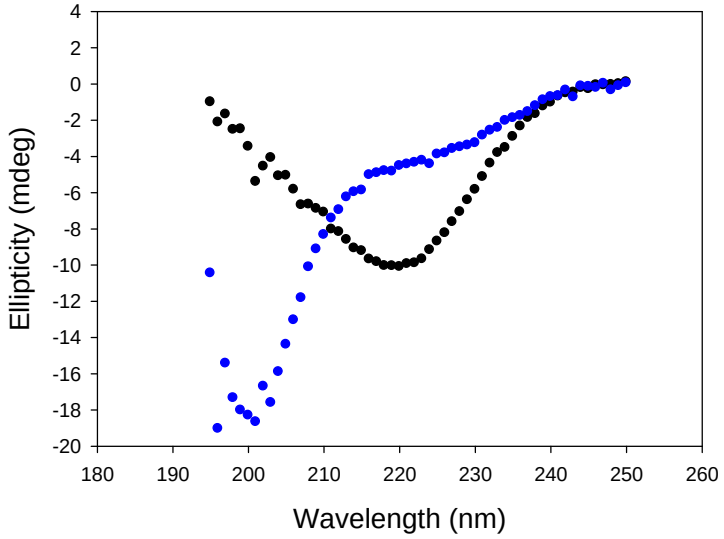

Figure 4-7: CD spectra of $A\beta_{1-40}$ and of the mixture of $A\beta_{1-40}$ with the two inhibitors**.** Aliquots were removed at the end of the various thioflavin-T monitored kinetic experiments displayed in Figure 4-3. $A\beta_{1-40}$ alone (black), 1:0.5:0.5 mixture of $A\beta_{1-40}$ with the G24P-IAPP and I26P-IAPP (blue). The total concentration of inhibitor was equal to 24 μM $A\beta_{1-40}$. Thus the 1:0.5:0.5 mixture contained 24 μM $A\beta_{1-40}$, 12 μM G24P-IAPP and 12 μM I26P-IAPP.

5. Sulfated triphenyl methane derivatives are potent inhibitors of amyloid formation by human islet amyloid polypeptide and protect against the toxic effects of amyloid formation

Abstract

Islet amyloid polypeptide (IAPP), also known as amylin, is responsible for amyloid formation in type 2 diabetes. The formation of islet amyloid is believed to contribute to the pathology of the disease by killing β-cells and it may also contribute to islet transplant failure. The design of inhibitors of amyloid formation is an active area of research, but comparatively little attention has been paid to inhibitors of IAPP in contrast to the large body of work on Aβ and most small molecule inhibitors of IAPP amyloid are generally effective only when used at a significant molar excess. Here we show that the simple sulphonated triphenyl methane derivative acid fuchsin, (3-(1-(4-Amino-3-methyl-5-sulphonatophenyl)-1-(4-amino-3-sulphonatophenyl) methylene) cyclohexa-1,4-dienesulphonic acid), is a potent inhibitor of *in vitro* amyloid formation by IAPP at substoichiometric levels and protects cultured rat INS-1 cells against the toxic effects of human IAPP. Fluorescence detected thioflavin-T binding assays, circular dichroism and TEM measurements confirm that the compound prevents amyloid fibril formation. Ionic strength dependent studies show that the effects are

mediated in part by electrostatic interactions. Experiments in which the compound is added at different time points before amyloid formation has commenced reveal that it arrests amyloid formation by trapping intermediate species. The compound is less effective against the Aβ peptide, indicating specificity in its ability to inhibit amyloid formation.

NOTE: The material presented in this chapter has been published (Fanling Meng, Andisheh Abedini, Annette Plesner, Katherine J. Potter, Chris T. Middleton, Martin T. Zanni, C. Bruce Verchere and Daniel P. Raleigh. "Sulfated Triphenyl Methane Derivatives are Potent Inhibitors of Amyloid Formation by Human Islet Amyloid Polypeptide and Protect against the Toxic Effect of Amyloid Formation" (2010) *Journal of Molecular Biology* In press). This chapter contains direct excerpts from the manuscript which was written by me with suggestions and revisions from Professor Daniel P. Raleigh. Cell toxicity experiments were performed by Dr. Andisheh Abedini at the University of British Columbia in Professor Verchere's laboratory. They are included in this chapter for completeness.

5.1 Introduction

There is considerable interest in developing inhibitors of amyloid formation as potential therapeutics, and as reagents to probe pathways of amyloid assembly. There is a large body of work on inhibitors of the Alzheimer beta amyloid peptide (Aβ), but less attention has been paid to the development of IAPP amyloid inhibitors, although several reports of effective large peptide based inhibitors have appeared, such as those which incorporate proline residues or N-methylated amino acids into the full IAPP sequence (*85, 119, 121, 148-150, 156-158*). In striking contrast, many small molecule and small peptide inhibitors of IAPP amyloid have often proven effective only when added in large molar excess. Here I use kinetic assays, CD and transmission electron microscopy (TEM) to show that the simple sulfonated triphenylmethyl derivative, acid fuchsin, (3-(1-(4-Amino-3-methyl-5-sulphonatophenyl)-1-(4-amino-3-sulphonatophenyl) methylene) cyclohexa-1,4-dienesulphonic acid), is potent inhibitor of amyloid formation by IAPP at substoichiometric ratios (Figure 5-1). The compound protects cultured INS-1 cells against the toxic effects of IAPP amyloid formation. Acid fuchsin is an interesting lead structure since a number of derivatives are readily available.

5.2 Material and methods

5.2.1 Peptide synthesis and purification

Human IAPP was synthesized on a 0.25 mmol scale using an applied Biosystems 433A peptide synthesizer, by 9-fluornylmethoxycarbonyl (Fmoc) chemistry as described

(*113*). Pseudoprolines were incorporated to facilitate the synthesis. *In vivo,* IAPP contains an amidated N-terminus, thus 5-(4'-fmoc-aminomethyl-3',5-dimethoxyphenol) valeric acid (PAL-PEG) resin was used to afford an amidated C-terminal. Standard Fmoc reaction cycles were used. The first residue attached to the resin, β-branched residues, residues directly following β-branched residues, and pseudoprolines were double coupled. Crude peptide was oxidized by dimethyl sulfoxide (DMSO) for 24 hours at room temperature (*140*). IAPP was purified by reverse-phase HPLC using a Vydac C18 preparative column. A two-buffer system was utilized. Buffer A consists of H_2O and 0.045% HCl (v/v). Buffer B consists of 80% acetonitrile, 20% H_2O, and 0.045% HCl (v/v). The gradient used was 0-70% buffer B in 70 minutes. The pure peptide eludated out at 50 minutes, which is 50% buffer B. Analytical HPLC was used to check the purity of the peptides. The identity of the pure peptide was confirmed by mass spectrometry using a Bruker MALDI-TOF MS (observed 3904.6, expected 3904.8). The $A\beta_{1-40}$ peptide was synthesized using a similar protocol except that a 5-(4'-fmoc-aminomethyl-3',5-dimethoxyphenol) -L-Valine-valeric acid (PAL-PEG) resin was used to provide a free C-terminus. The crude peptide was purified by HPLC and its identity confirmed by mass spectrometry (observed 4329.5, expected 4329.8).

5.2.2 Sample preparation for biophysical assays

For IAPP experiments, a 1.58 mM peptide stock solution was prepared in 100% hexafluoroisopropanol (HFIP) and stored at -4^{o}C. Acid fuchsin was obtained from

Sigma-Aldrich (lot number R3501) and dissolved at 1.58 mM in 20 mM Tris-HCl (pH 7.4) buffer. Samples for the experiments with the $A\beta_{1-40}$ peptide were prepared as follows: 1.0 mg $A\beta_{1-40}$ peptide was dissolved in 400 μL 100mM Tris-HCl (pH 7.4). The solution was vortexed for 10 sec and then centrifuged for 4 min at 17,200g. The supernatant was immediately withdrawn and peptide concentration was determined by UV-Vis at 280 nm. This supernatant was used for the amyloid assays.

5.2.3 Thioflavin-T fluorescence assays

All fluorescence experiments were performed with an Applied Photontechnology Fluorescence Spectrophotometer. An excitation wavelength of 450 nm and emission wavelength of 485 nm was used for the thioflavin-T studies. The excitation and emission slits were set at 6 nm. A 1.0 cm cuvette was used and each point was averaged over 1 min. For these studies, solutions of IAPP were prepared by diluting filtered peptide stock solution (0.45μm filter) into a Tris-HCl buffered (20mM, pH 7.4) thioflavin-T solution immediately before the measurement. The final concentration was 16 μM IAPP and 25 μM thioflavin-T with or without acid fuchsin in 2% HFIP. For $A\beta_{1-40}$ experiments, aliquots of an $A\beta_{1-40}$ stock solution were diluted into 100 mM tris-HCl (pH 7.4) to initiate the reactions in the presence or absence of acid fuchsin. Aliquots were withdrawn at different time points and diluted into Tris-HCl buffered (100mM, pH 7.4) thioflavin-T solution before the measurement.

5.2.4 Transmission electron microscopy (TEM)

Aliquots of fluorescence monitored kinetic assays were analyzed by TEM to characterize morphologies of the species in solution. 15 μL of peptide solution was placed on a carbon-coated Formvar 300 mesh copper grid for 1 min and then negatively stained with saturated uranyl acetate for 1 min.

5.2.5 Circular dichroism spectroscopy (CD)

CD experiments were conducted using an Applied Photophysics Chirascan circular dichroism spectrometer. Aliquots were removed from the kinetic studies when the time course of amyloid formation was complete and CD spectra recorded. Far-UV CD experiments were performed using a 0.1cm quartz cuvette. Wavelength scans were recorded at 25^{o}C and pH 7.4 over a range of 190 to 260 nm. Data points were recorded at 1 nm intervals and averaged over 0.5 sec. Final spectra are the average of 5 repeats. Background spectra were subtracted from the collected data. Samples contained 2% HFIP and 20 mM Tris-HCl (pH 7.4).

5.2.6 Right angle light scattering

Right angle light scattering experiments were conducted using an Applied Photontechnology Fluorescence Spectrophotometer. An irradiation wavelength of 400 nm was used. The samples do not absorb at this wavelength. Samples were prepared in an identical fashion as described for the thioflavin-T studies except that thioflavin-T was

omitted.

5.2.7 Cytotoxicity assays

Transfomed rat insulinoma (INS-1) beta cells were used to assess the ability of acid fuschin to protect against the toxic effects of human IAPP. INS-1 cells were grown in RPMI 1640 (Gibco-BRL) supplemented with 10% fetal bovine serum (FBS), 11 mM glucose, 10 mM Hepes, 2 mM L-glutamine, 1 mM sodium pyruvate, 50 μM β-mercaptoethanol, 100 U/ml penicillin (Gibco-BRL), and 100 U/ml streptomycin (Gibco-BRL). Cells were maintained at 37^{o}C in a humidified environment supplemented with 5% CO_2. Cells were grown for two passages prior to use and used in assays between passages 59 and 65. For toxicity experiments, cells were seeded at a density of 30,000 cells per well in 96-well plates and cultured for 24 hours prior to addition of solutions. Peptide samples and samples of peptide plus acid fuchsin were prepared in Tris-HCl buffer (pH 7.4) and added directly to cells (30% final media concentration) after 11 hours of incubation at room temperature. Alamar blue (Biosource International, CA) reduction was used to assess INS-1 cell toxicity. Alamar blue was diluted ten-fold in 30% culture media and cells were incubated for 5 hours at 37^{o}C. Fluorescence (excitation 530 nm; emission 590 nm) was measured with a Fluoroskan Ascent plate reader (Thermo Labsystems, Helsinki, Finland). Data represent a minimum of three independent experiments performed in triplicate and are plotted as mean +/- standard deviation.

5.2.8 Light microscopy

Changes in cell morphology were examined by light microscopy to provide a second method of evaluating cell viability. Transformed rat INS-1 beta cells were photographed immediately prior to assessment of toxicity by alamar blue cell viability assays. Images were taken using an Olympus BX-61 light microscope.

5.3 Results and discussion

5.3.1 Acid fuchsin is a highly effective inhibitor of *in vitro* amyloid formation by IAPP

The structure of acid fuchsin is displayed in Figure 1. Each of the three rings of the triphenylmethane core is sulfonated and contains an amino group, while one of the rings has an additional methyl substitution. The compound is widely used as a component of histological stains and the sodium salt is commercially available, but its ability to inhibit amyloid formation has not been tested. The primary sequence of human IAPP (IAPP) is also displayed in Figure 5-1. The 37 residue hormone contains a disulfide bond and is amidated.

Figure 5-2 displays the results of a kinetic experiment in which the rate of amyloid formation was measured in the presence and in the absence of acid fuchsin. The kinetics of amyloid formation typically follow a sigmoidal time course consisting of a lag phase during which no amyloid is produced followed by a growth phase which generates amyloid fibrils. The reaction reaches a plateau in which amyloid fibrils are in equilibrium with soluble peptide. The curves displayed in Figure 5-2 represent fluorescence-detected thioflavin-T binding experiments. Thioflavin-T is a small molecule whose fluorescent quantum yield increases significantly when it binds to amyloid fibrils. The mode of dye binding is not known, but it is generally thought to bind to grooves formed by the in-register rows of side chains generated from the regular β-sheet structure of the amyloid fibril (*10*). At a 1:1 ratio of IAPP to inhibitor, no detectable thioflavin-T binding is

observed consistent with the prevention of amyloid formation. Acid fuchsin also inhibits IAPP amyloid formation at substoichiometric concentrations. Significant inhibition is still observed at a ratio of IAPP to acid fuchsin of 5:1 i.e. at a five-fold excess of peptide to inhibitor. The lag phase is increased by a factor of 2 and the final thioflavin-T intensity is reduced to only 25% of that observed in the absence of inhibitor. Inhibition is still observed even at a ratio of IAPP to drug of 10:1. The effects are less pronounced but lag phase is increased while the final fluorescence is reduced by roughly half.

It is important to verify the results of thioflavin-T assays with independent techniques since compounds which show inhibitory effects in thioflavin-T assays can do so because they inhibit thioflavin-T binding to amyloid fibrils or quench the fluorescence of bound thioflavin-T instead of actually inhibiting amyloid formation. Such effects have been observed with IAPP (*159*). Consequently, TEM images were recorded of aliquots removed at the end of the reaction. The TEM images of the sample without inhibitor revealed a dense mat of fibrils with morphologies typical of those reported for *in vitro* IAPP amyloid deposits (Figure 5-2B). In contrast, no fibrils were observed when acid fuchsin was present at a 1:1 ratio (Figure 5-2C). Sparse deposits of fibrils are detected on the grids for the 5:1 peptide to inhibitor sample (Figure 5-2D) and more extensive deposits are observed for the 10:1 peptide to inhibitor sample (Figure 5-2E), but the fibrils appear to be somewhat thinner than those formed by IAPP alone. CD spectra of each sample were also recorded at the end of reaction. CD is sensitive to the presence or absence of secondary structure, and the CD spectrum of IAPP fibrils is consistent with

β-sheet formation. Thus, CD offers a third independent probe of the effectiveness of the inhibitors. In the absence of the inhibitor a CD spectrum is obtained which indicates considerable β-structure (Figure 5-3A). The spectrum is very similar to those reported for fibrillar samples of IAPP. The spectrum of the 1:1 mixture of IAPP and acid fuchsin is very different and indicates less β-structure (Figure 5-3B). Right angle light scattering experiments were also conducted (Figure 5-4). In the absence of acid fuchsin, a sigmoidal increase in scattering was observed with a lag time that is good agreement with that observed in the thioflavin-T fluorescence assay. In contrast, no light scattering is observed over the time course of an experiment when acid fuchsin is present at a 1:1 molar ratio. The results of the TEM, CD and light scattering experiments are all completely consistent with the results of thioflavin-T studies, and provide independent confirmation that the compound effectively inhibits amyloid formation.

5.3.2 Acid fuchsin interrupts the process of amyloid formation if it is added in the lag phase

The observation that acid fuchsin exhibits effects when added at substoichiometric concentrations suggests that it may interact with oligomeric species. If true, then acid fuchsin should also be an effective inhibitor if it is added in the lag phase after amyloid formation has been initiated. This is precisely what is observed. Figure 5-5A shows the effect of adding acid fuchsin in the lag phase. The thioflavin-T fluorescence monitored time course for IAPP in the absence of inhibitor is shown in black. Addition of acid

fuchsin to the lag phase prevents the development of species which are competent to bind thioflavin-T. Interestingly, TEM measurements suggest that acid fuchsin interrupts the process of amyloid formation and may partially trap the species which are populated when it is added. Figure 5-5B shows a TEM image of IAPP in the middle of the lag phase in the absence of inhibitor. An aliquot of the reaction mixture was removed at the midpoint of the lag phase, blotted onto a TEM grid and imaged. A collection of small spherical species are observed with a range of sizes. The experiment was repeated, but acid fuchsin was added at the midpoint of the lag phase, (red arrow), and the reaction allowed to continue for a total of 60 minutes before samples were removed for TEM analysis. This is a time which is more than sufficient for uninhibited IAPP to form amyloid. The micrograph (Figure 5-5C) reveals a collection of spherical objects which are similar, albeit somewhat larger than those observed in the absence of inhibitor, even though the sample with inhibitor was incubated for an additional 55 minutes. The experiment was repeated a second time, but acid fuchsin was added at the end of the lag phase (green arrow). The results of a control experiment are displayed in Figure 5-5D. In this experiment an aliquot of the reaction conducted in the absence of inhibitor was removed at the end of the lag phase, and the TEM image was recorded. If acid fuchsin is added at the end of the lag phase and the reaction then allowed to continue for a total of 60 minutes, a set of short fibril like species are detected (Figure 5-5E) which differ considerably in appearance from mature fibrils, but resemble the species formed at the end of the lag phase in the absence of acid fuchsin (Figure 5-5D). Once again, acid

fuchsin arrests amyloid formation.

5.3.3 Acid fuchsin protects rat INS-1beta cells against IAPP toxicity

We tested the ability of acid fuschin to protect against the toxic effects of IAPP amyloid formation using transformed rat insulinoma (INS-1) beta cells. This is a standard cell line for IAPP toxicity studies. Thirty micromolar human IAPP proved toxic to cells and reduced cell viability by 90% relative to control cells treated with acid fuchsin alone (Figure 5-6A). In contrast, a 1:1 molar ratio mixture of 30 μM hIAPP and 30 μM acid fuschsin protected cells from IAPP toxicity, leading to a loss of only 10% cell viability compared to control cells. Differences in INS-1 cell morphology were apparent between the 30 μM IAPP-treated and acid fuchsin/IAPP-treated cells under the light microscope. The 30 μM hIAPP-treated cells showed extensive cell shrinkage and detachment of the cells from the cell culture substratum (Figure 5-6). These changes, which are characteristic of apoptotic cells, were absent in acid fuchsin/hIAPP-treated and acid fuchsin control cells (Figure 5-6C and D) confirming the results of the alamar blue cell viability assays.

5.3.4 Not all sulfonated molecules inhibit IAPP amyloid formation, but electrostatic interactions appear to be important for the interaction of acid fuchsin and IAPP.

A range of simple sulphonated compounds have been used as inhibitors of amyloid formation by other peptides, and several low molecular weight sulfonated molecules have

entered clinical trials. For example, Tramiprosate (3-amino-1-propane sulfonic acid) has been shown to be an effective inhibitor of *in vitro* amyloid formation by Aβ and reduces the amyloid burden in TgCRND8 mice, while eprodisate (1, 3-propanedisulfonic acid) has been tested as a potential therapeutic agent for AA amyloidosis (*80-83, 160*). These studies together with the results reported here for acid fuchsin may give the impression that merely using a sulfonated small molecule leads to an inhibitor of IAPP amyloid, but this is not the case. For example, we tested the ability of Tramiposate to inhibit amyloid formation by IAPP. The compound had virtually no effect even when added in a 20 fold excess by weight which corresponds to a 562 fold molar excess. The lag time observed during thioflavin-T monitored kinetic experiments was essentially unchanged and TEM studies revealed that extensive fibrils were still formed even in the presence of a large excess of the compound (Figure 5-7). Furthermore, it is well documented that some sulfated glycosaminoglycans are potent enhancers of amyloid formation by IAPP (*47-48*). Thus, the potent effects of acid fuchsin are not simply a consequence of it being sulfonated. Electrostatic interactions are, however, important for the effective interaction of acid fuchsin with IAPP. We tested the ability of acid fuchsin to inhibit IAPP amyloid formation in the presence of 500 mM NaCl. The compound is a much less effective inhibitor under high salt concentrations as judged by thioflavin-T kinetic experiments and TEM. Figure 5-8 shows that the addition of acid fuchsin at a 1:1 ratio has a very small effect on the time course of amyloid formation in the presence of high salt. Note that amyloid formation is faster under high salt conditions because of the screening of

electrostatic interactions among IAPP molecules (*161*). TEM images collected at the end of the reaction reveal that both samples formed amyloid.

5.3.5 Acid fuchsin is not as an effective inhibitor of amyloid formation by the Aβ peptide.

IAPP and the Aβ peptide share some features in common, and some inhibitors of IAPP amyloid formation have proven effective against Aβ *in vitro* (*162-163*). Thus, it is reasonable to test the ability of acid fuchsin to inhibit amyloid formation by Aβ, especially given that some other sulfonated compounds are inhibitors of amyloid formation by Aβ. Acid fuchsin does have some effect on the ability of Aβ to form amyloid, but the results are much less dramatic than observed with IAPP. The time required to reach 50% completion of amyloid formation, t_{50}, is modestly longer in the presence of 25 μM acid fuchsin and TEM images collected at the end of the kinetic experiments (Figure 5-9) suggest that fewer amyloid fibrils are formed, but the overall effect is considerably less than observed with IAPP. These results indicate that acid fuchsin exhibits some specificity toward IAPP.

5.4 Conclusions

The data presented here clearly demonstrate that the simple sulfonated triphenylmethane derivative acid fuchsin is an effective inhibitor of amyloid formation by IAPP, and also confers protection from the toxic effects of human IAPP in cell culture.

The efficiency of the compound is not simply a consequence of it being sulfonated since prior work has demonstrated that some sulfonated compounds are enhancers of amyloid formation by IAPP and the work reported here shows that other sulphonated low molecular weight inhibitors of amyloid formation by Aβ are not effective inhibitors of amyloid formation by IAPP. However, electrostatic interactions are clearly important since the compound is a much less effective inhibitor in the presence of high salt. The fact that acid fuchsin displays noticeable effects even at substoichiometric ratios suggests that it can bind to oligomeric species, a conjecture which was suggested by the studies in which it was added during the lag phase. The experiments with the Aβ peptide show that acid fuchsin displays some specificity in its ability to inhibit amyloid. Acid fuchsin is an interesting lead compound and offers a new structural class of potential amyloid inhibitors to explore.

(A)

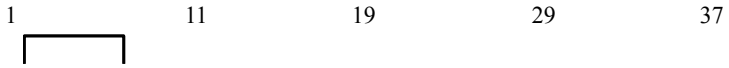

(B)

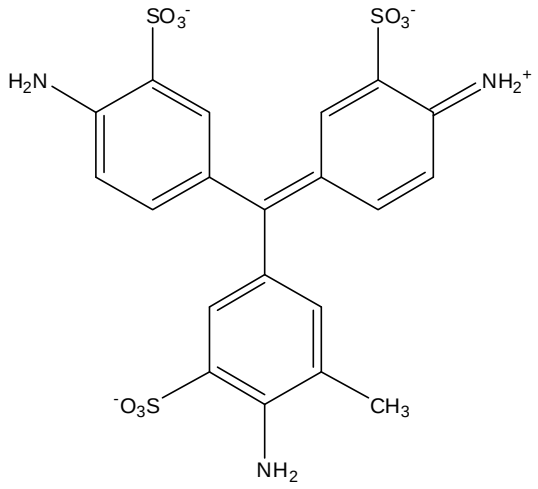

Figure 5-1: (A) The primary sequence of human IAPP. The peptide contains a disulfide bridge between Cys-2 and Cys-7 and has an amidated C-terminus. (B) The structure of acid fuchsin.

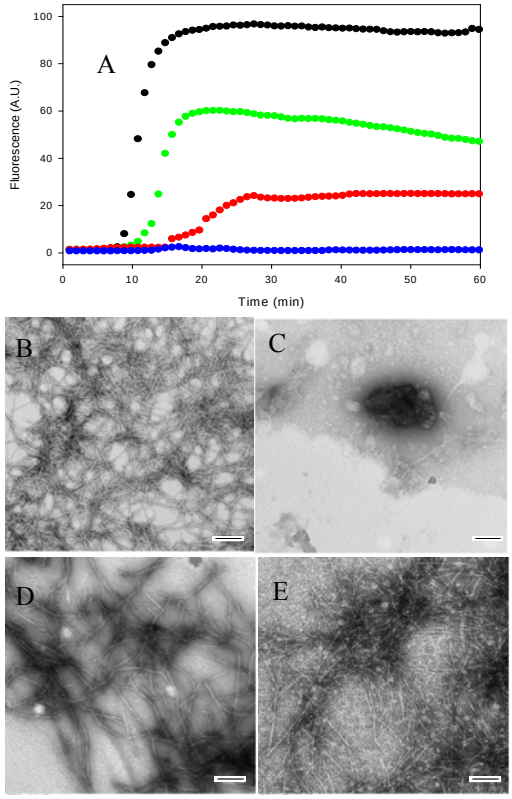

Figure 5-2: Acid fuchsin inhibits amyloid formation by human IAPP. (A) Fluorescent detected thioflavin-T kinetic assays are displayed: IAPP alone (black); A 1:1 molar ratio mixture of acid fuchsin and IAPP (blue) samples were 16 μM IAPP and 16 μM acid fuchsin; A 5:1 molar ratio mixture of IAPP and acid fuchsin (red), samples were 16 μM IAPP and 3.2 μM acid fuchsin; A 10:1 molar ratio mixture of IAPP and acid fuchsin (green), samples were 16 μM IAPP and 1.6 μM acid fuchsin. Peptide solutions contained 20 mM Tris-HCl buffer (pH 7.4) and 2% HFIP by volume and were continually stirred at 25^{o}C. (B-E) TEM studies confirm that acid fuchsin inhibits amyloid formation by IAPP. (B) Image of IAPP alone. (C) Image of a 1:1 mixture of IAPP and acid fuchsin. (D) Image of a 5:1 mixture of IAPP and acid fuchsin. (E) Image of a mixture of 10:1 mixture of IAPP and acid fuchsin. Samples were those used for the kinetic experiments depicted in Figure A. Aliquots were removed from the kinetic experiments after 60 minutes. Scale bars represent 100 nm.

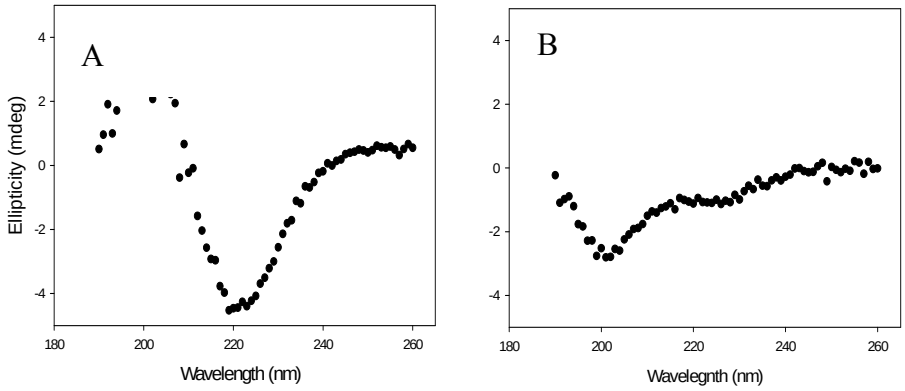

Figure 5-3: Far UV CD spectra further confirm that acid fuchsin is a good inhibitor of amyloid fibril formation. (A) Wildtype IAPP. (B) A 1:1 mixture of wildtype IAPP and acid fuchsin. The samples were those used for the kinetic assays depicted in Figure 2. Aliquots were removed at 60 minutes. Solutions contained 2% HFIP, 20 mM Tris-HCl (pH 7.4) and 25μM thioflavin-T. Spectra were recorded at 25 ºC.

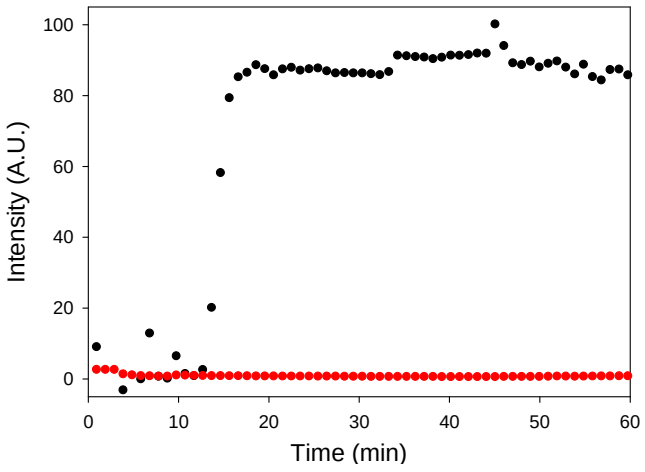

Figure 5-4: Right angle light scattering confirms that acid fuchsin inhibits amyloid formation by IAPP. Black, IAPP alone; Red, IAPP:acid fuchsin at a 1:1 molar ratio. Samples were 16 μM IAPP, 20 mM Tris-HCl, pH 7.4, 2% HFIP. Acid fuchsin, when present, was at 16 μM. Experiments were conducted with constant stirring. The wavelength of irradiation was 400 nm.

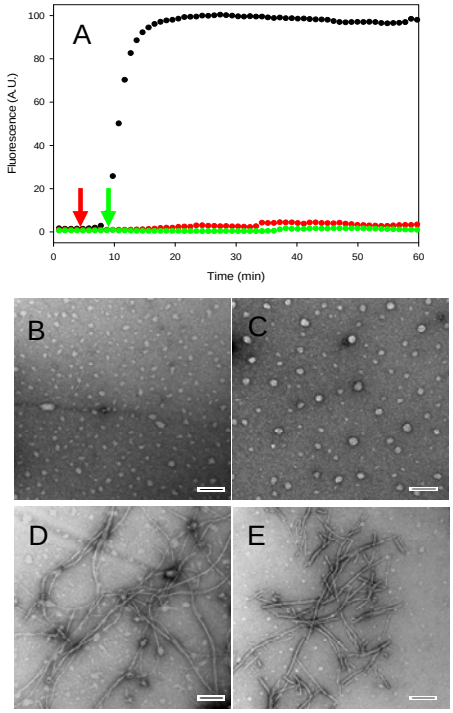

Figure 5-5: Acid fuschin inhibits amyloid formation if it is added during the lag phase. (A) Fluorescent detected thioflavin-T kinetic assays are displayed: IAPP alone (black); A 1:1 molar ratio mixture of acid fuchsin and IAPP with acid fuchsin added at 5 minutes (red arrow); A 1:1 molar ratio mixture of IAPP and acid fuchsin with acid fuchsin added at 9 minutes (green arrow). (B) TEM image of IAPP alone at 5 minutes (C) Image of 1:1 mixture of acid fuchsin and IAPP. Acid Fuchsin was added at 5 minutes and the reaction allowed to proceed for an additional 55 minutes before an aliquot was removed for TEM analysis. (D) Image of IAPP alone at 9 minutes. (E) Image of a 1:1 mixture of acid fuchsin and IAPP. Acid fuchsin was added at 9 minutes and the reaction allowed to proceed for an additional 51 minutes before an aliquot was removed for TEM analysis. Samples were 16 μM IAPP and 16 μM acid fuchsin; Solutions contained 20 mM Tris-HCl buffer (pH 7.4) and 2% HFIP by volume and were continually stirred at 25^{o}C.

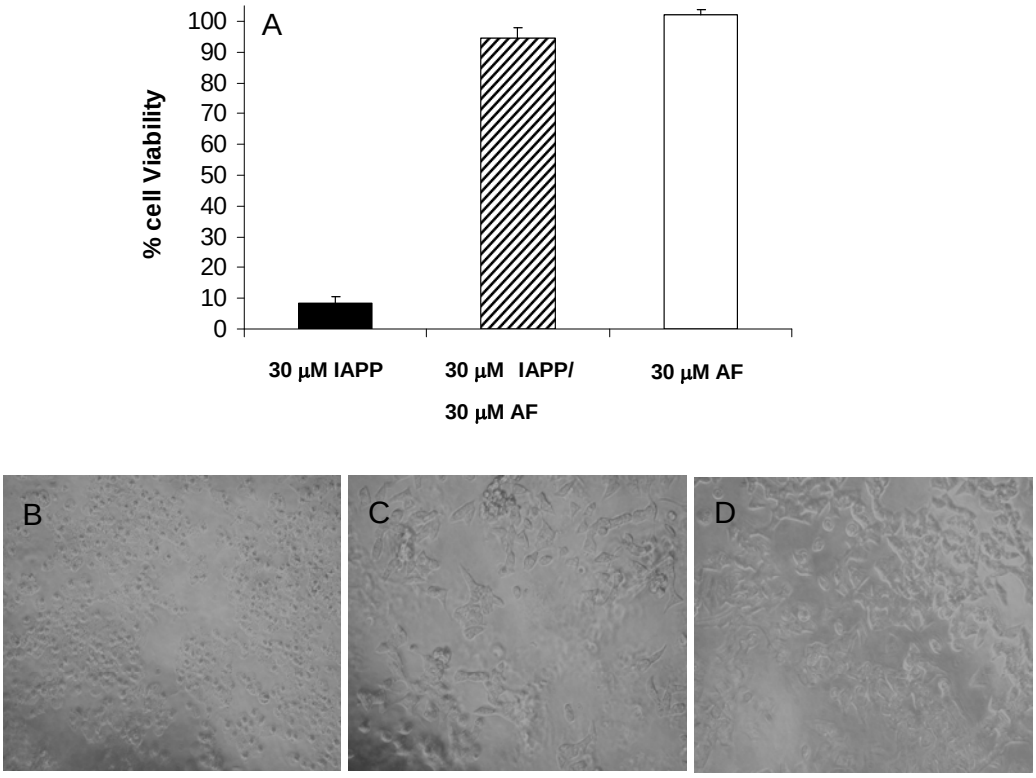

Figure 5-6: Acid fuschin is not cytotoxic and protects rat INS-1 beta cells from human IAPP induced toxicity**.** (A) Alamar blue cell viability assays. Data are plotted as percent cell viability relative to control cells treated with buffer only. Data represent a minimum of three independent experiments performed in triplicate and are plotted as mean +/- standard deviation. (B-D) Evaluation of cell morphology by light microscopy**.** (B) Transformed rat INS-1 beta cells treated with 30 μM human IAPP show cell rounding and detachment from the cell culture substratum, indicative of apoptosis. By contrast, INS-1 cells treated with either (C) a 1:1 molar ratio of 30 μM human IAPP plus 30 μM acid fuschin or (D) 30 μM acid fuschin alone show few signs of apoptosis. Bright field images were obtained immediately before Alamar blue assays. Cell toxicity experiments were performed by Dr. Andisheh Abedini in Professor Verchere's laboratory at the University of British Columbia.

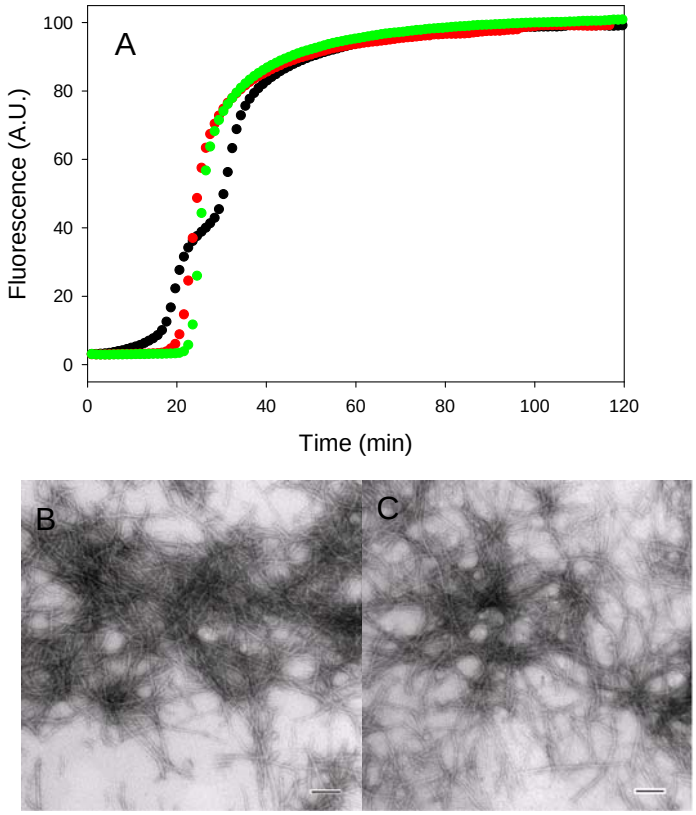

Figure 5-7: (A) Thioflavin-T monitored kinetic assays of the time course of IAPP amyloid formation in the presence of varying amounts of 3-aminopropane sulfonic acid (3APS, Tramprosate). Black, IAPP alone; Red, IAPP:3APS 1:20, i.e. 20 fold excess of 3APS on a molar basis; Green, IAPP:3APS 1:20 (w/w), i.e. a 20 fold excess on a weight to weight basis. This corresponds to a 562 fold excess on a molar basis. Samples were pH 7.4 in 20 mM Tris-HCl buffers and 25 μM thioflavin-T. The concentration of IAPP was 16 μM IAPP. The solutions contained 2% HFIP by volume and were continually stirred at 25^{o}C. (B) TEM image of IAPP:3APS 1:20, i.e. 20 fold excess of 3APS on a molar basis; (C) TEM image of IAPP:3APS 1:20 (w/w) i.e. a 20 fold excess on a weight to weight basis. Scale bars represent 100nm.

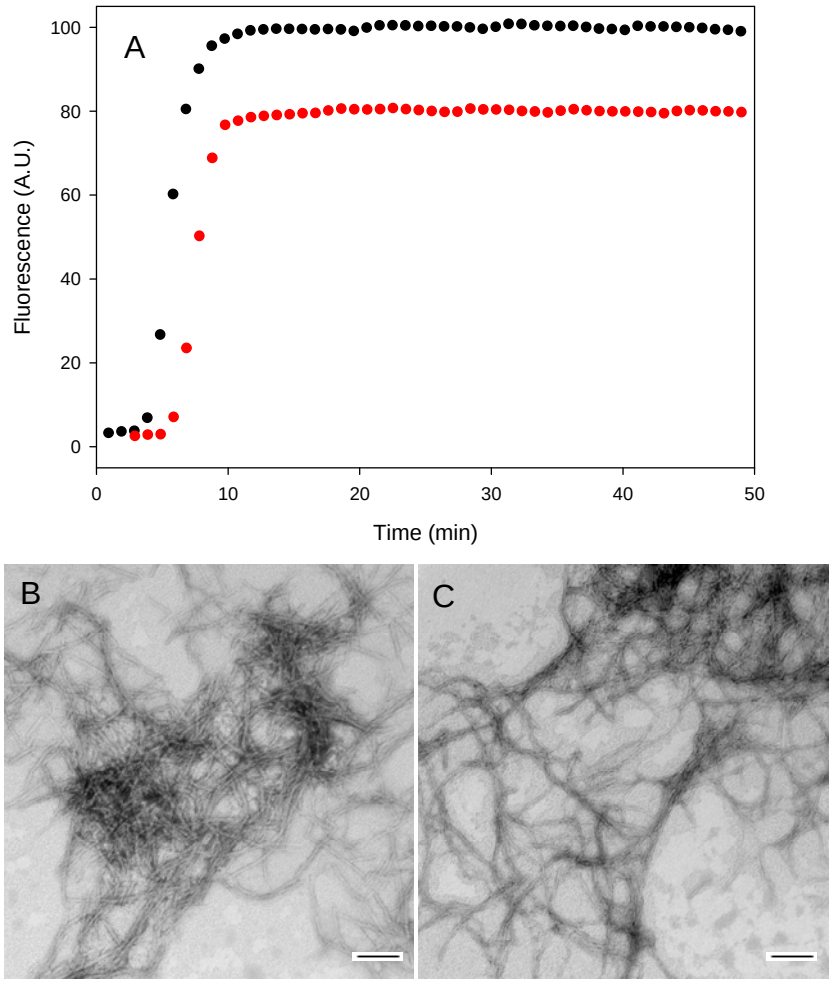

Figure 5-8: Electrostatic interactions are important for effective inhibition of IAPP amyloid formation. (A) Thioflavin-T fluorescence monitored kinetic experiments in the presence of 500 mM NaCl: IAPP alone (black); a 1:1 mixture of acid fuchsin and IAPP (red). (B) TEM image of a sample of IAPP from the end of the kinetic experiment. (C) TEM image of an aliquot of the 1:1 mixture of IAPP and acid fuchsin collected at the end of the kinetic experiment. Samples were 16 μM IAPP with or without 16 μM acid fuchsin. Solutions contained 20 mM Tris-HCl buffer (pH 7.4), 500 mM NaCl and 2% HFIP by volume and were continually stirred at 25^{o}C. Scale bars represent 100 nm.

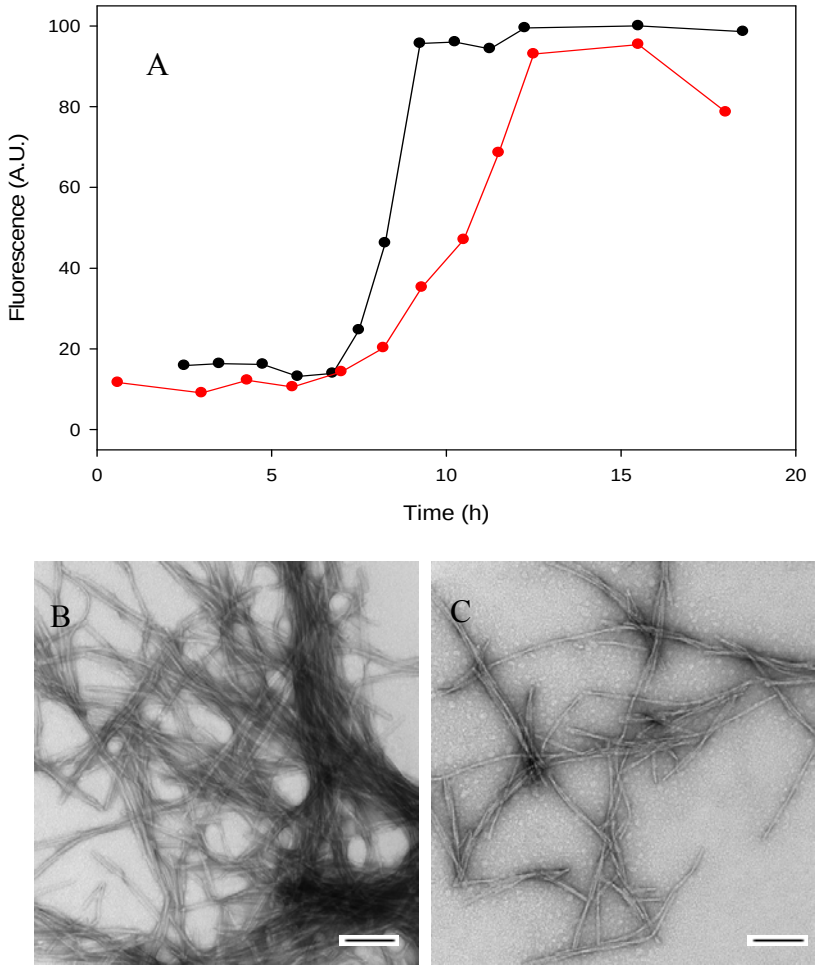

Figure 5-9: Acid fuchsin is a less effective inhibitor of amyloid formation by the $A\beta_{1\text{-}40}$ peptide. (a) Thioflavin-T fluorescence monitored kinetic experiments. $A\beta_{1\text{-}40}$ alone (black); a 1:1 mixture of acid fuchsin and $A\beta_{1\text{-}40}$ (red). (b) TEM image of a sample of $A\beta_{1\text{-}40}$ from the end of the kinetic experiment. (c) TEM image of a sample of the 1:1 mixture of $A\beta_{1\text{-}40}$ and acid fuchsin collected at the end of the kinetic experiments. Samples were 25 μM $A\beta_{1\text{-}40}$ with or without 25 μM acid fuchsin. Solutions contained 100 mM Tris-HCl buffer (pH 7.4) and were continually stirred at 25°C. Scale bars represent 100 nm.

6. Sulfated triphenyl methane derivatives are potent inhibitors of amyloid formation by pro-islet amyloid polypeptide processing intermediates and inhibit glycosaminoglycan mediated amyloid formation.

Abstract

Islet amyloid polypeptide, (IAPP also known as amylin), is responsible for islet amyloid formation in type 2 diabetes and IAPP induced toxicity is believed to contribute to the loss of β-cell mass associated with the late stages of type 2 diabetes. Islet amyloid formation may also play a role in graft failure after transplantation. IAPP is produced as a prohormone, proIAPP, and processed in the secretory granules of the pancreatic beta cells. Partially processed forms of proIAPP are found in amyloid deposits. Most notably, a 48 residue intermediate, $proIAPP_{1-48}$, which includes the N-terminal pro extension, but which has been properly processed at the C-terminus has been identified. It has been suggested that incomplete processing plays a role in amyloid formation by promoting interactions with sulfated proteoglycans of the extracellular matrix. Here we show that acid fuchsin (3-(1-(4-Amino-3-methyl-5-sulphonatophenyl)-1-(4-amino-3-sulphonatophenyl) methylene) cyclohexa-1,4-dienesulphonic acid), a simple sulfonated triphenyl methyl derivative, is a potent inhibitor of amyloid formation by the $proIAPP_{1-48}$ intermediate.

The more complicated triphenyl methane derivative fast green FCF, {ethyl-[4-[[4-[ethyl -[(3-sulfophenyl) methyl] amino] phenyl]-(4-hydroxy-2- sulfophenyl) methylidene]-1-cyclohexa-2,5-dienylidene]- [(3-sulfophenyl) methyl] azanium}, also inhibits amyloid formation by mature IAPP and the proIAPP processing intermediate. Both compounds inhibit amyloid formation by mixtures of the proIAPP intermediate and the model glycosaminoglycan heparan sulfate. The ability to inhibit amyloid formation is not just a consequence of the compounds being sulfonated, since the sulfonated inhibitor of Aβ 3-amino-1-propanesulfonic acid, tramprosate, does not inhibit amyloid formation by $proIAPP_{1-48}$ even when added in 40 fold excess.

NOTE: The material presented in this chapter has been submitted (Fanling Meng and Daniel P. Raleigh "Inhibit Glycosaminoglycan Mediated Amyloid Formation by Islet Amyloid Polypeptide and pro-Islet Amyloid Polypeptide Processing Intermediate"). This chapter contains direct excerpts from the manuscript which was written by me with suggestions and revisions from Professor Daniel P. Raleigh.

6.1 Introduction

IAPP is stored in the pancreatic β-cells in the same secretory granules as insulin, processed in parallel with insulin and secreted in response to the same stimuli (*16, 164-167*). IAPP is produced as a 89 residue preprohormone, preproIAPP. Cleavage of the signal sequence generates a 67 residue pro-form, denoted as proIAPP. ProIAPP is further processed to yield the mature 37 residue hormone by the enzymes prohormone convertase 2 and 1/3 which cleave proIAPP at the N-terminus and the C-terminus respectively. Cleavage at the C-terminus is followed by a series of steps leading to an amidated C-terminus (*16, 44, 106-108*). Immunohistochemical studies of islet amyloid have demonstrated the presence of a processing intermediate which corresponds to the first 48 residues of proIAPP (proIAPP$_{1-48}$) that contains the N-terminal prosequence, but not the C-terminal prosequence (Figure 6-1) (*42-43, 103-105*). Abnormal processing of proIAPP has been suggested to play an important role in islet amyloid formation and increased levels of incomplete processing have been suggested to correlate with cell death (*103-104, 168*).

In one model of islet amyloid formation, incomplete processing of proIAPP leads to interactions with heparan sulfate proteoglycans (HSPGs) of the basement membrane which promotes amyloid formation by generating a high local concentration of an amyloidogenic polypeptide (*45-46, 169*). The amyloid fibrils thus formed act as a seed to induce additional partially processed IAPP and mature IAPP to form amyloid. HSPGs are well known to be associated with *in vivo* amyloid deposits, including islet amyloid (*47-50,*

52, 109, 170). The model makes several predictions; first, proIAPP$_{1-48}$ is predicted to bind to HSPG's and second, the binding is predicted to enhance the rate of amyloid formation. The amyloid thus formed is also predicted to be able to seed amyloid fibril formation by fully processed mature IAPP. Verchere and cowokers have shown that proIAPP$_{1-48}$ binds to HSPGs and the binding site has been localized via peptide fragment studies (*45-46*). Our recent *in vitro* experiments have provided proof of principle evidence that HSPGs promote amyloid formation by the proIAPP$_{1-48}$ intermediate and have also shown that fibrils formed by the interaction of proIAPP$_{1-48}$ with glycosaminoglycans (GAGs) can seed amyloid formation by mature IAPP (*169*).

The development of inhibitors of amyloid formation is an active area of research, both because of their possible therapeutic applications, and because they can serve as reagents to probe mechanisms of toxicity and pathways of amyloid assembly (*69, 85, 121, 148-150*). There are a number of reports of inhibitors of amyloid formation by IAPP, but to the best of our knowledge, there have been no reported amyloid inhibitors designed to target amyloid formation by proIAPP intermediates or glycosaminoglycan (GAG) mediated amyloid formation by proIAPP processing intermediates (*75, 85, 93, 119, 121, 156-158, 171*).

The simple sulfonated triphenylmethyl derivative, acid fuchsin, (3-(1-(4-Amino-3-methyl-5-sulphonatophenyl)-1-(4-amino-3-sulphonatophenyl) methylene) cyclohexa-1,4-dienesulphonic acid) is an potent inhibitor of amyloid formation by mature IAPP in the absence of GAGs (*171*). Here we show that acid fuchsin

inhibits amyloid formation by proIAPP processing intermediates and by mixtures of proIAPP and heparan sulfate (Figure 6-1). We also report that a second sulfonated triphenyl derivative fast green FCF, {ethyl-[4-[[4-[ethyl -[(3-sulfophenyl) methyl] amino] phenyl]-(4-hydroxy-2- sulfophenyl) methylidene]-1-cyclohexa-2,5-dienylidene]-[(3-sulfophenyl) methyl] azanium}, is an effective inhibitor of amyloid formation by IAPP and proIAPP processing intermediates, and inhibits GAG mediated amyloid formation.

6.2 Materials and Methods

6.2.1 Peptide synthesis and purification

Peptides were synthesized on a 0.25 mmol scale using an applied Biosystems 433A peptide synthesizer, by 9-fluornylmethoxycarbonyl (Fmoc). Pseudoprolines were incorporated to facilitate the synthesis (*113*). 5-(4'-fmoc-aminomethyl-3',5-dimethoxyphenol) valeric acid (PAL-PEG) resin was used to afford an amidated C-terminal. Standard Fmoc reaction cycles were used. The first residue attached to the resin, β-branched residues, residues directly following β-branched residues and pseudoprolines were double coupled. Crude peptides were oxidized by dimethyl sulfoxide (DMSO) for 24 hours at room temperature (*140*). The peptides were purified by reverse-phase HPLC using a Vydac C18 preparative column. A two-buffer system was utilized. Buffer A consists of H_2O and 0.045% HCl (v/v). Buffer B consists of 80% acetonitrile, 20% H_2O, and 0.045% HCl (v/v). The gradient used was 0-70%

buffer B in 70 minutes. The pure IAPP and proIAPP$_{1-48}$ peptides eludated out at 50 (50% buffer B) and 52 minutes (52% buffer B) respectivly. Analytical HPLC was used to check the purity of the peptides. The identity of the pure peptides was confirmed by mass spectrometry using a Bruker MALDI-TOF MS (IAPP observed 3904.6, expected 3904.8; proIAPP$_{1-48}$ observed 5209.5, expected 5209.9).

6.2.2 Sample preparation

1.58 mM peptide stock solutions were prepared in 100% hexafluoroisopropanol (HFIP) and stored at 4^{o}C. Acid fuchsin and fast green FCF were obtained from Sigma-Aldrich, lot numbers F8129 and F7252 respectively, and dissolved at 1.58 mM in 20 mM Tris-HCl (pH 7.4) buffer. Heparan sulfate was obtained from Sigma-Aldrich. A heparan sulfate stock solution was prepared in 20 mM Tris-HCl (pH 7.4) buffer at 2mg/2.2ml.

6.2.3 Thioflavin-T fluorescence

All fluorescence experiments were performed with an Applied Photontechnology Fluorescence Spectrophotometer. An excitation wavelength of 450 nm and emission wavelength of 485 nm was used for the thioflavin-T studies (*10*). The excitation and emission slits were set at 6 nm. A 1.0 cm cuvette was used and each point was averaged for 1 minute. Solutions were prepared by diluting filtered stock solution (0.45μm filter) into a Tris-HCl buffered (20mM, pH 7.4) thioflavin-T solution immediately before the

measurement. The final composition of the solutions was 32 μM peptide and 25 μM thioflavin-T with or without inhibitor in 2% HFIP. For experiments which involve proIAPP$_{1-48}$/heparan sulfate mixtures, the final conditions were 32 μM peptide, 2.7 μM heparan sulfate and 25 μM thioflavin-T in 20 mM Tris-HCl buffer (pH 7.4) 2% HFIP. All solutions were stirred during the fluorescence experiments.

6.2.4 Transmission electron microscopy (TEM)

15 μL samples of peptide solution were removed at the end of the thioflavin-T monitored kinetic experiments and placed on a carbon-coated Formvar 300 mesh copper grid for 1 min and then negatively stained with saturated uranyl acetate for 1 min. The same solutions that were used for the fluorescence measurements were used so that samples could be compared under as similar conditions as possible.

6.2.5 Circular dichroism spectroscopy (CD)

CD experiments were conducted using an Applied Photophysics Chirascan circular dichroism spectrometer. Far-UV CD experiments were performed using a 0.1cm quartz cuvette. Wavelength scans were recorded at 25^{o}C, pH 7.4 over a range of 190 to 260nm, at 1nm intervals with an averaging time of 0.5 second and are the result of 5 repeats. Background spectra were subtracted from the collected data. Samples were in pH 7.4, 2% HFIP and 20mM Tris-HCl.

6.3 Results and discussion

6.3.1 Acid fuchsin is a potent inhibitor of amyloid formation by proIAPP$_{1-48}$

The sequence of proIAPP$_{1-48}$ and mature IAPP are shown in Figure 6-1. The 11 additional residues found in proIAPP$_{1-48}$ decrease the overall hydrophobicity and increase the net charge of the polypeptide relative to mature IAPP, but they significantly increase the ability to bind GAGs (*45-46, 169*). The structure of acid fuchsin and fast green FCF are displayed in Figure 6-1 and are built off a triphenylmethane core. Each ring in acid fuchsin is sulfonated and has an amino substituant, while one of the three rings has a methyl substituant. The structure of fast green FCF is more complex, but it is based on the same triphenylmethane core and it is sulfonated.

We have previously shown that acid fuchsin is an effective inhibitor of amyloid formation by mature IAPP, but its effect on amyloid formation by proIAPP$_{1-48}$ has not been examined (*171*). The ability of fast green FCF to inhibit amyloid formation by mature IAPP or proIAPP$_{1-48}$ has not yet been studied. Figure 6-2 displays the results of a kinetic experiment in which the rate of amyloid formation by proIAPP$_{1-48}$ was measured in the presence and in the absence of acid fuchsin using fluorescence detected thioflavin-T binding assays. Thioflavin-T is a widely used small molecule probe of amyloid formation. The fluorescent quantum yield of the dye increases significantly when it binds to amyloid fibrils, although the exact mode of dye binding is not known (*10*). In the absence of acid fuchsin, proIAPP$_{1-48}$ displays the classic sigmoidal curve expected for amyloid formation. ProIAPP$_{1-48}$ is less amyloidgenic than mature IAPP in

homogeneous solution and the lag time is longer for proIAPP$_{1-48}$ than for mature IAPP (*169, 172*). No detectable thioflavin-T binding is observed at a 1:1 ratio of proIAPP$_{1-48}$ to inhibitor, consistent with the prevention of fibril formation. It is important to independently confirm the results of thioflavin-T binding assays, since they can sometimes give false positives or false negatives (*159*). Therefore, CD and TEM studies were conducted. TEM images of proIAPP$_{1-48}$ display numerous amyloid fibrils in the absence of acid fuchsin, but no fibrils are detectable in the presence of inhibitor (Figure 6-2). The CD spectrum of proIAPP$_{1-48}$ at the end of reaction has an intense β-sheet signal in the absence of acid fuchsin, which is not detected when acid fuchsin is present (Figure 6-3). The CD and TEM studies confirm the conclusions of the thioflavin-T assays and provide further evidence that the compound effectively inhibits amyloid formation by proIAPP$_{1-48}$.

6.3.2 Acid fuchsin inhibits glycosaminoglycan (GAG) promoted amyloid formation by proIAPP$_{1-48}$

The N-terminal region of proIAPP promotes binding to GAGs, and GAGs such as heparan sulfate have been shown to catalyzed amyloid formation by proIAPP$_{1-48}$ (*169*). Thus, we tested the effects of acid fuchsin on amyloid formation by mixtures of proIAPP$_{1-48}$ and heparan sulfate. Mixtures of proIAPP$_{1-48}$ and heparan sulfate form amyloid very quickly under the conditions of our studies (Figure 6-4). The proIAPP$_{1-48}$ heparan sulfate mixture has a lag phase of only 6 minutes under the conditions of these

experiments, while $proIAPP_{1-48}$ in the absence of GAG has a lag phase on the order of 25 minutes. The $proIAPP_{1-48}$ heparan sulfate complex has higher initial fluorescence intensity than $proIAPP_{1-48}$ alone, probably because heparan sulfate accelerates aggregation and β-sheet structure formation which leads to the rapid formation of a structure which can bind thioflavin-T (*169*). In the presence of an equimolar amount of acid fuchsin, the $proIAPP_{1-48}$ heparan sulfate mixture shows only a modest total increase in thioflavin-T fluorescence intensity during an 80 minute kinetic run and the final thioflavin-T intensity is only 50% of that observed for $proIAPP_{1-48}$ and heparan sulfate in the absence of inhibitor. The effects of acid fuchsin are more pronounced when the compound is added in 10 fold molar excess. In this case, acid fuchsin abolishes amyloid formation by the $proIAPP_{1-48}$ heparan sulfate mixture. The ability of acid fuchsin to inhibit heparan sulfate catalyzed amyloid formation by $proIAPP_{1-48}$ was confirmed by TEM (Figure 6-4). In the absence of inhibitor, a dense network of amyloid fibrils was observed for the sample of $proIAPP_{1-48}$ plus heparan sulfate at the end of the reaction. Addition of acid fuchsin at a 1:1 ratio results in much thinner and less prevalent fibrils, while the 10:1 mixture (acid fuchsin in 10 fold excess) was devoid of fibrils. Consistent with the TEM results, CD spectroscopy confirmed some β-sheet formation for the 1:1 mixture of inhibitor with $proIAPP_{1-48}$ heparan sulfate (Figure 6-3). A 10:1 ratio of inhibitor to peptide could not be tested by CD or thioflavin-T fluorescence because the high absorbance of acid fuchsin interfered with the CD measurement and led to strong inner filter effects in fluorescence measurements.

6.3.3 Fast green FCF inhibits amyloid formation by mature IAPP and proIAPP$_{1-48}$, but is less effective than acid fuchsin

We first examined the ability of fast green FCF to inhibit amyloid formation by mature IAPP. No thioflavin-T fluorescence is observed when fast green FCF is present at a 1:1 ratio of compound to IAPP (Figure 6-5). TEM images recorded at the end of the kinetic experiment, (80 minutes), reveal narrow, short, bent structures which differ from classic amyloid fibrils on some portions of the grid and more typical fibrils on others (Figure 6-5). CD spectroscopy reveals that the material contains β-sheet structure. We also examined the effects of fast green FCF when it is added in a 10 fold excess relative to IAPP. Inner filter effects prevent thioflavin-T experiments and CD spectra can not be recorded because of the high absorbance of the sample, but no fibrils are observed in the TEM images collected after 80 minutes. The data indicates that fast green FCF does inhibit amyloid formation by mature IAPP, but is noticeably less effective than acid fuchsin. Acid fuchsin has been shown to have significant effects even at substoichiometric ratios of compound to mature IAPP and no fibrils like aggregates were detected in a 1:1 sample of acid fuchsin with mature IAPP while CD spectroscopy indicated no significant β-sheet structure formation (*171*).

Fast green FCF also inhibits amyloid formation by the proIAPP$_{1-48}$ intermediate, but again, less effectively than does acid fuchsin. Figure 6-6 displays the thioflavin-T monitored kinetics of proIAPP$_{1-48}$ amyloid formation in the presence and in the absence

of fast green FCF. The sample of proIAPP$_{1-48}$ without fast green FCF shows a typical sigmoidal kinetic curve and dense mats of fibrils are observed by TEM. No significant thioflavin-T fluorescence is observed for the 1:1 mixture of fast green FCF with proIAPP$_{1-48}$ and the TEM images recorded from samples removed at the end of the kinetic run, (80 minutes), are very different from those observed in the absence of inhibitor. Small, bent, elongated structures are detected in most images, while some show more fibril like objects (Figure 6-6). The CD spectrum of the 1:1 mixture of compound with proIAPP$_{1-48}$ reveals significant β-structure (Figure 6-7). Experiments were also conducted with a 10 fold excess of fast green FCF. Again, the high absorbance of the sample prevents thioflavin-T studies and CD measurements, but TEM images recorded after 80 minutes of incubation were devoid of fibril like structures (Figure 6-6). Thus, the results obtained with proIAPP$_{1-48}$ are similar to those obtained with mature IAPP; fast green FCF is an inhibitor of amyloid formation but is less effective than acid fuchsin. It is also worth noting that the studies with fast green FCF provide another example of the difficulty of relying only on thioflavin-T based assays since the thioflavin-T studies would suggest, erroneously, that fast green FCF was as effective at inhibiting amyloid formation as acid fuchsin.

6.3.4 Fast green FCF also inhibits amyloid formation by proIAPP$_{1-48}$ in the presence of heparan sulfate, but is less effective than acid fuchsin

Fast green FCF also has an effect on GAG mediated amyloid formation by

proIAPP$_{1-48}$. Figure 6-8 displays the results of a kinetic experiment involving a mixture of proIAPP$_{1-48}$ and heparan sulfate conducted in the presence and absence of compound. Thioflavin-T curves are included for completeness, but as noted above, can be misleading for fast green FCF in the absence of additional data. More informative are the TEM images. The images collected of the 1:1 mixture of fast green FCF with proIAPP$_{1-48}$ heparan sulfate differ from those recorded for samples which lacked the compound. More pronounced differences are observed when the compound is added in a 10 fold excess (Figure 6-8). Some short fibril like species are detected, but the morphology is different from the fibrils formed in the absence of fast green FCF and they are less prevalent. None-the-less, the TEM data clearly indicates that a 10 fold excess of fast green FCF is less effective than acid fuchsin at inhibiting GAG mediated amyloid formation by the mixture of proIAPP$_{1-48}$ heparan sulfate. CD measurements (Figure 6-7) show that the proIAPP$_{1-48}$ heparan sulfate mixture forms β-structure in the presence of a 1:1 mixture of fast green FCF.

6.4 Conclusions

Acid fuchsin and fast green FCF are, to the best of our knowledge, the first compounds which have been shown to inhibit amyloid formation by the proIAPP$_{1-48}$ processing intermediate. Both also have effects upon GAG mediated amyloid formation. Acid fuchsin is the more effective inhibitor in both the presence and in the absence of GAG.

The ability of the compounds to inhibit amyloid formation is likely to be due in part to the presence of sulfonated groups (*171*), but additional features are required since not all sulfonated compounds are inhibitors of proIAPP$_{1-48}$ amyloid formation. GAGs such as heparan sulfate, for example, clearly accelerate the process. In addition, not all sulfonated small molecules are inhibitors. For example, tramprosate, which is an inhibitor of amyloid formation by the Aβ peptide (*82*), has no detectable effect on amyloid formation by proIAPP$_{1-48}$ (Figure 6-9). Aromatic aromatic interactions between inhibitors and IAPP have been proposed to be important (*119, 158*) and acid fuchsin may be an effective inhibitor because it combines an aromatic core with multiple sulfonates. The weaker effects observed with fast green FCF may reflect the different relative spacing of the sulfonates.

A

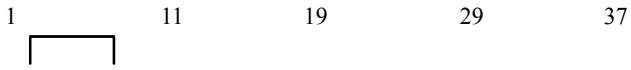

B

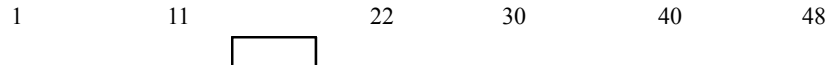

C

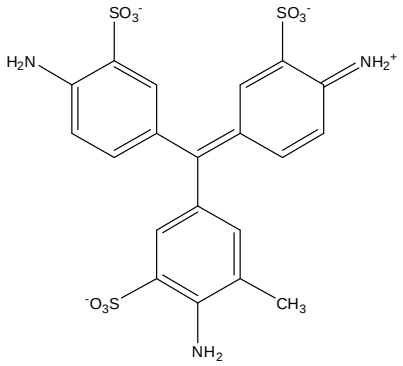

D

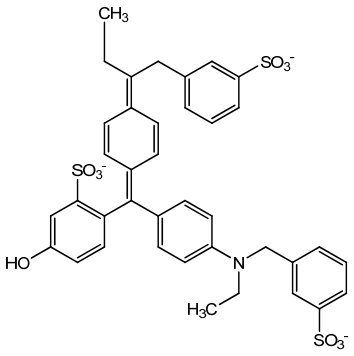

Figure 6-1: (A) The primary sequence of mature human IAPP. The peptide contains a disulfide bridge between Cys-2 and Cys-7 and has an amidated C-terminus. (B) The primary sequence of the proIAPP$_{1\text{-}48}$ processing intermediate. The sequence is numbered beginning at the first residue of the intermediate. The N-terminal extension is depicted in red and the sequence of the mature hormone in black. (C) The structure of acid fuchsin. (D) The structure of fast green FCF.

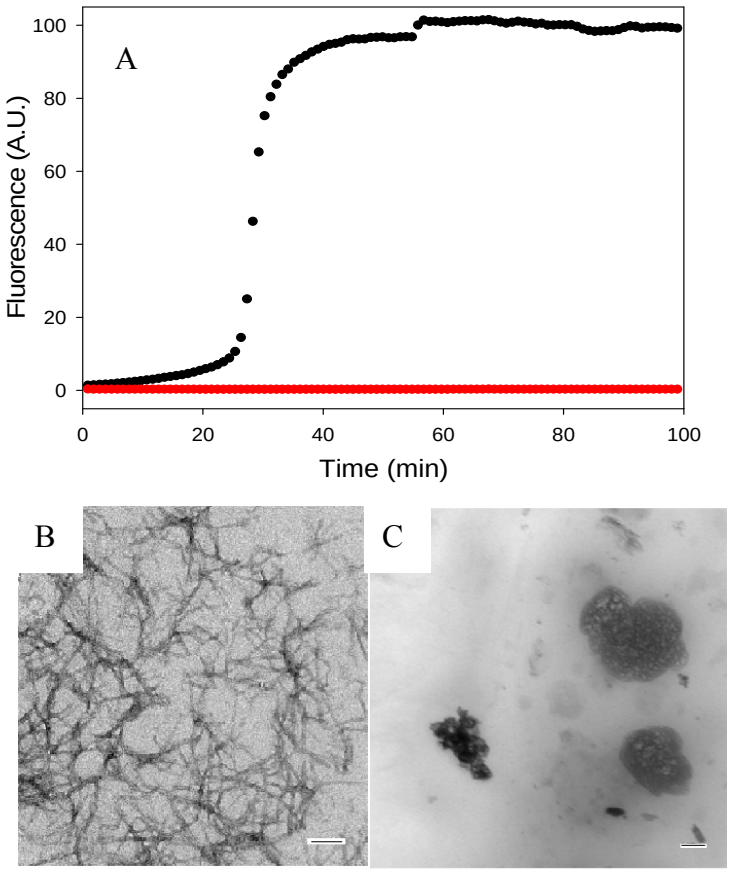

Figure 6-2: Acid fuchsin inhibits amyloid formation by proIAPP$_{1-48}$. (A) Time course of amyloid fibril formation monitored by thioflavin-T binding; proIAPP$_{1-48}$ in the absence of inhibitor (black), proIAPP$_{1-48}$ plus an equimolar amount of acid fuchsin (red). (B) TEM image of the amyloid fibrils formed by proIAPP$_{1-48}$ in the absence of acid fuchsin. Samples were removed 80 minutes after the start of the reaction. (C) TEM image of a sample of the acid fuchsin proIAPP$_{1-48}$ mixture collected 80 minutes after the initiation of the reaction. Scale bars represent 100 nm. The same solutions were used for the kinetic studies and for the TEM samples. The pH of the solutions was 7.4. The solutions contained 2% HFIP by volume, 20mM Tris-HCl, 25µM thioflavin-T, 32µM peptide and were continually stirred at 25^{o}C.

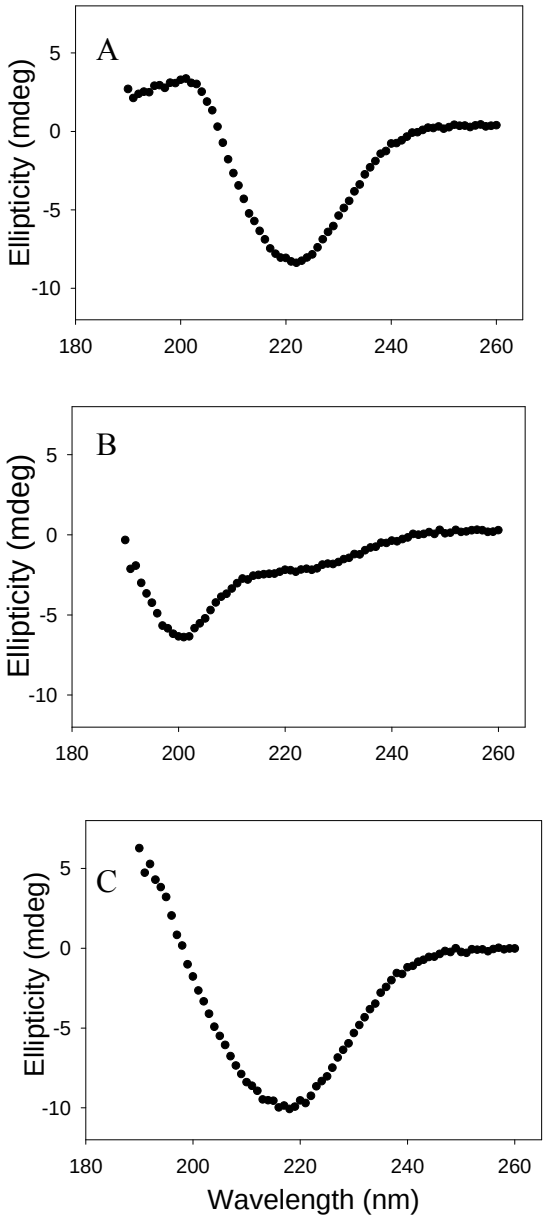

Figure 6-3: Far UV CD Spectra confirm that acid fuchsin is an inhibitor of amyloid fibril formation by proIAPP$_{1-48}$. (A) proIAPP$_{1-48}$ alone, (B) A 1:1 mixture of proIAPP$_{1-48}$ and acid fuchsin, (C) A 1:1 mixture of acid fuchsin with proIAPP$_{1-48}$/heparan sulfate. The samples were those used for the kinetic runs and contain 2% HFIP, 20 mM Tris-HCl pH 7.4, 25 μM thioflavin-T plus 32μM peptide. Aliquots were removed at 80 minutes. Spectra were recorded at 25 ºC.

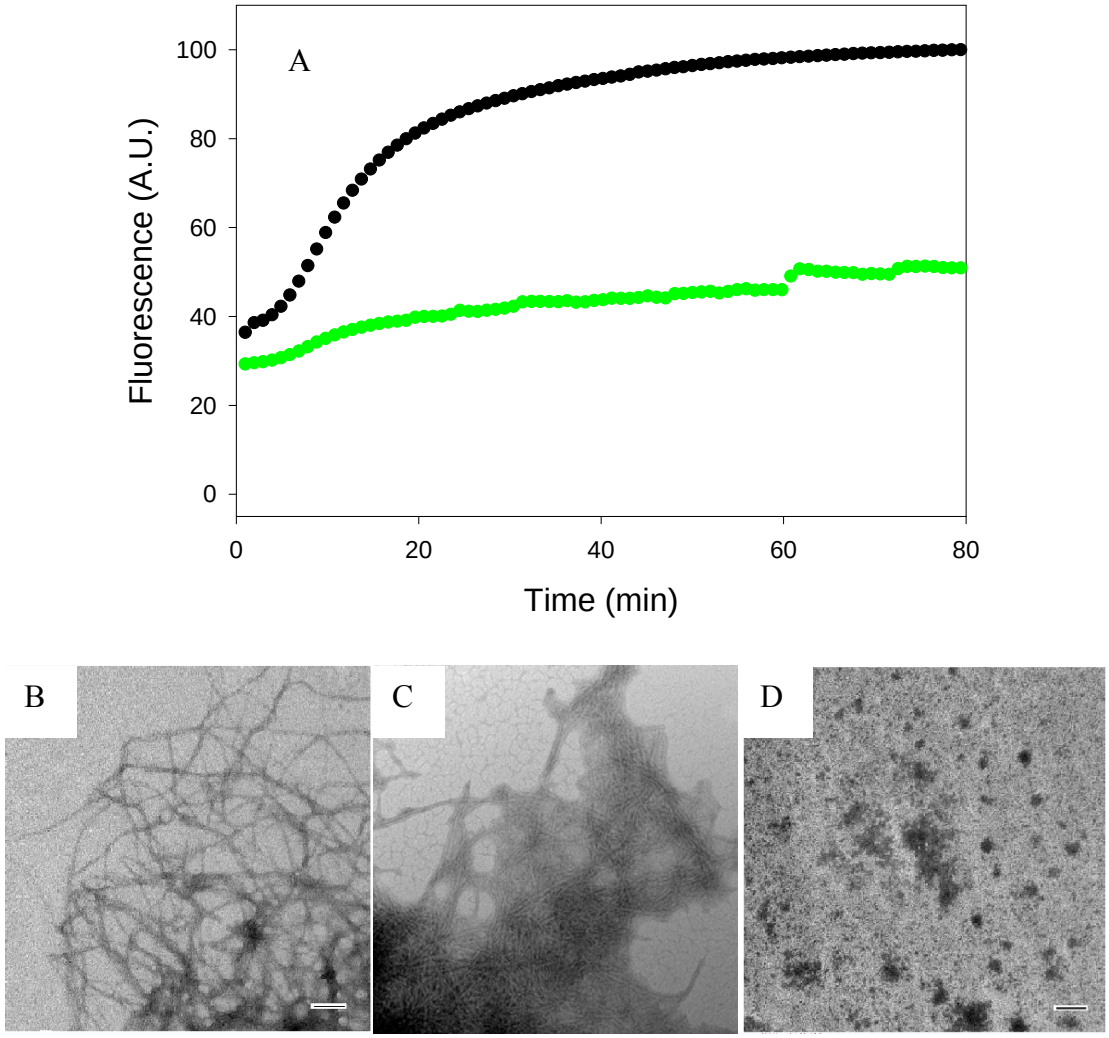

Figure 6-4: Acid fuchsin inhibits amyloid formation by a mixture of proIAPP$_{1-48}$ and heparan sulfate. (A) Time course of amyloid fibril formation monitored by thioflavin-T binding: proIAPP$_{1-48}$ with heparan sulfate in the absence of inhibitor (black); a 1:1 mixture of acid fuchsin with proIAPP$_{1-48}$/heparan sulfate (green). (B) TEM image of the amyloid fibrils formed by the proIAPP$_{1-48}$ heparan sulfate mixture in the absence of acid fuchsin. Samples were removed 80 minutes after the start of the reaction. (C) TEM image of a sample of the 1:1 mixture of acid fuchsin with proIAPP$_{1-48}$/heparan sulfate collected at 80 minutes after the initiation of the reaction. (D) TEM image of a sample of the 10:1 mixture of acid fuchsin with proIAPP$_{1-48}$/heparan sulfate collected at 80 minutes after the initiation of the reaction. Scale bars represent 100 nm. The same solutions were used for the kinetic studies and for the TEM samples. The pH of the solutions was 7.4. The solutions contained 2% HFIP by volume, 20mM Tris-HCl, 25μM thioflavin-T, 32μM peptide and were continually stirred at 25^{o}C.

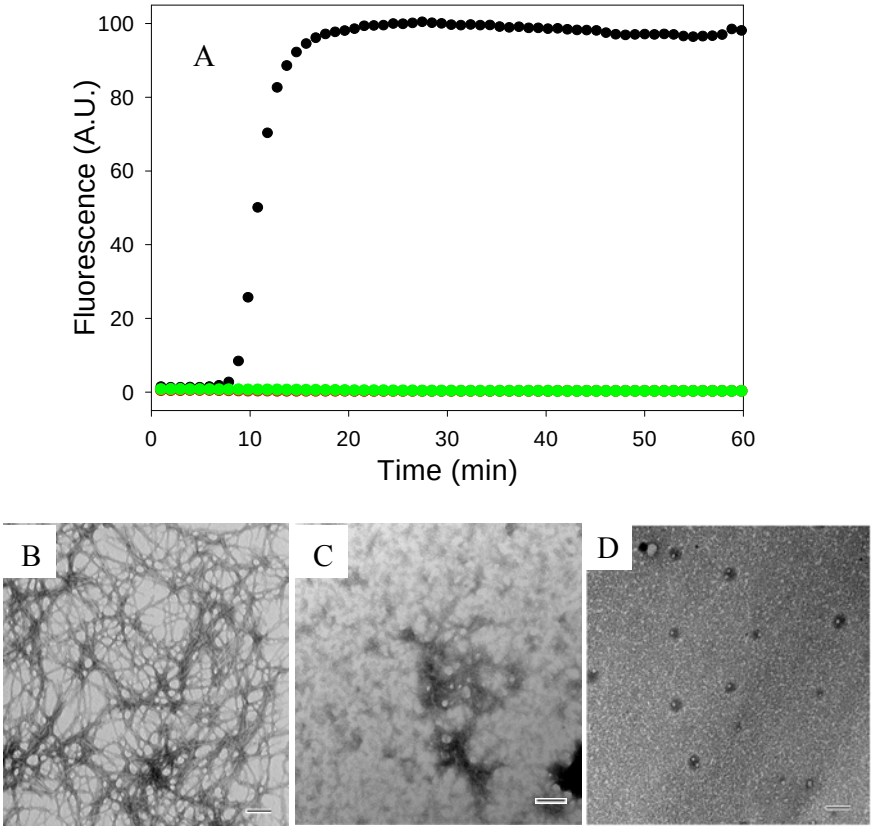

Figure 6-5: Fast green FCF inhibits amyloid formation by IAPP. (A) The effects of fast green FCF on the kinetics of mature IAPP monitored by thioflavin-T fluorescence: IAPP alone (black); a mixture of fast green FCF and IAPP at a ratio of 1:1 (red). (B) TEM image of a sample of IAPP in the absence of inhibitor. (C) TEM image of a 1:1 mixture of fast green FCF and IAPP. (D) TEM image of a 10:1 mixture of fast green FCF and IAPP. Aliquots were removed from solution 60 minutes after the reactions were started. All samples were examined at pH 7.4. Scale bars represent 100 nm. Solutions contained 20 mM Tris-HCl buffer, 25 μM thioflavin-T, 32 μM peptide 2% HFIP, and were continually stirred at 25ºC.

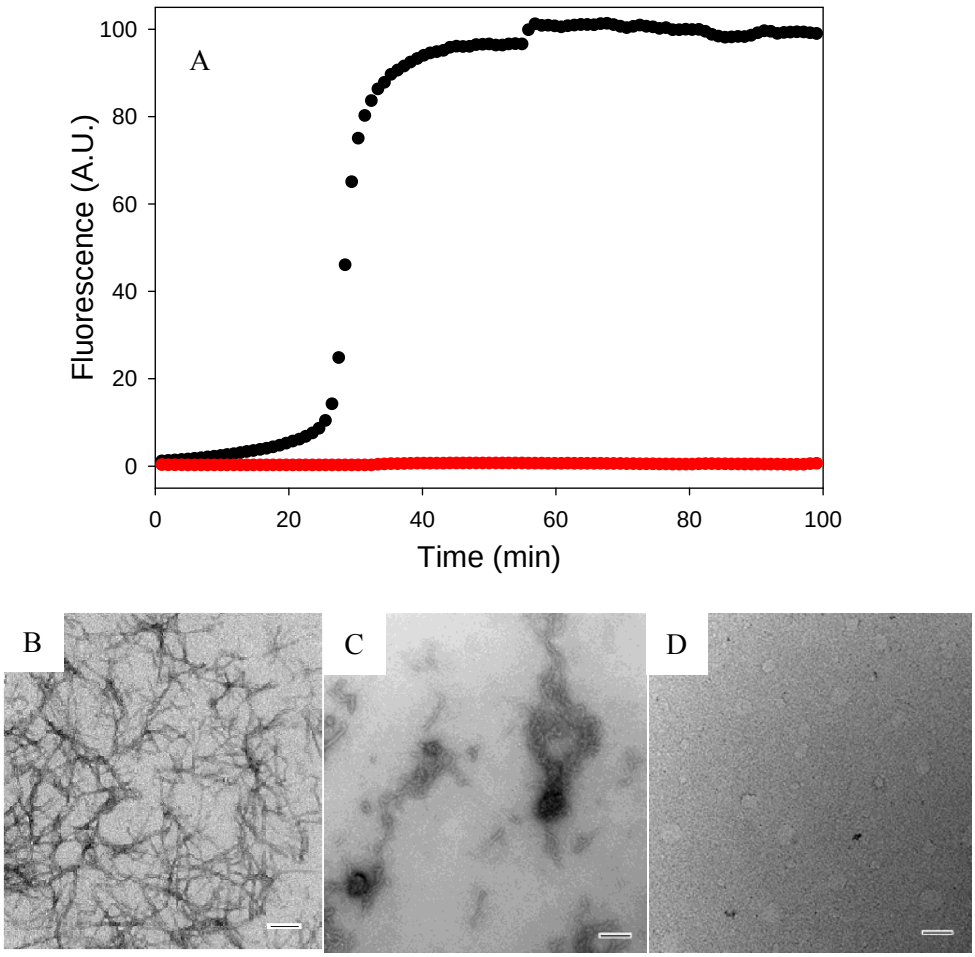

Figure 6-6: Fast green FCF inhibits amyloid formation by proIAPP$_{1-48}$. (A) The effects of fast green FCF on the kinetics of proIAPP$_{1-48}$ monitored by thioflavin-T fluorescence: proIAPP$_{1-48}$ alone (black); a mixture of fast green FCF and proIAPP$_{1-48}$ at a ratio of 1:1 (red). (B) TEM image of proIAPP$_{1-48}$ in the absence of inhibitor. (C) TEM image of a mixture of fast green FCF and proIAPP$_{1-48}$ at a 1:1 ratio. (D) TEM image of a mixture of fast green FCF and proIAPP$_{1-48}$ at a 10:1 ratio. Samples were those used for the experiments depicted in Figure A. All samples were examined at pH 7.4. Scale bars represent 100 nm. Solutions contained 20 mM Tris-HCl buffer (pH 7.4), 25 μM thioflavin-T, 32 μM peptide, 2% HFIP, and were continually stirred at 25ºC. The thioflavin-T curve shown and TEM images displayed for proIAPP$_{1-48}$ without inhibitor are the same as shown in Figure 6-4.

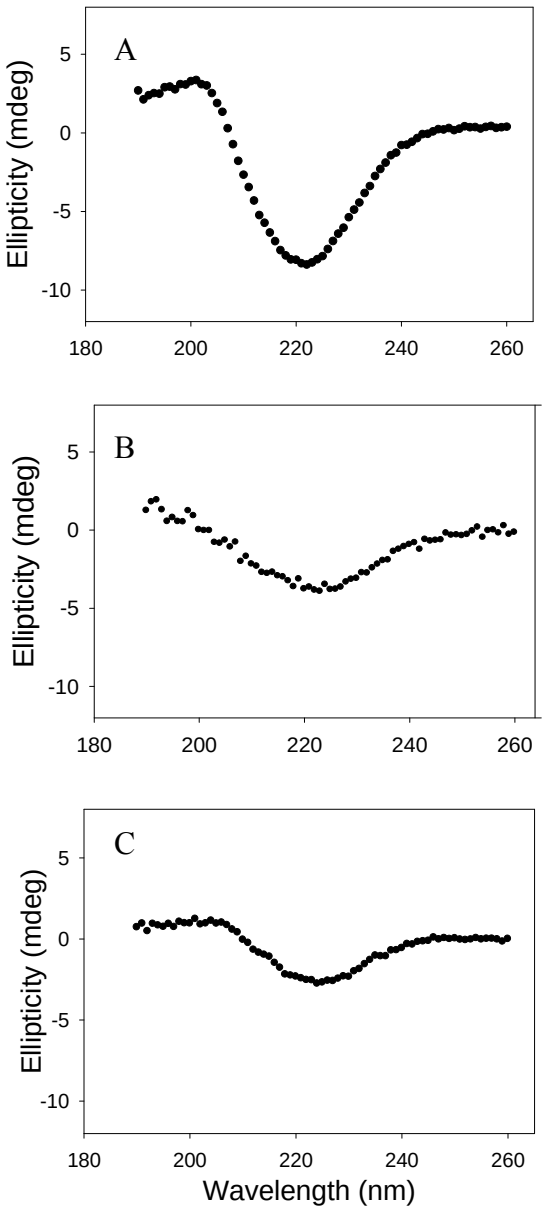

Figure 6-7: Far UV CD spectra of fast green FCF with proIAPP$_{1-48}$. (A) proIAPP$_{1-48}$ alone, (B) A 1:1 mixture of proIAPP$_{1-48}$ and fast green FCF, (C) A 1:1 mixture of fast green FCF with proIAPP$_{1-48}$/heparan sulfate. The samples were those used for the kinetic runs and contained 2% HFIP, 20 mM Tris-HCl pH 7.4, 25 μM thioflavin-T, 32 μM peptide. Aliquots were removed at 80 minutes. Spectra were recorded at 25 ºC.

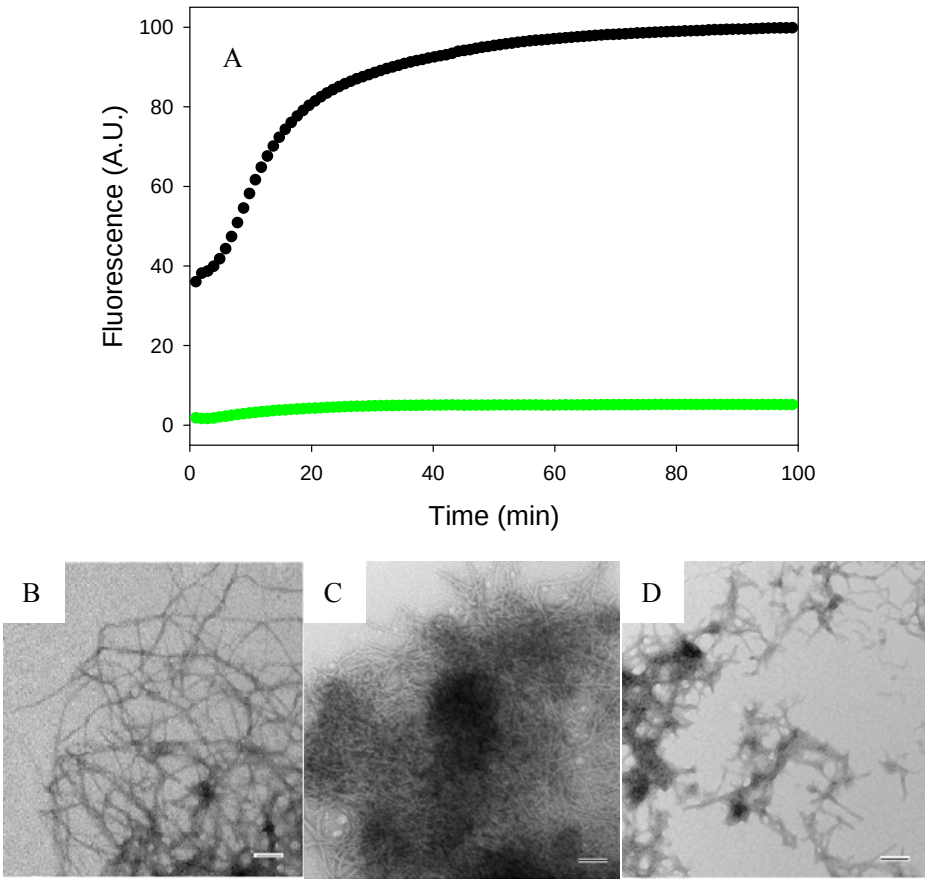

Figure 6-8: Fast green FCF inhibits amyloid formation by mixture of proIAPP$_{1-48}$ and heparan sulfate. (A) Time course of amyloid fibril formation monitored by fluorescence detected thioflavin-T binding: proIAPP$_{1-48}$/heparan sulfate (black); a 1:1 molar ratio mixture of fast green and proIAPP$_{1-48}$ heparan sulfate (green). (B) TEM image of proIAPP$_{1-48}$ heparan sulfate in the absence of inhibitor. (C) TEM image of a 1:1 molar ratio mixture of fast green and proIAPP$_{1-48}$ heparan sulfate. (D) TEM image of a 10:1 molar ratio mixture of fast green and proIAPP$_{1-48}$ heparan sulfate. The pH of the solutions was 7.4. The solutions contained 2% HFIP by volume, 20mM Tris-HCl, 25 μM thioflavin-T, 32 μM peptide and were continually stirred at 25^{o}C. The thioflavin-T curve shown and TEM images displayed for proIAPP$_{1-48}$ heparan sulfate without inhibitor are the same as shown in Figure 6-4.

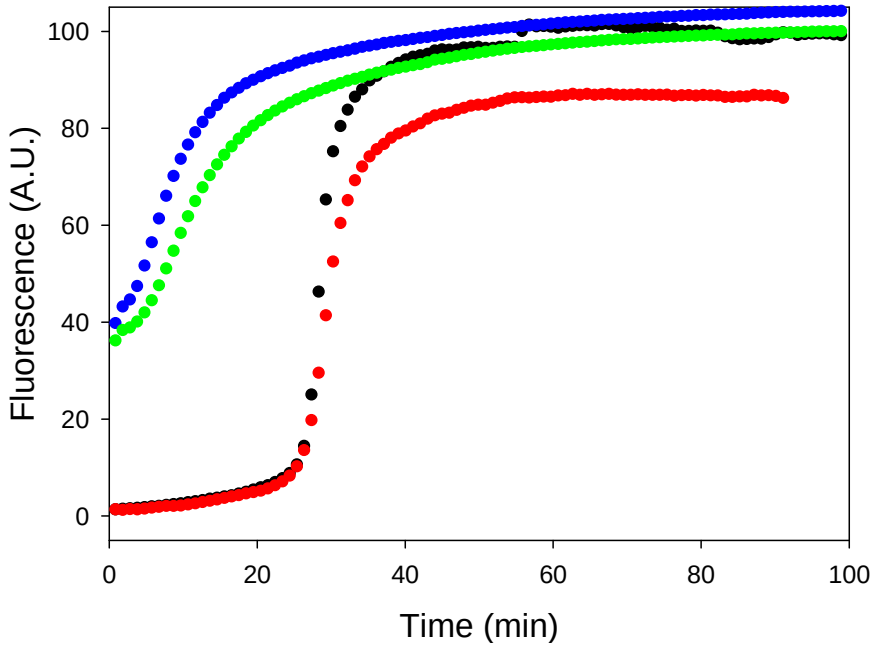

Figure 6-9: Tramprosate (3-amino-1-propane sulfonic acid) does not inhibit amyloid formation by proIAPP$_{1-48}$ or by the proIAPP$_{1-48}$ heparan sulfate mixture. Time course of amyloid fibril formation monitored by fluorescence detected thioflavin-T binding: proIAPP$_{1-48}$ alone (black); a 40:1 molar ratio mixture of tramprosate and proIAPP$_{1-48}$ (red); proIAPP$_{1-48}$/heparan sulfate (green); a 40:1 molar ratio mixture of tramprosate and proIAPP$_{1-48}$/heparan sulfate (blue). The pH of the solutions was 7.4. The solutions contained 2% HFIP by volume, 20mM Tris-HCl, 25 μM thioflavin-T, 32 μM peptide and were continually stirred at 25^{o}C.

7. The flavanol (–)-epigallocatechin 3-gallate inhibits amyloid formation by islet amyloid polypeptide, disaggregates amyloid fibrils and protects cultured cells against IAPP induced toxicity

Abstract

Islet amyloid polypeptide (IAPP, amylin) is the major protein component of islet amyloid deposits associated with type 2 diabetes. The polypeptide lacks a well−defined structure in its monomeric state, but readily assembles to form amyloid. Amyloid fibrils formed from IAPP, intermediates generated in the assembly of IAPP amyloid, or both are toxic to β-cells, suggesting that islet amyloid formation may contribute to the pathology of type 2 diabetes. There are relatively few reported inhibitors of amyloid formation by IAPP. Here we show that the tea−derived flavanol, (–)-Epigallocatechin 3-Gallate, [(2*R*,3*R*)-5,7-dihydroxy-2-(3,4,5-trihydroxyphenyl)-3,4-dihydro-2*H*-1-benzopyran-3-yl 3,4,5-trihydroxybenzoate], (EGCG), is an effective inhibitor of *in vitro* IAPP amyloid formation and disaggregates preformed amyloid fibrils derived from IAPP. The compound is thus one of a very small set of molecules which have been shown to disaggregate IAPP amyloid fibrils. Fluorescence detected thioflavin-T binding assays and transmission electron microscopy confirm that the compound inhibits unseeded amyloid fibril formation as well as disaggregates IAPP amyloid. Seeding studies show that the

complex formed by IAPP and EGCG does not seed amyloid formation by IAPP. In this regard, the behavior of IAPP is similar to the reported interactions of Aβ and α−synuclein with EGCG. Alamar blue assays and light microscopy indicate that the compound protects cultured rat INS-1 cells against IAPP−induced toxicity. Thus, EGCG offers an interesting lead structure for further development of inhibitors of IAPP amyloid formation and for compounds that disaggregate IAPP amyloid.

NOTE: The material presented in this chapter has been has been submitted for publication (Fanling Meng, Andisheh Abedini, Annette Plesner, C. Bruce Verchere and Daniel P. Raleigh. "The flavanol (–)-epigallocatechin 3-gallate inhibits amyloid formation by islet amyloid polypeptide, disaggregates amyloid fibrils and protects cultured cells against IAPP induced toxicity" (2010) *Submitted to Biochemistry*). This chapter contains direct excerpts from the manuscript which was written by me with suggestions and revisions from Professor Daniel P. Raleigh. Cell toxicity experiments were performed by Dr. Andisheh Abedini in Professor Verchere's laboratory at the University of British Columbia. They are included in this chapter for completeness.

7.1 Introduction

IAPP has been identified in all mammalian species examined, and is a member of the calcitonin-like family of peptides which includes calcitonin, adrenomedullin, and calcitonin gene-related peptide (*173*). IAPP normally functions as an endocrine partner to insulin, is processed in parallel with insulin in the pancreatic β-cells, and is secreted in response to the same stimuli that lead to insulin secretion (*164-166*). Synthetic aggregates of human IAPP are toxic to pancreatic β-cells, arguing that the process of IAPP amyloid fibril formation contributes to islet cell death in type 2 diabetes (*27-29, 66, 99*). Longitudinal studies using animal models suggest a role for islet amyloid in type 2 diabetes, while autopsies indicate varying amounts of amyloid deposits in individuals diagnosed with type 2 diabetes (*100, 174*). Recent work has highlighted a potentially deleterious role for IAPP amyloid formation in islet transplantation (*175-178*). Thus, there is considerable interest in the development of inhibitors of IAPP amyloid formation. There is a very large body of work on inhibitors of the Alzheimer beta amyloid peptide (Aβ), but much less attention has been paid to the development of IAPP amyloid inhibitors (*75, 80-81, 85, 119, 121, 148-150, 156-158*).

The ester of epigallocatechin and gallic acid, (–)-Epigallocatechin 3-Gallate [EGCG; (2*R*,3*R*)-5,7-dihydroxy-2-(3,4,5-trihydroxyphenyl)-3,4-dihydro-2*H*-1-benzopyran-3-yl 3,4,5-trihydroxybenzoate], is the most abundant biologically active compound in tea (*179-180*). This tea derived flavanol has been reported to attenuate Aβ−induced

neurotoxicity in cultured human neuronal cell lines, and to modulate both tau pathology and Aβ–mediated cognitive impairment in transgenic mouse models of Alzheimer disease (*181-183*). The molecular basis of these effects is not well understood, but has been postulated to be related to EGCG's radical scavenging properties, its potential to effect the processing of amyloid precursor protein, its ability to interfere with amyloid formation, or by its inhibition of c-Abl/FE65 nuclear translocation and GSK3 beta activation (*77, 183-184*).

Early studies using model homo-polymers of amino acids showed that catechins, a core component of the EGCG structure, interfered with and inhibited the coil to β-sheet transition (*185*). Recent work has shown that EGCG inhibits the *in vitro* amyloid formation of several natively unfolded polypeptides including Aβ, α-synuclein, and polyglutamine peptides and the model polypeptide κ-casein (*77-78, 186*). The compound has also been shown to induce a transition of the cellular form of the prion protein into a detergent insoluble form, which differs from the pathological scrapie protein conformation, and to eradicate formation of a variety of prion structures (*79, 187*). However, its ability to inhibit amyloid formation by IAPP has not been tested, nor has its ability to protect cells against the toxic effects of IAPP amyloid formation been examined. These observations promoted us to examine the ability of EGCG to inhibit amyloid formation by IAPP and disaggregate amyloid fibrils, and to also test its ability to protect cells against IAPP toxicity.

7.2 Materials and methods

7.2.1 Peptide synthesis and purification

Human IAPP was synthesized on a 0.25 mmol scale using an applied Biosystems 433A peptide synthesizer, by 9-fluornylmethoxycarbonyl (Fmoc) chemistry as described (*113*). Pseudoprolines were incorporated to facilitate the synthesis. 5-(4'-fmoc-aminomethyl-3',5-dimethoxyphenol) valeric acid (PAL-PEG) resin was used to afford an amidated C-terminal. The first residue attached to the resin, β-branched residues, residues directly following β-branched residues and pseudoprolines were double coupled. The peptide was cleaved from the resin using standard TFA protocols. Crude peptides were oxidized by dimethyl sulfoxide (DMSO) for 24 hours at room temperature (*140*). The peptides were purified by reverse-phase HPLC using a Vydac C18 preparative column. A two-buffer system was utilized. Buffer A consists of H_2O and 0.045% HCl (v/v). Buffer B consists of 80% acetonitrile, 20% H_2O, and 0.045% HCl (v/v). The gradient used was 0-70% buffer B in 70 minutes. The pure peptide eludated out at 50 minutes, which is 50% buffer B. HCl was used as the counter-ion since the presence of TFA has been shown to affect amyloid formation by some IAPP derived peptides (*188*). After the initial purification, the peptide was washed with ether, centrifuged, dried and then redissolved in HFIP and subjected to a second round of HPLC purification. This procedure was necessary to remove residual scavengers that can interfere with toxicity assays. Analytical HPLC was used to check the purity of the peptide. The identity of the pure peptide was confirmed by mass spectrometry using a Bruker MALDI-TOF MS;

IAPP observed 3904.6, expected 3904.8. An additional sample of human IAPP was purchased from Bachem.

7.2.2 Sample preparation for in vitro biophysical assays of amyloid formation

Stock solutions (1.58 mM) of IAPP were prepared in 100% hexafluoroisopropanol (HFIP), and stored at 4^{o}C. Aliquots of IAPP peptide in HFIP were filtered through a 0.45 μm filter and dried under vacuum. A Tris-HCl buffered (20 mM, pH 7.4) thioflavin-T solution was added to these samples to initiate amyloid formation. These conditions were chosen to match the method of sample preparation used for toxicity studies.

7.2.3 Thioflavin-T fluorescence

Fluorescence measurements were performed using a Beckman model D880 plate reader. The samples were incubated at 25 ^{o}C in 96-well plates. An excitation filter of 430 nm and an emission filter of 485 nm were used. All solutions for these studies were prepared by adding a Tris-HCl buffered (20 mM, pH 7.4) thioflavin-T solution into IAPP peptide (in dry form) immediately before the measurement. The final concentration was 32 μM peptide and 25 μM thioflavin-T with or without 32 μM EGCG in 20 mM Tris-HCl. Seeding experiments were performed by adding IAPP to either preformed amyloid or to the final products of an IAPP plus EGCG kinetic experiment. The final concentration of seeds for the IAPP and IAPP: EGCG complex seeding experiments were 3.2 μM IAPP and 3.2 μM IAPP: 3.2 μM EGCG respectively, in monomeric units. EGCG was

purchased from Sigma-Aldrich.

7.2.4 Transmission electron microscopy (TEM)

Peptide solution (5 μL) was blotted onto a carbon-coated Formvar 300 mesh copper grid for 1 min and then negatively stained with saturated uranyl acetate for 1 min. The same solutions that were employed for thioflavin-T fluorescence measurements were used for TEM studies so that samples could be compared under as similar conditions as possible.

7.2.5 Analysis of the effect of EGCG on IAPP-induced toxicity

Rat insulinoma (INS-1) beta cells were used to assess the ability of EGCG to protect against the toxic effects of human IAPP. INS-1 cells were grown in RPMI 1640 (Gibco-BRL) supplemented with 10% fetal bovine serum (FBS), 11 mM glucose, 10 mM Hepes, 2 mM L-glutamine, 1 mM sodium pyruvate, 50 μM β-mercaptoethanol, 100 U/ml penicillin (Gibco-BRL), and 100 U/ml streptomycin (Gibco-BRL). Cells were maintained at 37^{o}C in a humidified environment supplemented with 5% CO_2. Cells were grown for two passages prior to use and used in assays between passages 59 and 65. For toxicity experiments, cells were seeded at a density of 30,000 cells per well in 96-well plates and cultured for 24 hours prior to addition of solutions. Solutions of EGCG:IAPP at 1:1 molar ratio (30 μM IAPP and 30 μM EGCG) were prepared by adding aliquots of a 1.09 mM EGCG stock solution to dry IAPP (prepared as described in the sample preparation

subsection) and diluting with Tris-HCl buffer (pH 7.4). Peptide samples and samples of peptide plus EGCG in Tris-HCl buffer (pH 7.4) were added directly to cells (30% final media concentration) after 11 hours of incubation at room temperature. Alamar blue (Biosource International, CA) was used to assess INS-1 cell viability. Alamar blue was diluted ten-fold in 30% culture media and cells were incubated for 5 hours at 37^{o}C. Fluorescence (excitation 530; emission 590 nm) was measured with a Fluoroskan Ascent plate reader (Thermo Labsystems). Data are representative of a minimum of three independent experiments performed in triplicate. The experiments were repeated using human IAPP synthesized by two independent sources and similar results were obtained.

7.2.6 Light Microscopy

Changes in cell morphology were examined by light microscopy in order to provide a second method of evaluating cell viability. Transformed rat INS-1 beta cells were photographed immediately prior to assessment of toxicity by alamar blue cell viability assays. Images were captured using a Nikon Eclipse TS100 light microscope.

7.3 Results and discussion

7.3.1 EGCG inhibits amyloid formation by IAPP *in vitro*

The primary sequence of IAPP is shown in Figure 7-1, which also displays the structure of EGCG. The kinetics of *in vitro* amyloid formation are generally complex, and IAPP is no exception. Like other amyloidogenic polypeptides, it displays a lag phase during which no detectable amyloid fibrils are formed followed by a more rapid growth phase also called the elongation phase, which leads to a final state in which amyloid fibrils are in equilibrium with soluble peptide. The rate of amyloid formation by IAPP was measured in the presence and in the absence of EGCG using thioflavin-T binding assays. Thioflavin-T is a small molecule whose fluorescent quantum yield increases significantly when it binds to amyloid fibrils (*10*). The dye is thought to bind in grooves formed on the surface of the amyloid fibril which are generated by the in-register alignment of side chains in the regular cross β-sheet structure. Binding of the dye in a planar conformation eliminates rotation of the benzothiozole and benzaminic rings, and reduces self-quenching, resulting in an increase in fluorescence quantum yield.

Thioflavin-T monitored kinetic progress curves for IAPP in the presence and absence of EGCG are displayed in Figure 7-2. The sigmoidal curve observed in the absence of EGCG is typical of that observed for IAPP *in vitro*. The lag time is on the order of 20 hours for the IAPP sample in the absence of EGCG. The time course of amyloid formation observed here is comparable to other studies that have used similar sample preparation protocols, but is slower than has been observed for some biophysical

studies that were conducted with constant stirring, and which initiate amyloid formation by dilution of stock solutions of IAPP in fluorinated alcohols, typically HFIP, into buffer. Stirring is well known to increase the rate of amyloid formation, most likely by inducing fiber fragmentation, and small amounts of residual HFIP have been shown to drastically accelerate amyloid formation by IAPP (*161, 189-192*).

Experiments conducted in the presence of EGCG give strikingly different results than observed in the absence of the compound. No increase in thioflavin-T fluorescence is observed for the 1:1 mixture of IAPP with EGCG. The standard interpretation of curves such as those shown in Figure 2 is that the lack of thioflavin-T fluorescence indicates that no amyloid is formed. However, it is important to independently confirm the results of the thioflavin-T binding assays (*159*). Consequently, TEM images were recorded of aliquots removed at the end of the reaction. The TEM images of the sample without inhibitor revealed extensive amyloid fibrils with a morphology typical of that found for *in vitro* IAPP amyloid deposits (Figure 7-2B). In contrast, very few aggregates were observed on the grid when EGCG was present at the 1:1 ratio and the few fibrils detected had a different morphology (Figure 7-2C). The TEM and thioflavin-T studies indicate that EGCG inhibits amyloid formation by IAPP *in vitro*.

7.3.2 The complex formed by IAPP and EGCG does not seed amyloid formation

Studies with Aβ and α-synuclein have shown that the EGCG peptide complexes formed are unable to seed amyloid formation by the parent protein (*77*). Seeding refers to

the process of adding pre-aggregated species to a sample of unaggregated polypeptide. Seeding normally significantly accelerates amyloid formation by eliminating the lag phase. The inability of the EGCG: Aβ and the EGCG:α-synuclein complexes to seed aggregation of the parent proteins was taken as evidence that the species are off pathway (*77*). It is extremely difficult to determine if an intermediate is on or off pathway (*193*). Strictly speaking, the results with Aβ and α−synuclein indicate that the species formed are not capable of supporting growth of amyloid fibrils, but do not prove that they are off-pathway. Instead, EGCG may have trapped the respective polypeptides in an early intermediate state which is on pathway, but which has not yet reached the state where it is capable of promoting growth of cross β-structure. None-the-less, seeding experiments can provide important mechanistic insight. In particular, the observation of the ability to seed amyloid formation is consistent with the species being on pathway. Thus, a positive result in a seeding study is easily interpreted, while a negative result, although informative, is more ambiguous. Consequently, we investigated the ability of the material present at the end of the kinetic experiments to seed amyloid formation by IAPP. Figure 7-3 displays the results of IAPP seeding studies. Adding pure IAPP seeds eliminates the lag phase and leads to a thioflavin-T curve which is very similar to other reported seeding studies (*191*). In contrast, seeding by aliquots of the 1:1 EGCG: IAPP mixture collected at the end of the kinetic experiment displayed in Figure 7-2, had no detectable effect, indicating that the EGCG: IAPP complex does not seed amyloid formation by IAPP under these conditions (Figure 7-3).

7.3.3 EGCG disaggregates IAPP amyloid fibrils

We also tested the ability of EGCG to disaggregate IAPP amyloid fibrils. To the best of our knowledge, there are no small molecules which have been reported to disaggregate IAPP amyloid, although one large peptide-based inhibitor has been shown to do so (*85*). Figure 4 displays the results of a kinetic experiment for an IAPP control without EGCG; the second curve is from an experiment in which EGCG was added after the plateau region was reached. An initial rapid decrease in thioflavin-T fluorescence is observed after EGCG is added, followed by a slower decay of fluorescence. Samples of the solution were removed at various time points after addition of EGCG and used for TEM analysis. Images recorded from samples removed after the end of the initial, rapid, decay of thioflavin-T fluorescence revealed that the amyloid fibrils had converted to much shorter aggregates which, qualitatively appeared to have less tendency to clump together. Images were also recorded after the end of the second, slower decay phase. Most of the TEM grids were blank, while a few regions contained amorphous aggregates or very thin aggregates (Figure 7-4).

7.3.4 EGCG protects INS-1 beta cells against the toxic effects of human IAPP

We compared the effects of 30 μM human IAPP and a 1:1 mixture of 30 μM human IAPP and 30 μM EGCG on rat INS-1 cells in order to determine whether EGCG was able to protect beta cells from the toxic effects of human IAPP. Rat INS-1 cells are

transformed β-cell line which is widely used in studies of β-cell toxicity. Incubation of INS-1 cells with 30 μM human IAPP for 5 hours resulted in significant toxicity; cell viability was only 22 ± 0.3% relative to untreated control determined by alamar blue assays. The 1:1 mixture of EGCG and IAPP was significantly less toxic, increasing the percentage of viable cells to 77 ± 4% (Figure 7-5A). Changes in cell morphology were examined by light microscopy in order to provide a second method of evaluating cell viability. Cells were photographed immediately prior to assessment of toxicity by alamar blue assay. Analysis of 30 μM IAPP-treated INS-1 cells demonstrated induction of cell shrinkage and extensive detachment of cells from the cell culture substratum, indicative of cell death. In contrast, INS-1 cells treated with a 1:1 molar ratio of EGCG: IAPP, or with just EGCG demonstrated no observable signs of cell death (Figure 7-5).

The experiments demonstrate a significant level of EGCG-induced protection and indicate that EGCG is an effective inhibitor of human IAPP induced *in vitro* toxicity. Similar results were obtained using human IAPP from two independent sources, in-house prepared human IAPP and human IAPP purchased from Bachem. This is an important control since there have been reports of significant lot-to-lot variability in the toxicity of human IAPP from different sources (*68*).

7.4 Conclusions

The data reported here demonstrate that EGCG inhibits *in vitro* amyloid formation by IAPP and disaggregates IAPP amyloid. EGCG is the first small molecule that has been

shown to disaggregate IAPP-derived amyloid fibrils. Studies of the interaction of EGCG with α–synuclein and Aβ lead to the proposal, based in part on seeding studies, that EGCG functions by a universal mechanism which involves diverting polypeptides from their normal amyloid formation pathway into non-productive off pathway states (*77*). It is worth noting, however, that it is extraordinarily difficult to prove if a species is on or off the pathway of amyloid formation (*91, 193*). Along these lines, studies with another polyphenol, exifone [3,4,5,2',3',4'-Hexahydroxybenzophenone;[2,3,4-Trihydroxyphenyl) (3,4,5-trihydroxyphenyl) methanon], has provided evidence that such compounds can function by an alternative mechanism in which they trap amyloidogenic proteins in an on-pathway intermediate state (*194*). Recent work with reduced carboxymethylated κ-casein showed that EGCG maintained the protein in a pre-amyloid state, but did not redirect the normal aggregation pathway (*78*). Thus EGCG can inhibit amyloid by a variety of ways. Under the conditions used here, EGCG appears to interact with IAPP in a fashion more similar to its interaction with Aβ and α-synuclein. Irrespective of the details, it is clear that EGCG has the ability to interact with a broad range of natively unfolded proteins and inhibit their *in vitro* aggregation while at the same time protecting cultured cells against toxicity.

A

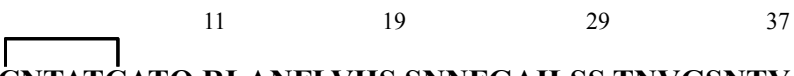

B

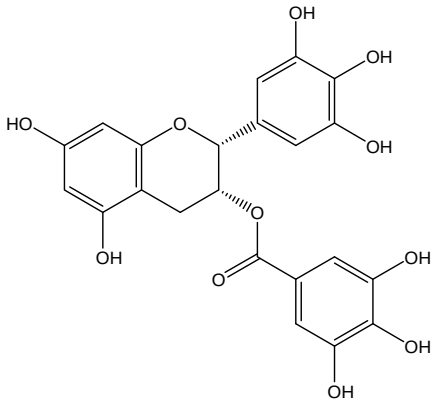

Figure 7-1: (A) The primary sequence of human IAPP. The peptide contains a disulfide bridge between Cys-2 and Cys-7 and has an amidated C-terminus. (B) The structure of EGCG.

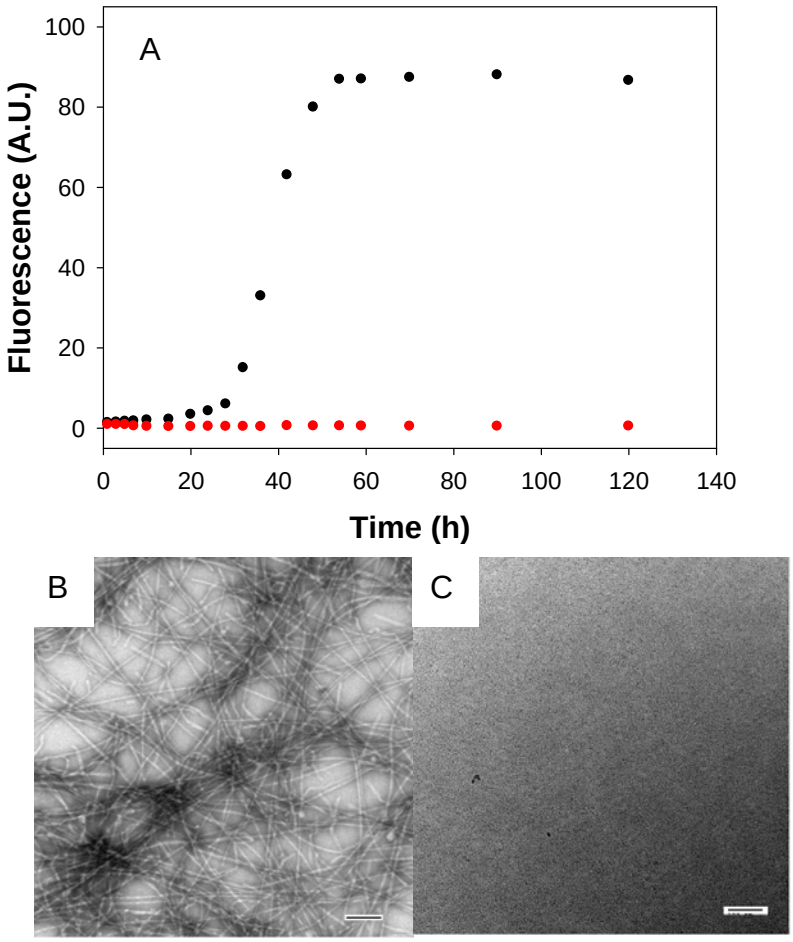

Figure 7-2: EGCG inhibits amyloid formation by IAPP *in vitro*. (A) Fluorescence detected thioflavin-T binding assays in the presence and absence of EGCG. IAPP alone (black); a 1:1 molar ratio mixture of EGCG and IAPP (*155*); (B) TEM image of IAPP alone. (C) TEM image of a 1:1 mixture of IAPP and EGCG. Aliquots were removed from the kinetic experiments depicted in panel A after 200 hours and blotted for TEM. Scale bars represent 100 nm. Samples contained 32 μM IAPP and experiments were performed in 20 mM Tris-HCl, pH 7.4, 25^{o}C.

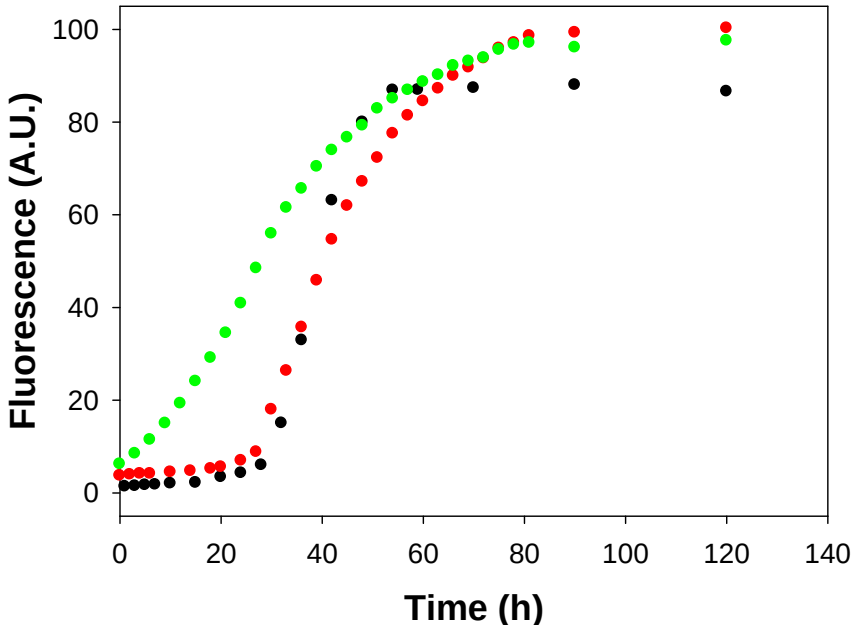

Figure 7-3: IAPP:EGCG complexes do not seed amyloid formation by IAPP. The results of thioflavin-T monitored kinetic experiments are shown. Black, unseeded IAPP; Green, IAPP seeded with IAPP amyloid fibrils; Red, IAPP seeded with the IAPP:EGCG complex. Experiments were conducted in 20mM Tris-HCl, pH 7.4, 25^{o}C. The IAPP concentration was 32 μM. Seeds, when present, were added at a concentration of 3.2 μM (monomer units).

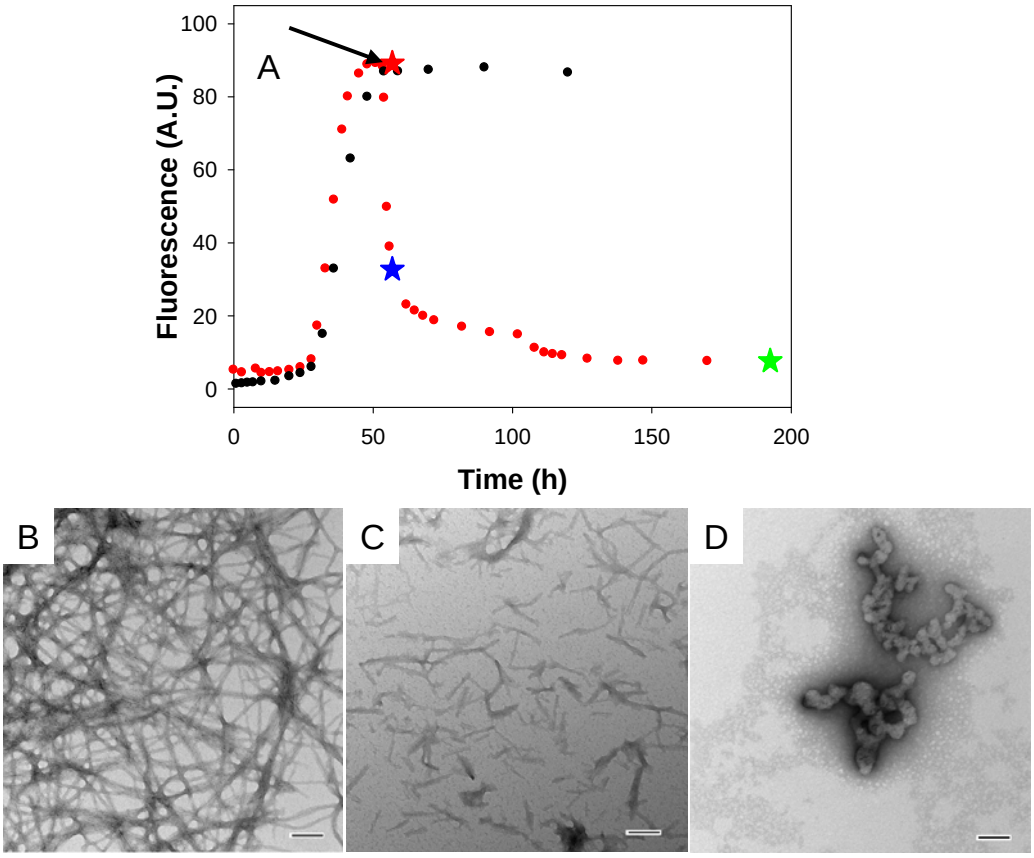

Figure 7-4: EGCG disaggregates IAPP amyloid fibrils. (A) thioflavin-T monitored kinetic experiments. Black, IAPP alone; Red, EGCG added at the point indicated by the arrow. (B) TEM image of IAPP before the addition of EGCG. The sample was removed at the time point indicated by the (★). (C) TEM images of IAPP after the addition of EGCG. The sample was removed at the time point indicated by the (★). (D) TEM image of IAPP after the addition of EGCG. The sample was removed at the time point indicated by the (★). Scale bars represent 100nm. Kinetic runs were conducted at pH 7.4, 25^{o}C, 20mM Tris-HCl with 32 μM IAPP.

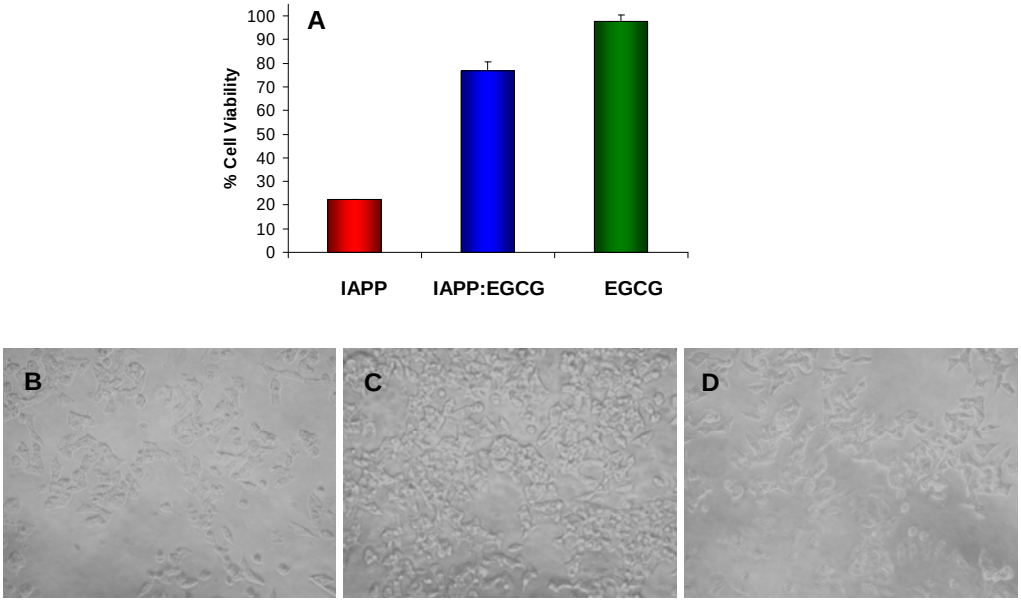

Figure 7-5: EGCG protects rat INS-1 cells against the toxic effects of human IAPP. (A) Cell viability as determined via alamar blue assays, plotted as percent viability. Red, the effect of the addition of a 30μM solution of human IAPP. Blue, the effect of a 1:1 mixture of human IAPP (30 μM) and EGCG (30 μM). Green, the effect of a 30μM solution of EGCG. All solutions were incubated at room temperature for 11 hrs and then applied to rat INS-1 cells in 96-well plates. Values are relative to those of control cells treated with buffer only. All values represent means ± SEM (n=3). (B) Evaluation of apoptotic cell morphology by light microscopy. Transformed rat INS-1 beta cells were photographed immediate prior to assessment of cell viability by alamar blue. (B) The effect of the addition of 30 μM human IAPP. (C) The effect of a 1:1 mixture of human IAPP (30 μM) and EGCG (30 μM). (D) The effect of a 30 μM solution of EGCG. Cell toxicity experiments were performed by Dr. Andisheh Abedini at the University of British Columbia in Professor Verchere's laboratory.

References

1. Sipe, J. D. (1994) Amyloidosis, *Crit. Rev. Clin. Lab. Sci. 31*, 325-354.
2. Selkoe, D. J. (2004) Cell biology of protein misfolding: The examples of alzheimer's and parkinson's diseases, *Nat. Cell Biol. 6*, 1054-1061.
3. Kajava, A. V., Aebi, U., and Steven, A. C. (2005) The parallel superpleated beta-structure as a model for amyloid fibrils of human amylin, *J. Mol. Biol. 348*, 247-252.
4. Goldsbury, C., Goldie, K., Pellaud, J., Seelig, J., Frey, P., Muller, S. A., Kistler, J., Cooper, G. J. S., and Aebi, U. (2000) Amyloid fibril formation from full-length and fragments of amylin, *J. Struct. Biol. 130*, 352-362.
5. Goldsbury, C., Kistler, J., Aebi, U., Arvinte, T., and Cooper, G. J. S. (1999) Watching amyloid fibrils grow by time-lapse atomic force microscopy, *J. Mol. Biol. 285*, 33-39.
6. Goldsbury, C. S., Cooper, G. J. S., Goldie, K. N., Muller, S. A., Saafi, E. L., Gruijters, W. T. M., and Misur, M. P. (1997) Polymorphic fibrillar assembly of human amylin, *J. Struct. Biol. 119*, 17-27.
7. Makin, O. S., and Serpell, L. C. (2005) Structures for amyloid fibrils, *FEBS J. 272*, 5950-5961.
8. Sunde, M., Serpell, L. C., Bartlam, M., Fraser, P. E., Pepys, M. B., and Blake, C. C. F. (1997) Common core structure of amyloid fibrils by synchrotron x-ray diffraction, *J. Mol. Biol. 273*, 729-739.
9. Johnston, N. (2005) Gamma-secretase makes a splash, *Scientist 19*, 24-25.
10. Levine, H. (1995) Thioflavine-t interaction with amyloid beta-sheet structures, *Amyloid-International Journal of Experimental and Clinical Investigation 2*, 1-6.
11. Krebs, M. R. H., Bromley, E. H. C., and Donald, A. M. (2005) The binding of thioflavin-t to amyloid fibrils: Localisation and implications, *J. Struct. Biol. 149*, 30-37.
12. Padrick, S. B., and Miranker, A. D. (2001) Islet amyloid polypeptide: Identification of long-range contacts and local order on the fibrillogenesis pathway, *J. Mol. Biol. 308*, 783-794.
13. Jarrett, J. T., and Lansbury, P. T. (1993) Seeding one-dimensional crystallization of amyloid - a pathogenic mechanism in alzheimers-disease and scrapie, *Cell 73*, 1055-1058.
14. Lomakin, A., Chung, D. S., Benedek, G. B., Kirschner, D. A., and Teplow, D. B. (1996) On the nucleation and growth of amyloid beta-protein fibrils: Detection of nuclei and quantitation of rate constants, *Proc. Natl. Acad. Sci. U. S. A. 93*, 1125-1129.
15. Soto, C., Saborio, G. P., and Anderes, L. (2002) Cyclic amplification of protein misfolding: Application to prion-related disorders and beyond, *Trends Neurosci. 25*, 390-394.

16. Cooper, G. J. S. (1994) Amylin compared with calcitonin-gene-related peptide - structure, biology, and relevance to metabolic disease, *Endocr. Rev. 15*, 163-201.
17. Kahn, S. E., Andrikopoulos, S., and Verchere, C. B. (1999) Islet amyloid: A long-recognized but underappreciated pathological feature of type 2 diabetes, *Diabetes 48*, 241-253.
18. Kahn, S. E., Dalessio, D. A., Schwartz, M. W., Fujimoto, W. Y., Ensinck, J. W., Taborsky, G. J., and Porte, D. (1990) Evidence of cosecretion of islet amyloid polypeptide and insulin by beta-cells, *Diabetes 39*, 634-638.
19. Sanke, T., Hanabusa, T., Nakano, Y., Oki, C., Okai, K., Nishimura, S., Kondo, M., and Nanjo, K. (1991) Plasma islet amyloid polypeptide (amylin) levels and their responses to oral glucose in type-2 (non-insulin-dependent) diabetic-patients, *Diabetologia 34*, 129-132.
20. Castillo, M. J., Scheen, A. J., and Lefebvre, P. J. (1995) Amylin islet amyloid polypeptide - biochemistry, physiology, pathophysiology, *Diabetes Metab. 21*, 3-25.
21. Leighton, B., and Cooper, G. J. S. (1988) Pancreatic amylin and calcitonin gene-related peptide cause resistance to insulin in skeletal-muscle invitro, *Nature 335*, 632-635.
22. Akesson, B., Panagiotidis, G., Westermark, P., and Lundquist, I. (2003) Islet amyloid polypeptide inhibits glucagon release and exerts a dual action on insulin release from isolated islets, *Regulatory Peptides 111*, 55-60.
23. Ohsawa, H., Kanatsuka, A., Yamaguchi, T., Makino, H., and Yoshida, S. (1989) Islet amyloid polypeptide inhibits glucose-stimulated insulin-secretion from isolated rat pancreatic-islets, *Biochem. Biophys. Res. Commun. 160*, 961-967.
24. Makin, O. S., and Serpell, L. C. (2004) Structural characterisation of islet amyloid polypeptide fibrils, *J. Mol. Biol. 335*, 1279-1288.
25. Sanke, T., Bell, G. I., Sample, C., Rubenstein, A. H., and Steiner, D. F. (1988) An islet amyloid peptide is derived from an 89-amino acid precursor by proteolytic processing, *J. Biol. Chem. 263*, 17243-17246.
26. Marzban, L., and Verchere, C. B. (2004) Pro-islet amyloid polypeptide and its n-terminally extended intermediate are secreted from both the regulated and constitutive secretory pathways of beta-cells, *Diabetes 53*, A395-a395.
27. Clark, A., Wells, C. A., Buly, I. D., Cruickshank, J. K., Vanhegan, R. I., Matthews, D. R., Cooper, G. J. S., Holman, R. R., and Turner, R. C. (1988) Islet amyloid, increased alpha cells, reduced beta cells and exocrine fibrosis: Quantitative changes in the pancreas in type 2 diabetes, *Diabetes Res. Clin. Pract. 9*, 151-159.
28. Butler, A. E., Janson, J., Bonner-Weir, S., Ritzel, R., Rizza, R. A., and Butler, P. C. (2003) Beta-cell deficit and increased beta-cell apoptosis in humans with type 2 diabetes, *Diabetes 52*, 102-110.
29. Hull, R. L., Westermark, G. T., Westermark, P., and Kahn, S. E. (2004) Islet amyloid: A critical entity in the pathogenesis of type 2 diabetes, *J. Clin.*

Endocrinol. Metab. 89, 3629-3643.

30. Wimalawansa, S. J. (1997) Amylin, calcitonin gene-related peptide, calcitonin, and adrenomedullin: A peptide superfamily, *Crit. Rev. Neurobiol. 11*, 167-239.
31. Westermark, P., Engstrom, U., Johnson, K. H., Westermark, G. T., and Betsholtz, C. (1990) Islet amyloid polypeptide - pinpointing amino-acid-residues linked to amyloid fibril formation, *Proc. Natl. Acad. Sci. U. S. A. 87*, 5036-5040.
32. Chou, P. Y., and Fasman, G. D. (1978) Empirical predictions of protein conformation, *Annu. Rev. Biochem 47*, 251-276.
33. Ashburn, T. T., and Lansbury, P. T. (1993) Interspecies sequence variations affect the kinetics and thermodynamics of amyloid formation - peptide models of pancreatic amyloid, *J. Am. Chem. Soc. 115*, 11012-11013.
34. Moriarty, D. F., and Raleigh, D. P. (1999) Effects of sequential proline substitutions on amyloid formation by human amylin(20-29), *Biochemistry 38*, 1811-1818.
35. Abedini, A., and Raleigh, D. P. (2006) Destabilization of human iapp amyloid fibrils by proline mutations outside of the putative amyloidogenic domain: Is there a critical amyloidogenic domain in human IAPP?, *J. Mol. Biol. 355*, 274-281.
36. Porte, D., and Kahn, S. E. (1989) Hyperproinsulinemia and amyloid in niddm - clues to etiology of islet beta-cell dysfunction, *Diabetes 38*, 1333-1336.
37. Kahn, S. E., and Halban, P. A. (1997) Release of incompletely processed proinsulin is the cause of the disproportionate proinsulinemia of NIDDM, *Diabetes 46*, 1725-1732.
38. Badman, M. K., Shennan, K. I. J., Jermany, J. L., Docherty, K., and Clark, A. (1996) Processing of pro-islet amyloid polypeptide (proIAPP) by the prohormone convertase PC2, *Febs Letters 378*, 227-231.
39. Higham, C. E., Hull, R. L., Lawrie, L., Shennan, K. I. J., Morris, J. F., Birch, N. P., Docherty, K., and Clark, A. (2000) Processing of synthetic pro-islet amyloid polypeptide (proiapp) 'amylin' by recombinant prohormone convertase enzymes, pc2 and pc3, in vitro, *Eur. J. Biochem. 267*, 4998-5004.
40. Krampert, M., Bernhagen, J., Schmucker, J., Horn, A., Schmauder, A., Brunner, H., Voelter, W., and Kapurniotu, A. (2000) Amyloidogenicity of recombinant human pro-islet amyloid polypeptide (proiapp), *Chem. Biol. 7*, 855-871.
41. Hull, R. I., Jaikaran, E. T. A. S., Serpell, L. C., Fraser, P. E., Clark, A., and Landon, M. (1998) Synthetic human pro-islet amyloid polypeptide forms amyloid-like fibrils in vitro., *Diabetologia 41*, A168-A168.
42. Westermark, P., Engstrom, U., Westermark, G. T., Johnson, K. H., Permerth, J., and Betsholtz, C. (1989) Islet amyloid polypeptide (iapp) and pro-iapp immunoreactivity in human islets of langerhans, *Diabetes Res. Clin. Pract. 7*, 219-226.
43. Westermark, G. T., Steiner, D. F., Gebre-Medhin, S., Engstrom, U., and

Westermark, P. (2000) Proislet amyloid polypeptide immunoreactivity in the islets of langerhans, *Upsala J. Med. Sci. 105*, 97-106.

44. Furuta, M., Yano, H., Zhou, A., Rouille, Y., Holst, J. J., Carroll, R., Ravazzola, M., Orci, L., Furuta, H., and Steiner, D. F. (1997) Defective prohormone processing and altered pancreatic islet morphology in mice lacking active spc2, *Proc. Natl. Acad. Sci. U. S. A. 94*, 6646-6651.
45. Park, K., and Verchere, C. B. (2001) Identification of a heparin binding domain in the n-terminal cleavage site of pro-islet amyloid polypeptide - implications for islet amyloid formation, *J. Biol. Chem. 276*, 16611-16616.
46. Abedini, A., Tracz, S. M., Cho, J. H., and Raleigh, D. P. (2006) Characterization of the heparin binding site in the n-terminus of human pro-islet amyloid polypeptide: Implications for amyloid formation, *Biochemistry 45*, 9228-9237.
47. Castillo, G. M., Cummings, J. A., Yang, W. H., Judge, M. E., Sheardown, M. J., Rimvall, K., Hansen, J. B., and Snow, A. D. (1998) Sulfate content and specific glycosaminoglycan backbone of perlecan are critical for perlecan's enhancement of islet amyloid polypeptide (amylin) fibril formation, *Diabetes 47*, 612-620.
48. Watson, D. J., Lander, A. D., and Selkoe, D. J. (1997) Heparin-binding properties of the amyloidogenic peptides a beta and amylin - dependence on aggregation state and inhibition by congo red, *J. Biol. Chem. 272*, 31617-31624.
49. Snow, A. D., Bramson, R., Mar, H., Kisilevsky, R., Hassell, J. R., Kimata, K., and Wight, T. N. (1989) Immuno-identification and localization of heparin sulfate proteoglycans to aa amyloid fibrils in an experimental mouse model of inflammation-associated amyloidosis, *Clin. Res. 37*, A223-a223.
50. Inoue, S. (2001) Basement membrane and beta amyloid fibrillogenesis in alzheimer's disease, *International Review of Cytology - a Survey of Cell Biology, Vol 210 210*, 121-161.
51. Ancsin, J. B. (2003) Amyloidogenesis: Historical and modern observations point to heparan sulfate proteoglycans as a major culprit, *Amyloid-Journal of Protein Folding Disorders 10*, 67-79.
52. Potter-Perigo, S., Hull, R. L., Tsoi, C., Braun, K. R., Andrikopoulos, S., Teague, J., Verchere, C. B., Kahn, S. E., and Wight, T. N. (2003) Proteoglycans synthesized and secreted by pancreatic islet beta-cells bind amylin, *Arch. Biochem. Biophys. 413*, 182-190.
53. Knight, J. D., and Miranker, A. D. (2004) Phospholipid catalysis of diabetic amyloid assembly, *J. Mol. Biol. 341*, 1175-1187.
54. Knight, J. D., Hebda, J. A., and Miranker, A. D. (2006) Conserved and cooperative assembly of membrane-bound alpha-helical states of islet amyloid polypeptide, *Biochemistry 45*, 9496-9508.
55. Jayasinghe, S. A., and Langen, R. (2005) Lipid membranes modulate the structure of islet amyloid polypeptide, *Biochemistry 44*, 12113-12119.
56. Quist, A., Doudevski, L., Lin, H., Azimova, R., Ng, D., Frangione, B., Kagan, B.,

Ghiso, J., and Lal, R. (2005) Amyloid ion channels: A common structural link for protein-misfolding disease, *Proc. Natl. Acad. Sci. U. S. A. 102*, 10427-10432.
57. Anguiano, M., Nowak, R. J., and Lansbury, P. T. (2002) Protofibrillar islet amyloid polypeptide permeabilizes synthetic vesicles by a pore-like mechanism that may be relevant to type ii diabetes, *Biochemistry 41*, 11338-11343.
58. Green, J. D., Kreplak, L., Goldsbury, C., Blatter, X. L., Stolz, M., Cooper, G. S., Seelig, A., Kist-Ler, J., and Aebi, U. (2004) Atomic force microscopy reveals defects within mica supported lipid bilayers induced by the amyloidogenic human amylin peptide, *J. Mol. Biol. 342*, 877-887.
59. Furth, A. J. (1997) Glycated proteins in diabetes, *Br. J. Biomed. Sci. 54*, 192-200.
60. Kapurniotu, A., Bernhagen, J., Greenfield, N., Al-Abed, Y., Teichberg, S., Frank, R. W., Voelter, W., and Bucala, R. (1998) Contribution of advanced glycosylation to the amyloidogenicity of islet amyloid polypeptide, *Eur. J. Biochem. 251*, 208-216.
61. Westermark, P., Skinner, M., and Cohen, A. S. (1975) P-component of amyloid of human islets of langerhans, *Scand. J. Immunol. 4*, 95-97.
62. Wisniewski, T., and Frangione, B. (1992) Apolipoprotein-e - a pathological chaperone protein in patients with cerebral and systemic amyloid, *Neurosci. Lett. 135*, 235-238.
63. Botto, M., Hawkins, P. N., Bickerstaff, M. C. M., Herbert, J., Bygrave, A. E., McBride, A., Hutchinson, W. L., Tennent, G. A., Walport, M. J., and Pepys, M. B. (1997) Amyloid deposition is delayed in mice with targeted deletion of the serum amyloid p component gene, *Nat Med 3*, 855-859.
64. Mahley, R. W. (1988) Apolipoprotein-e - cholesterol transport protein with expanding role in cell biology, *Science 240*, 622-630.
65. Caughey, B., and Lansbury, P. T. (2003) Protofibrils, pores, fibrils, and neurodegeneration: Separating the responsible protein aggregates from the innocent bystanders, *Annu. Rev. Neurosci. 26*, 267-298.
66. Lorenzo, A., Razzaboni, B., Weir, G. C., and Yankner, B. A. (1994) Pancreatic-islet cell toxicity of amylin associated with type-2 diabetes-mellitus, *Nature 368*, 756-760.
67. Janson, J., Ashley, R. H., Harrison, D., McIntyre, S., and Butler, P. C. (1999) The mechanism of islet amyloid polypeptide toxicity is membrane disruption by intermediate-sized toxic amyloid particles, *Diabetes 48*, 491-498.
68. Konarkowska, B., Aitken, J. F., Kistler, J., Zhang, S. P., and Cooper, G. J. S. (2006) The aggregation potential of human amylin determines its cytotoxicity towards islet beta-cells, *FEBS J. 273*, 3614-3624.
69. Lansbury, P. T., and Lashuel, H. A. (2006) A century-old debate on protein aggregation and neurodegeneration enters the clinic, *Nature 443*, 774-779.
70. Kirkitadze, M. D., Bitan, G., and Teplow, D. B. (2002) Paradigm shifts in alzheimer's disease and other neuro degenerative disorders: The emerging role of

oligomeric assemblies, *J Neurosci Res 69*, 567-577.

71. Walsh, D. M., Townsend, M., Podlisny, M. B., Shankar, G. M., Fadeeva, J. V., El Agnaf, O., Hartley, D. M., and Selkoe, D. J. (2005) Certain inhibitors of synthetic amyloid beta-peptide (a beta) fibrillogenesis block oligomerization of natural a beta and thereby rescue long-term potentiation, *Journal of Neuroscience 25*, 2455-2462.
72. Lee, S. C., Hashim, Y., Li, J. K. Y., Ko, G. T. C., Critchley, J. A. J. H., Cockram, C. S., and Chan, J. C. N. (2001) The islet amyloid polypeptide (amylin) gene s20g mutation in chinese subjects: Evidence for associations with type 2 diabetes and cholesterol levels, *Clin. Endocrinol. (Oxf). 54*, 541-546.
73. Luca, S., Yau, W. M., Leapman, R., and Tycko, R. (2007) Peptide conformation and supramolecular organization in amylin fibrils: Constraints from solid-state nmr, *Biochemistry 46*, 13505-13522.
74. Ono, K., Condron, M. M., and Teplow, D. B. (2009) Structure-neurotoxicity relationships of amyloid beta-protein oligomers, *Proc. Natl. Acad. Sci. U. S. A. 106*, 14745-14750.
75. Mishra, R., Sellin, D., Radovan, D., Gohlke, A., and Winter, R. (2009) Inhibiting islet amyloid polypeptide fibril formation by the red wine compound resveratrol, *ChemBioChem 10*, 445-+.
76. Evers, F., Jeworrek, C., Tiemeyer, S., Weise, K., Sellin, D., Paulus, M., Struth, B., Tolan, M., and Winter, R. (2009) Elucidating the mechanism of lipid membrane-induced iapp fibrillogenesis and its inhibition by the red wine compound resveratrol: A synchrotron x-ray reflectivity study, *J. Am. Chem. Soc. 131*, 9516-9521.
77. Ehrnhoefer, D. E., Bieschke, J., Boeddrich, A., Herbst, M., Masino, L., Lurz, R., Engemann, S., Pastore, A., and Wanker, E. E. (2008) Egcg redirects amyloidogenic polypeptides into unstructured, off-pathway oligomers, *Nature Structural & Molecular Biology 15*, 558-566.
78. Hudson, S. A., Ecroyd, H., Dehle, F. C., Musgrave, I. F., and Carver, J. A. (2009) (-)-epigallocatechin-3-gallate (egcg) maintains kappa-casein in its pre-fibrillar state without redirecting its aggregation pathway, *J. Mol. Biol. 392*, 689-700.
79. Rambold, A. S., Miesbauer, M., Olschewski, D., Seidel, R., Riemer, C., Smale, L., Brumm, L., Levy, M., Gazit, E., Oesterhelt, D., Baier, M., Becker, C. F. W., Engelhard, M., Winklhofer, K. F., and Tatzelt, J. (2008) Green tea extracts interfere with the stress-protective activity of prpc and the formation of prpsc, *Journal of Neurochemistry 107*, 218-229.
80. Aisen, P. S., Gauthier, S., Vellas, B., Briand, R., Saurnier, D., Laurin, J., and Garceau, D. (2007) Alzhemed: A potential treatment for alzheimer's disease, *Current Alzheimer Research 4*, 473-478.
81. Kisilevsky, R., Lemieux, L. J., Fraser, P. E., Kong, X. Q., Hultin, P. G., and Szarek, W. A. (1995) Arresting amyloidosis in-vivo using small-molecule anionic

sulfonates or sulfates - implications for alzheimers-disease, *Nat Med 1*, 143-148.

82. Gervais, F., Paquette, J., Morissette, C., Krzywkowski, P., Yu, M., Azzi, M., Lacombe, D., Kong, X. Q., Aman, A., Laurin, J., Szarek, W. A., and Tremblay, P. (2007) Targeting soluble a beta peptide with tramiprosate for the treatment of brain amyloidosis, *Neurobiology of Aging 28*, 537-547.
83. Dember, L. M., Hawkins, P. N., Hazenberg, B. P. C., Gorevic, P. D., Merlini, G., Butrimiene, I., Livneh, A., Lesnyak, O., Puechal, X., Lachmann, H. J., Obici, L., Balshaw, R., Garceau, D., Hauck, W., Skinner, M., and Gr, E. A. A. T. (2007) Eprodisate for the treatment of renal disease in aa amyloidosis, *New Engl J Med 356*, 2349-2360.
84. Soto, C., Sigurdsson, E. M., Morelli, L., Kumar, R. A., Castano, E. M., and Frangione, B. (1998) Beta-sheet breaker peptides inhibit fibrillogenesis in a rat brain model of amyloidosis: Implications for alzheimer's therapy, *Nat Med 4*, 822-826.
85. Yan, L. M., Tatarek-Nossol, M., Velkova, A., Kazantzis, A., and Kapurniotu, A. (2006) Design of a mimic of nonamyloidogenic and bioactive human islet amyloid polypeptide (iapp) as nanomolar affinity inhibitor of iapp cytotoxic fibrillogenesis, *Proceedings of the National Academy of Sciences of the United States of America 103*, 2046-2051.
86. Rijkers, D. T. S., Hoppener, J. W. M., Posthuma, G., Lips, C. J. M., and Liskamp, R. M. J. (2002) Inhibition of amyloid fibril formation of human amylin by n-alkylated amino acid and alpha-hydroxy acid residue containing peptides, *Chem-Eur J 8*, 4285-4291.
87. Mason, J. M., Kokkoni, N., Stott, K., and Doig, A. J. (2003) Design strategies for anti-amyloid agents, *Curr. Opin. Struct. Biol. 13*, 526-532.
88. Chiti, F., Taddei, N., Stefani, M., Dobson, C. M., and Ramponi, G. (2001) Reduction of the amyloidogenicity of a protein by specific binding of ligands to the native conformation, *Protein Sci. 10*, 879-886.
89. Luo, Y., Smith, J. V., Paramasivam, V., Burdick, A., Curry, K. J., Buford, J. P., Khan, L., Netzer, W. J., Xu, H. X., and Butko, P. (2002) Inhibition of amyloid-beta aggregation and caspase-3 activation by the ginkgo biloba extract egb761, *Proc. Natl. Acad. Sci. U. S. A. 99*, 12197-12202.
90. Potter, K. J., Scrocchi, L. A., Warnock, G. L., Ao, Z. L., Younker, M. A., Rosenberg, L., Lipsett, M., Verchere, C. B., and Fraser, P. E. (2009) Amyloid inhibitors enhance survival of cultured human islets, *Bba-Gen Subjects 1790*, 566-574.
91. Abedini, A., and Raleigh, D. P. (2009) A critical assessment of the role of helical intermediates in amyloid formation by natively unfolded proteins and polypeptides, *Protein Eng Des Sel 22*, 453-459.
92. Hebda, J. A., Saraogi, I., Magzoub, M., Hamilton, A. D., and Miranker, A. D. (2009) A peptidomimetic approach to targeting pre-amyloidogenic states in type ii

diabetes, *Chem. Biol. 16*, 943-950.
93. Cao, P., Meng, F., Abedini, A., and Raleigh, D. P. (2010) The ability of rodent islet amyloid polypeptide to inhibit amyloid formation by human islet amyloid polypeptide has important implications for the mechanism of amyloid formation and the design of inhibitors, *Biochemistry 49*, 872-881.
94. Kapurniotu, A., Buck, A., Weber, M., Schmauder, A., Hirsch, T., Bernhagen, J., and Tatarek-Nossol, M. (2003) Conformational restriction via cyclization in beta-amyloid peptide a beta(1-28) leads to an inhibitor of a beta(1-28) amyloidogenesis and cytotoxicity, *Chem. Biol. 10*, 149-159.
95. Ferreira, S. T., Vieira, M. N. N., and De Felice, F. G. (2007) Soluble protein oligomers as emerging toxins in alzheimer's and other amyloid diseases, *Iubmb Life 59*, 332-345.
96. Vendruscolo, M., Zurdo, J., MacPhee, C. E., and Dobson, C. M. (2003) Protein folding and misfolding: A paradigm of self-assembly and regulation in complex biological systems, *Philos T Roy Soc A 361*, 1205-1222.
97. Westermark, P., Wernstedt, C., Wilander, E., Hayden, D. W., Obrien, T. D., and Johnson, K. H. (1987) Amyloid fibrils in human insulinoma and islets of langerhans of the diabetic cat are derived from a neuropeptide-like protein also present in normal islet cells, *Proc. Natl. Acad. Sci. U. S. A. 84*, 3881-3885.
98. Cooper, G. J. S., Willis, A. C., Clark, A., Turner, R. C., Sim, R. B., and Reid, K. B. M. (1987) Purification and characterization of a peptide from amyloid-rich pancreases of type-2 diabetic-patients, *Proc. Natl. Acad. Sci. U. S. A. 84*, 8628-8632.
99. Clark, A., Lewis, C. E., Willis, A. C., Cooper, G. J. S., Morris, J. F., Reid, K. B. M., and Turner, R. C. (1987) Islet amyloid formed from diabetes-associated peptide may be pathogenic in type-2 diabetes, *Lancet 2*, 231-234.
100. Rocken, C., Linke, R. P., and Saeger, W. (1992) Immunohistology of islet amyloid polypeptide in diabetes-mellitus - semiquantitative studies in a postmortem series, *Virchows Archiv a-Pathological Anatomy and Histopathology 421*, 339-344.
101. Rushing, P. A., Hagan, M. M., Seeley, R. J., Lutz, T. A., D'Alessio, D. A., Air, E. L., and Woods, S. C. (2001) Inhibition of central amylin signaling increases food intake and body adiposity in rats, *Endocrinology 142*, 5035-5038.
102. Clementi, G., Caruso, A., Cutuli, V. M. C., deBernardis, E., Prato, A., and AmicoRoxas, M. (1996) Amylin given by central or peripheral routes decreases gastric emptying and intestinal transit in the rat, *Experientia 52*, 677-679.
103. Paulsson, J. F., and Westermark, G. T. (2005) Aberrant processing of human proislet amyloid polypeptide results in increased amyloid formation, *Diabetes 54*, 2117-2125.
104. Marzban, L., Rhodes, C. J., Steiner, D. F., Haataja, L., Halban, P. A., and Verchere, C. B. (2006) Impaired nh2-terminal processing of human proislet amyloid polypeptide by the prohormone convertase pc2 leads to amyloid formation and

cell death, *Diabetes 55*, 2192-2201.
105. Paulsson, J. F., Andersson, A., Westermark, P., and Westermark, G. T. (2006) Intracellular amyloid-like deposits contain unprocessed pro-islet amyloid polypeptide (proiapp) in beta cells of transgenic mice overexpressing the gene for human iapp and transplanted human islets, *Diabetologia 49*, 1237-1246.
106. Marcinkiewicz, M., Ramla, D., Seidah, N. G., and Chretien, M. (1994) Developmental expression of the prohormone convertases pc1 and pc2 in mouse pancreatic-islets, *Endocrinology 135*, 1651-1660.
107. Wang, J., Xu, J., Finnerty, J., Furuta, M., Steiner, D. F., and Verchere, C. B. (2001) The prohormone convertase enzyme 2 (pc2) is essential for processing pro-islet amyloid polypeptide at the nh2-terminal cleavage site, *Diabetes 50*, 534-539.
108. Marzban, L., Trigo-Gonzales, G., Zhu, X. R., Rhodes, C. J., Halban, P. A., Steiner, D. F., and Verchere, C. B. (2004) Role of beta-cell prohormone convertase (pc) 1/3 in processing of pro-islet antyloid polypeptide, *Diabetes 53*, 141-148.
109. Young, I. D., Ailles, L., Narindrasorasak, S., Tan, R., and Kisilevsky, R. (1992) Localization of the basement-membrane heparan-sulfate proteoglycan in islet amyloid deposits in type-ii diabetes-mellitus, *Arch. Pathol. Lab. Med. 116*, 951-954.
110. Castillo, G. M., Ngo, C., Cummings, J., Wight, T. N., and Snow, A. D. (1997) Perlecan binds to the beta-amyloid proteins (a beta) of alzheimer's disease, accelerates a beta fibril formation, and maintains a beta fibril stability, *Journal of Neurochemistry 69*, 2452-2465.
111. Yamamoto, S., Yamaguchi, I., Hasegawa, K., Tsutsumi, S., Goto, Y., Gejyo, F., and Naiki, H. (2004) Glycosaminoglycans enhance the trifluoroethanol-induced extensionof beta(2)-microglobulin-related amyloid fibrils at a neutral ph, *J. Am. Soc. Nephrol. 15*, 126-133.
112. Suk, J. Y., Zhang, F. M., Balch, W. E., Linhardt, R. J., and Kelly, J. W. (2006) Heparin accelerates gelsolin amyloidogenesis, *Biochemistry 45*, 2234-2242.
113. Abedini, A., and Raleigh, D. P. (2005) Incorporation of pseudoproline derivatives allows the facile synthesis of human iapp, a highly amyloidogenic and aggregation-prone polypeptide, *Organic Letters 7*, 693-696.
114. Teplow, D. B., Lazo, N. D., Bitan, G., Bernstein, S., Wyttenbach, T., Bowers, M. T., Baumketner, A., Shea, J. E., Urbanc, B., Cruz, L., Borreguero, J., and Stanley, H. E. (2006) Elucidating amyloid beta-protein folding and assembly: A multidisciplinary approach, *Acc. Chem. Res. 39*, 635-645.
115. Kirkitadze, M. D., Condron, M. M., and Teplow, D. B. (2001) Identification and characterization of key kinetic intermediates in amyloid beta-protein fibrillogenesis, *J. Mol. Biol. 312*, 1103-1119.
116. Elimova, E., Kisilevsky, R., Szarek, W. A., and Ancsin, J. B. (2004) Amyloidogenesis recapitulated in cell culture: A peptide inhibitor provides direct evidence for the role of heparan sulfate and suggests a new treatment strategy,

Faseb Journal 18, 1749-+.

117. Conde-Knape, K. (2001) Heparan sulfate proteoglycans in experimental models of diabetes: A role for perlecan in diabetes complications, *Diabetes Metab Res 17*, 412-421.
118. Cohen, T., Frydman-Marom, A., Rechter, M., and Gazit, E. (2006) Inhibition of amyloid fibril formation and cytotoxicity by hydroxyindole derivatives, *Biochemistry 45*, 4727-4735.
119. Porat, Y., Mazor, Y., Efrat, S., and Gazit, E. (2004) Inhibition of islet amyloid polypeptide fibril formation: A potential role for heteroaromatic interactions, *Biochemistry 43*, 14454-14462.
120. Scrocchi, L. A., Chen, Y., Waschuk, S., Wang, F., Cheung, S., Darabie, A. A., McLaurin, J., and Fraser, P. E. (2002) Design of peptide-based inhibitors of human islet amyloid polypeptide fibrillogenesis, *J. Mol. Biol. 318*, 697-706.
121. Abedini, A., Meng, F. L., and Raleigh, D. P. (2007) A single-point mutation converts the highly amyloidogenic human islet amyloid polypeptide into a potent fibrillization inhibitor, *J. Am. Chem. Soc. 129*, 11300-+.
122. Pepys, M. B. (2001) Pathogenesis, diagnosis and treatment of systemic amyloidosis, *Philos T Roy Soc B 356*, 203-210.
123. Walsh, D. M., and Selkoe, D. J. (2004) Oligomers in the brain: The emerging role of soluble protein aggregates in neurodegeneration, *Protein Peptide Lett 11*, 213-228.
124. Kayed, R., Head, E., Thompson, J. L., McIntire, T. M., Milton, S. C., Cotman, C. W., and Glabe, C. G. (2003) Common structure of soluble amyloid oligomers implies common mechanism of pathogenesis, *Science 300*, 486-489.
125. Isaacs, A. M., Senn, D. B., Yuan, M. L., Shine, J. P., and Yankner, B. A. (2006) Acceleration of amyloid beta-peptide aggregation by physiological concentrations of calcium, *J. Biol. Chem. 281*, 27916-27923.
126. Hori, Y., Hashimoto, T., Wakutani, Y., Urakami, K., Nakashima, K., Condron, M. M., Tsubuki, S., Saido, T. C., Teplow, D. B., and Iwatsubo, T. (2007) The tottori (d7n) and english (h6r) familial alzheimer disease mutations accelerate a beta fibril formation without increasing protofibril formation, *J. Biol. Chem. 282*, 4916-4923.
127. Grudzielanek, S., Velkova, A., Shukla, A., Smirnovas, V., Tatarek-Nossol, M., Rehage, H., Kapurniotu, A., and Winter, R. (2007) Cytotoxicity of insulin within its self-assembly and amyloidogenic pathways, *J. Mol. Biol. 370*, 372-384.
128. Meier, J. J., Kayed, R., Lin, C. Y., Gurlo, T., Haataja, L., Jayasinghe, S., Langen, R., Glabe, C. G., and Butler, P. C. (2006) Inhibition of human iapp fibril formation does not prevent beta-cell death: Evidence for distinct actions of oligomers and fibrils of human iapp, *Am J Physiol-Endoc M 291*, E1317-E1324.
129. Namba, Y., Kawatsu, K., Izumi, S., Ueki, A., and Ikeda, K. (1992) Neurofibrillary tangles and senile plaques in brain of elderly leprosy patients, *Lancet 340*,

978-978.

130. Chui, D. H., Tabira, T., Izumi, S., Koya, G., and Ogata, J. (1994) Decreased beta-amyloid and increased abnormal tau-deposition in the brain of aged patients with leprosy, *Am. J. Pathol. 145*, 771-775.
131. Tomiyama, T., Asano, S., Suwa, Y., Morita, T., Kataoka, K., Mori, H., and Endo, N. (1994) Rifampicin prevents the aggregation and neurotoxicity of amyloid-beta protein in-vitro, *Biochem. Biophys. Res. Commun. 204*, 76-83.
132. Matsuzaki, K., Noguch, T., Wakabayashi, M., Ikeda, K., Okada, T., Ohashi, Y., Hoshino, M., and Naiki, H. (2007) Inhibitors of amyloid beta-protein aggregation mediated by gm1-containing raft-like membranes, *Bba-Biomembranes 1768*, 122-130.
133. Tomiyama, T., Shoji, A., Kataoka, K., Suwa, Y., Asano, S., Kaneko, H., and Endo, N. (1996) Inhibition of amyloid beta protein aggregation and neurotoxicity by rifampicin - its possible function as a hydroxyl radical scavenger, *J. Biol. Chem. 271*, 6839-6844.
134. Lieu, V. H., Wu, J. W., Wang, S. S. S., and Wu, C. H. (2007) Inhibition of amyloid fibrillization of hen egg-white lysozymes by rifampicin and p-benzoquinone, *Biotechnol. Progr. 23*, 698-706.
135. Li, J., Zhu, M., Rajamani, S., Uversky, V. N., and Fink, A. L. (2004) Rifampicin inhibits alpha-synuclein fibrillation and disaggregates fibrils, *Chem. Biol. 11*, 1513-1521.
136. Xu, J., Wei, C. Z., Xu, C. Q., Bennett, M. C., Zhang, G. H., Li, F. C., and Tao, E. X. (2007) Rifampicin protects pc12 cells against mpp+-induced apoptosis and inhibits the expression of an alpha-synuclein multimer, *Brain Research 1139*, 220-225.
137. Tomiyama, T., Kaneko, H., Kataoka, K., Asano, S., and Endo, N. (1997) Rifampicin inhibits the toxicity of pre-aggregated amyloid peptides by binding to peptide fibrils and preventing amyloid-cell interaction, *Biochem. J 322*, 859-865.
138. Haataja, L., Gurlo, T., Huang, C. J., and Butler, P. C. (2008) Islet amyloid in type 2 diabetes, and the toxic oligomer hypothesis, *Endocr. Rev. 29*, 303-316.
139. Harroun, T. A., Bradshaw, J. P., and Ashley, R. H. (2001) Inhibitors can arrest the membrane activity of human islet amyloid polypeptide independently of amyloid formation, *Febs Letters 507*, 200-204.
140. Abedini, A., Singh, G., and Raleigh, D. P. (2006) Recovery and purification of highly aggregation-prone disulfide-containing peptides: Application to islet amyloid polypeptide, *Anal. Biochem. 351*, 181-186.
141. Benetton, S. A., Kedor-Hackmann, E. R. M., Santoro, M. I. R. M., and Borges, V. M. (1998) Reversed-phase high performance liquid chromatographic determination of rifampin in the presence of its acid-induced degradation products, *J. Liq. Chromatogr. Rel. Technol. 21*, 3215-3221.
142. Furesz, S. (1970) Chemical and biological properties of rifampicin, *Antibiotica Et*

Chemotherapia 16, 316-&.
143. Marek, P., Gupta, R., and Raleigh, D. P. (2008) The fluorescent amino acid p-cyanophenylalanine provides an intrinsic probe of amyloid formation, *ChemBioChem 9*, 1372-1374.
144. Tucker, M. J., Oyola, R., and Gai, F. (2006) A novel fluorescent probe for protein binding and folding studies: P-cyano-phenylalanine, *Biopolymers 83*, 571-576.
145. Chiti, F., and Dobson, C. M. (2006) Protein misfolding, functional amyloid, and human disease, *Annu. Rev. Biochem 75*, 333-366.
146. Cohen, F. E., and Kelly, J. W. (2003) Therapeutic approaches to protein-misfolding diseases, *Nature 426*, 905-909.
147. Chen, S. M., Berthelier, V., Hamilton, J. B., O'Nuallain, B., and Wetzel, R. (2002) Amyloid-like features of polyglutamine aggregates and their assembly kinetics, *Biochemistry 41*, 7391-7399.
148. Blazer, L. L., and Neubig, R. R. (2009) Small molecule protein-protein interaction inhibitors as cns therapeutic agents: Current progress and future hurdles, *Neuropsychopharmacology 34*, 126-141.
149. Takahashi, T., and Mihara, H. (2008) Peptide and protein mimetics inhibiting amyloid beta-peptide aggregation, *Acc. Chem. Res. 41*, 1309-1318.
150. Feng, B. Y., Toyama, B. H., Wille, H., Colby, D. W., Collins, S. R., May, B. C. H., Prusiner, S. B., Weissman, J., and Shoichet, B. K. (2008) Small-molecule aggregates inhibit amyloid polymerization, *Nat. Chem. Biol. 4*, 197-199.
151. Kapurniotu, A. (2001) Arnyloidogenicity and cytotoxicity of islet amyloid polypeptide, *Biopolymers 60*, 438-459.
152. Mazor, Y., Gilead, S., Benhar, I., and Gazit, E. (2002) Identification and characterization of a novel molecular-recognition and self-assembly domain within the islet amyloid polypeptide, *J. Mol. Biol. 322*, 1013-1024.
153. Yan, L. M., Velkova, A., Tatarek-Nossol, M., Andreetto, E., and Kapurniotu, A. (2007) Lapp mimic blocks a beta cytotoxic self-assembly: Cross-suppression of amyloid toxicity of a beta and iapp suggests a molecular link between alzheimer's disease and type ii diabetes, *Angewandte Chemie-International Edition 46*, 1246-1252.
154. Berthelier, V., and Wetzel, R. (2006) Screening for modulators of aggregation with a microplate elongation assay, *Amyloid, Prions, and Other Protein Aggregates, Pt C 413*, 313-325.
155. Lazar, K. L., Kurutz, J. W., Tycko, R., and Meredith, S. C. (2006) Encapsulation and nmr on an aggregating peptide before fibrillogenesis, *J. Am. Chem. Soc. 128*, 16460-16461.
156. Scrocchi, L. A., Chen, Y., Wang, F., Han, K., Ha, K., Wu, L., and Fraser, P. E. (2003) Inhibitors of islet amyloid polypeptide fibrillogenesis, and the treatment of type-2 diabetes, *Lett. Pept. Sci. 10*, 545-551.
157. Mishra, R., Bulic, B., Sellin, D., Jha, S., Waldmann, H., and Winter, R. (2008)

Small-molecule inhibitors of islet amyloid polypeptide fibril formation, *Angewandte Chemie-International Edition 47*, 4679-4682.

158. Porat, Y., Abramowitz, A., and Gazit, E. (2006) Inhibition of amyloid fibril formation by polyphenols: Structural similarity and aromatic interactions as a common inhibition mechanism, *Chemical Biology & Drug Design 67*, 27-37.
159. Meng, F. L., Marek, P., Potter, K. J., Verchere, C. B., and Raleigh, D. P. (2008) Rifampicin does not prevent amyloid fibril formation by human islet amyloid polypeptide but does inhibit fibril thioflavin-t interactions: Implications for mechanistic studies beta-cell death, *Biochemistry 47*, 6016-6024.
160. Rajkumar, S. V., and Gertz, M. A. (2007) Advances in the treatment of amyloidosis, *New Engl J Med 356*, 2413-2415.
161. Abedini, A., and Raleigh, D. P. (2005) The role of his-18 in amyloid formation by human islet amyloid polypeptide, *Biochemistry 44*, 16284-16291.
162. Velkova, A., Tatarek-Nossol, M., Andreetto, E., and Kapurniotu, A. (2008) Exploiting cross-amyloid interactions to inhibit protein aggregation but not function: Nanomolar affinity inhibition of insulin aggregation by an iapp mimic, *Angewandte Chemie-International Edition 47*, 7114-7118.
163. O'Nuallain, B., Williams, A. D., Westermark, P., and Wetzel, R. (2004) Seeding specificity in amyloid growth induced by heterologous fibrils, *J. Biol. Chem. 279*, 17490-17499.
164. Marzban, L., Park, K., and Verchere, C. B. (2003) Islet amyloid polypeptide and type 2 diabetes, *Exp. Gerontol. 38*, 347-351.
165. Hutton, J. C. (1989) The insulin secretory granule, *Diabetologia 32*, 271-281.
166. Nishi, M., Sanke, T., Nagamatsu, S., Bell, G. I., and Steiner, D. F. (1990) Islet amyloid polypeptide - a new beta-cell secretory product related to islet amyloid deposits, *J. Biol. Chem. 265*, 4173-4176.
167. Bonner-Weir, S., and O'Brien, T. D. (2008) Islets in type 2 diabetes: In honor of dr. Robert c. Turner, *Diabetes 57*, 2899-2904.
168. Marzban, L., Tomas, A., Becker, T. C., Rosenberg, L., Oberholzer, J., Fraser, P. E., Halban, P. A., and Verchere, C. B. (2008) Small interfering rna-mediated suppression of proislet amyloid polypeptide expression inhibits islet amyloid formation and enhances survival of human islets in culture, *Diabetes 57*, 3045-3055.
169. Meng, F., Abedini, A., Song, B., and Raleigh, D. P. (2007) Amyloid formation by pro-islet amyloid polypeptide processing intermediates: Examination of the role of protein heparan sulfate interactions and implications for islet amyloid formation in type 2 diabetes, *Biochemistry 46*, 12091-12099.
170. Hull, R. L., Zraika, S., Udayasankar, J., Kisilevsky, R., Szarek, W. A., Wight, T. N., and Kahn, S. E. (2007) Inhibition of glycosaminoglycan synthesis and protein glycosylation with was-406 and azaserine result in reduced islet amyloid formation in vitro, *American Journal of Physiology-Cell Physiology 293*,

C1586-C1593.

171. Meng, F., Abedini, A., Plesner, A., Middleton, C. T., Potter, K. J., Zanni, M. T., Verchere, C. B., and Raleigh, D. P. (2010) The sulfated triphenyl methane derivative acid fuchsin is a potent inhibitor of amyloid formation by human islet amyloid polypeptide and protects against the toxic effects of amyloid formation, *J. Mol. Biol. doi:10.1016/j.jmb.2010.05.001*.
172. Yonemoto, I. T., Kroon, G. J. A., Dyson, H. J., Balch, W. E., and Kelly, J. W. (2008) Amylin proprotein processing generates progressively more amyloidogenic peptides that initially sample the helical state, *Biochemistry 47*, 9900-9910.
173. Westermark, P., Wernstedt, C., Wilander, E., and Sletten, K. (1986) A novel peptide in the calcitonin gene related peptide family as an amyloid fibril protein in the endocrine pancreas, *Biochem. Biophys. Res. Commun. 140*, 827-831.
174. Hayden, M. R., Karuparthi, P. R., Manrique, C. M., Lastra, G., Habibi, J., and Sowers, J. R. (2007) Longitudinal ultrastructure study of islet amyloid in the hip rat model of type 2 diabetes mellitus, *Exp Biol Med 232*, 772-779.
175. Westermark, G. T., Westermark, P., Berne, C., Korsgren, O., and Transpla, N. N. C. I. (2008) Widespread amyloid deposition in transplanted human pancreatic islets, *New Engl J Med 359*, 977-979.
176. Westermark, G. T., Westermark, P., Nordin, A., Tornelius, E., and Andersson, A. (2003) Formation of amyloid in human pancreatic islets transplanted to the liver and spleen of nude mice, *Upsala J Med Sci 108*, 193-203.
177. Udayasankar, J., Kodama, K., Hull, R. L., Zraika, S., Aston-Mourney, K., Subramanian, S. L., Tong, J., Faulenbach, M. V., Vidal, J., and Kahn, S. E. (2009) Amyloid formation results in recurrence of hyperglycaemia following transplantation of human iapp transgenic mouse islets, *Diabetologia 52*, 145-153.
178. Potter, K. J., Abedini, A., Marek, P., Klimek, A. M., Butterworth, S., Driscoll, M., Baker, R., Nilsson, M. R., Warnock, G. L., Oberholzer, J., Bertera, S., Trucco, M., Korbutt, G. S., Fraser, P. E., Raleigh, D. P., and Verchere, C. B. (2010) Islet amyloid deposition limits the viability of human islet grafts but not porcine islet grafts, *Proc. Natl. Acad. Sci. U. S. A. 107*, 4305-4310.
179. Higdon, J. V., and Frei, B. (2003) Tea catechins and polyphenols: Health effects, metabolism, and antioxidant functions, *Critical Reviews in Food Science and Nutrition 43*, 89-143.
180. Jeong, W. S., and Kong, A. N. T. (2004) Biological properties of monomeric and polymeric catechins: Green tea catechins and procyanidins, *Pharmaceutical Biology 42*, 84-93.
181. Rezai-Zadeh, K., Arendash, G. W., Hou, H. Y., Fernandez, F., Jensen, M., Runfeldt, M., Shytle, R. D., and Tan, J. (2008) Green tea epigallocatechin-3-gallate (egcg) reduces beta-amyloid mediated cognitive impairment and modulates tau pathology in alzheimer transgenic mice, *Brain Research 1214*, 177-187.

182. Li, Q., Gordon, M., Tan, J., and Morgan, D. (2006) Oral administration of green tea epigallocatechin-3-gallate (egcg) reduces amyloid beta deposition in transgenic mouse model of alzheimer's disease, *Experimental Neurology 198*, 576-576.
183. Rezai-Zadeh, K., Shytle, D., Sun, N., Mori, T., Hou, H. Y., Jeanniton, D., Ehrhart, J., Townsend, K., Zeng, J., Morgan, D., Hardy, J., Town, T., and Tan, J. (2005) Green tea epigallocatechin-3-gallate (egcg) modulates amyloid precursor protein cleavage and reduces cerebral amyloidosis in alzheimer transgenic mice, *Journal of Neuroscience 25*, 8807-8814.
184. Lin, C. L., Chen, T. F., Chiu, M. J., Way, T. D., and Lin, J. K. (2009) Epigallocatechin gallate (egcg) suppresses beta-amyloid-induced neurotoxicity through inhibiting c-abl/fe65 nuclear translocation and gsk3 beta activation, *Neurobiology of Aging 30*, 81-92.
185. Tilstra, L. F., Maeda, H., and Mattice, W. L. (1988) Interaction of (+)-catechin with the edge of the beta-sheet formed by poly-(s-carboxymethyl-l-cysteine), *Journal of the Chemical Society-Perkin Transactions 2*, 1613-1616.
186. Bieschke, J., Russ, J., Friedrich, R. P., Ehrnhoefer, D. E., Wobst, H., Neugebauer, K., and Wanker, E. E. (2010) Egcg remodels mature alpha-synuclein and amyloid-beta fibrils and reduces cellular toxicity, *Proc. Natl. Acad. Sci. U. S. A. 107*, 7710-7715.
187. Roberts, B. E., Duennwald, M. L., Wang, H., Chung, C., Lopreiato, N. P., Sweeny, E. A., Knight, M. N., and Shorter, J. (2009) A synergistic small-molecule combination directly eradicates diverse prion strain structures, *Nat. Chem. Biol. 5*, 936-946.
188. Nilsson, M. R., and Raleigh, D. P. (1999) Analysis of amylin cleavage products provides new insights into the amyloidogenic region of human amylin, *J. Mol. Biol. 294*, 1375-1385.
189. Collins, S. R., Douglass, A., Vale, R. D., and Weissman, J. S. (2004) Mechanism of prion propagation: Amyloid growth occurs by monomer addition, *PLoS Biol. 2*, 1582-1590.
190. Knowles, T. P. J., Waudby, C. A., Devlin, G. L., Cohen, S. I. A., Aguzzi, A., Vendruscolo, M., Terentjev, E. M., Welland, M. E., and Dobson, C. M. (2009) An analytical solution to the kinetics of breakable filament assembly, *Science 326*, 1533-1537.
191. Larson, J. L., and Miranker, A. D. (2004) The mechanism of insulin action on islet amyloid polypeptide fiber formation, *J. Mol. Biol. 335*, 221-231.
192. Xue, W. F., Homans, S. W., and Radford, S. E. (2008) Systematic analysis of nucleation-dependent polymerization reveals new insights into the mechanism of amyloid self-assembly, *Proc. Natl. Acad. Sci. U. S. A. 105*, 8926-8931.
193. Ling, Y. L., Strasfeld, D. B., Shim, S. H., Raleigh, D. P., and Zanni, M. T. (2009) Two-dimensional infrared spectroscopy provides evidence of an intermediate in

the membrane-catalyzed assembly of diabetic amyloid, *J. Phys. Chem. B 113*, 2498-2505.

194. Masuda, M., Hasegawa, M., Nonaka, T., Oikawa, T., Yonetani, M., Yamaguchi, Y., Kato, K., Hisanaga, S., and Goedert, M. (2009) Inhibition of alpha-synuclein fibril assembly by small molecules: Analysis using epitope-specific antibodies, *Febs Letters 583*, 787-791.